

UNIVERSITY OF OKLAHOMA

GRADUATE COLLEGE

AN OPTIMALLY WELL LOCALIZED MULTI-CHANNEL
PARALLEL PERFECT RECONSTRUCTION FILTER BANK

A Dissertation

SUBMITTED TO THE GRADUATE FACULTY

in partial fulfillment of the requirements for the

degree of

Doctor of Philosophy

By

PETER C. TAY
Norman, Oklahoma
2003

UMI Number: 3107288

INFORMATION TO USERS

The quality of this reproduction is dependent upon the quality of the copy submitted. Broken or indistinct print, colored or poor quality illustrations and photographs, print bleed-through, substandard margins, and improper alignment can adversely affect reproduction.

In the unlikely event that the author did not send a complete manuscript and there are missing pages, these will be noted. Also, if unauthorized copyright material had to be removed, a note will indicate the deletion.

UMI[®]

UMI Microform 3107288

Copyright 2004 by ProQuest Information and Learning Company.

All rights reserved. This microform edition is protected against unauthorized copying under Title 17, United States Code.

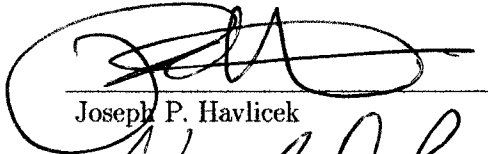
ProQuest Information and Learning Company
300 North Zeeb Road
P.O. Box 1346
Ann Arbor, MI 48106-1346

©Copyright by PETER C. TAY 2003
All Rights Reserved.

AN OPTIMALLY WELL LOCALIZED MULTI-CHANNEL
PARALLEL PERFECT RECONSTRUCTION FILTER BANK

A Dissertation APPROVED FOR THE
SCHOOL OF ELECTRICAL AND COMPUTER
ENGINEERING

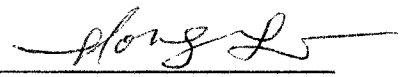
BY



Joseph P. Havlicek



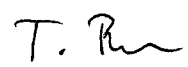
Victor DeBrunner



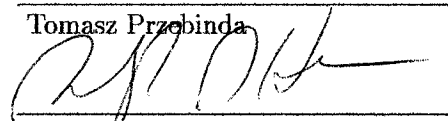
Hong Liu



Murad Özaydin



Tomasz Przebinda



Ralph Hamerla

This dissertation is dedicated to my mother
Nellie Chu Ai Tay
and to the memory of my father
Samuel Soo Lam Tay.

Acknowledgements

I would like to thank each committee member for serving. Our openly candid, scientific, and philosophical discussions has help me grow as an engineer, mathematician, and historian. A hardy appreciation goes to Professor Joesph “Joejob” Havlicek and Professor Victor DeBrunner. In addition to teaching me everything I know about signal and image processing and funding my education and professional development, they have given me a wide range of valuable advice and much encouragement throughout the years.

My arrival to this important point in my life and the completion of this dissertation would not have been possible without the generous support of the ORISE fellowship program which placed me in the Radar Operation Center of the National Weather Service. This program was largely funded by the National Oceanic and Atmospheric Administration (NOAA). I am greatly indebted to William “Bill” Armstrong for this appointment.

Lastly I like to thank the most supportive person in my life, my sister, Elizabeth Tay McVicker. It is her scholarly accomplishments which gave me the courage to dream *the dream* and believe in myself.

Table of Contents

Acknowledgements	v
List of Tables	viii
List of Figures	x
Abstract	xiii
Chapter 1. Introduction	1
1.1 Overview	1
1.2 Original Contributions	2
1.3 Notation and Nomenclature	3
Chapter 2. Background	7
2.1 Historical Background	7
2.2 AM-FM Image Models	10
2.3 Wavelets	15
2.3.1 Orthogonal Case	16
2.3.2 Biorthogonal Case	19
2.4 Time-Bandwidth Measures	21
2.4.1 Uncertainty for Infinite Discrete Time Sequences	21
2.4.2 Uncertainty for Finite Discrete Time Sequences	28
Chapter 3. Problem Statement	32
Chapter 4. Novel Measure of Uncertainty	36
4.1 Quantifying Uncertainty and Localization	36
4.2 Equivalence Classes of Sequences	38
Chapter 5. Application to Scaling Functions	45

Chapter 6. Optimal Scaling Function	55
6.1 A Best In Time and Best In Frequency Lower Bound	55
6.2 Magnitude of an Orthogonal Scaling Function	57
6.3 A Linear Phase Response	62
6.4 A Search Algorithm to Determine the Lower Bound	76
6.4.1 Orthogonal Case	76
6.4.2 Biorthogonal Case	82
Chapter 7. Multi-Channel Parallel Filter Bank Realizations	90
7.1 $L - 1$ Level Discrete Wavelet Transform	90
7.2 Uncertainty of a Multi-Channel Filter Bank	94
7.3 Optimal Multi-Channel Filter Bank	99
Chapter 8. Image Analysis	102
8.1 Analysis and Synthesis Algorithm	102
8.2 Evaluation Using Some Well-Known QMF's	112
Chapter 9. Conclusion and Future Work	137
9.1 Conclusion	137
9.2 Future Work	140
Bibliography	143
Appendices	
Appendix A. Plots of Functions Γ_{\max} and Γ_{\min}	150
Appendix B. Search Results of Section 6.4.1	159
Appendix C. Well Known Quadrature Mirror Filter Banks	165

List of Tables

5.1	Frequency variance of haar _N , symlet and db _N , and the ideal magnitude response for lengths 2 – 20.	52
5.2	Time variance of a symmetric filter with phase given in equation (5.3), symlet, and db _N for lengths 2 – 20. All three types of filters have the same magnitude $ F[k] $	53
5.3	Uncertainty measure of haar _N , symlet, and db _N for lengths 2 – 20.	53
6.1	Lower bounds for uncertainty measure for filter lengths 2 – 20 given by $\sigma_{n, [\mathbf{haar}_N]}^2 \sigma_{\omega, [\mathbf{d}_N]}^2$ in the second leftmost column and as determined by the search algorithm in subsection 6.4.1 in the second rightmost column.	81
6.2	Length-six biorthogonal QMF	87
6.3	Length-eight biorthogonal QMF	89
7.1	Two, three, four, five channel filter bank uncertainties using the length 6 Coiflet (Coif), Daubechies length 6 (DB_6), the biorthogonal 6/2 (BO6/2), the biorthogonal 3/5 (BO3/5), and the biorthogonal 4/4 (BO4/4), QMFs.	101
8.1	Reconstruction <i>CSE</i> of <i>lena</i> using the length six Coiflet (Coif) QMF, the Daubechies length 6 (DB_6) QMF, the biorthogonal 3/5 QMF (BO3/5), the biorthogonal 6/2 QMF (BO6/2), the biorthogonal 4/4 QMF (BO4/4).	113
8.2	Reconstruction <i>CSE</i> of <i>girl</i> using the length six Coiflet (Coif) QMF, the Daubechies length 6 (DB_6) QMF, the biorthogonal 3/5 QMF (BO3/5), the biorthogonal 6/2 QMF (BO6/2), the biorthogonal 4/4 QMF (BO4/4).	113
8.3	Reconstruction <i>CSE</i> of <i>gauss</i> using the length six Coiflet (Coif) QMF, the Daubechies length 6 (DB_6) QMF, the biorthogonal 3/5 QMF (BO3/5), the biorthogonal 6/2 QMF (BO6/2), the biorthogonal 4/4 QMF (BO4/4).	114
8.4	Reconstruction <i>CSE</i> of <i>burlap</i> using the length six Coiflet (Coif) QMF, the Daubechies length 6 (DB_6) QMF, the biorthogonal 3/5 QMF (BO3/5), the biorthogonal 6/2 QMF (BO6/2), the biorthogonal 4/4 QMF (BO4/4).	114

8.5	Reconstruction <i>CSE</i> of <i>mandril</i> using the length six Coiflet (Coif) QMF, the Daubechies length 6 (DB_6) QMF, the biorthogonal 3/5 QMF (BO3/5), the biorthogonal 6/2 QMF (BO6/2), the biorthogonal 4/4 QMF (BO4/4).	120
8.6	Reconstruction <i>CSE</i> of <i>clown</i> using the length six Coiflet (Coif) QMF, the Daubechies length 6 (DB_6) QMF, the biorthogonal 3/5 QMF (BO3/5), the biorthogonal 6/2 QMF (BO6/2), the biorthogonal 4/4 QMF (BO4/4).	124
8.7	Reconstruction <i>CSE</i> of <i>salesman</i> using the length six Coiflet (Coif) QMF, the Daubechies length 6 (DB_6) QMF, the biorthogonal 3/5 QMF (BO3/5), the biorthogonal 6/2 QMF (BO6/2), the biorthogonal 4/4 QMF (BO4/4).	125
8.8	Reconstruction <i>CSE</i> of <i>lady</i> using the length six Coiflet (Coif) QMF, the Daubechies length 6 (DB_6) QMF, the biorthogonal 3/5 QMF (BO3/5), the biorthogonal 6/2 QMF (BO6/2), the biorthogonal 4/4 QMF (BO4/4).	130
8.9	Reconstruction <i>CSE</i> of <i>baby</i> using the length six Coiflet (Coif) QMF, the Daubechies length 6 (DB_6) QMF, the biorthogonal 3/5 QMF (BO3/5), the biorthogonal 6/2 QMF (BO6/2), the biorthogonal 4/4 QMF (BO4/4).	130
C.1	The Daubechies length six (DB_6) QMF.	165
C.2	The biorthogonal 3/5 (BO3/5) QMF.	165
C.3	The biorthogonal 6/2 (BO6/2) QMF.	166
C.4	The biorthogonal 4/4 (BO4/4) QMF.	166
C.5	The length six Coiflet (<i>Coif</i>) QMF.	166

List of Figures

6.1	Plot of $\Gamma_{\max}(\lambda)$ of the length four filter \mathbf{f} defined in equation (6.46) for $0 \leq \lambda \leq 1$	74
6.2	Plot of $\Gamma_{\min}(\lambda)$ of the length four filter \mathbf{f} defined in equation (6.46) for $0 \leq \lambda \leq 1$	75
7.1	The three level discrete wavelet transform cascaded filter bank.	90
7.2	The three level inverse discrete wavelet transform cascaded filter bank.	91
7.3	The Noble identities.	91
7.4	A L channel parallel filter bank.	92
7.5	The magnitude terms of $H_1(z)$ using a Daubechies length 6 QMF to implement a four-channel parallel filter bank.	97
8.1	Log magnitude spectrum of $H_{3,3}(z)$	105
8.2	Output of $H_{3,3}(z)$ using the <i>lena</i> image.	106
8.3	Log magnitude spectrum of $H_{3,3,t}(z)$	107
8.4	Log magnitude spectrum of $H_{3,3,b}(z)$	108
8.5	Output of $H_{3,3,t}(z)$ using <i>lena</i> image.	109
8.6	Output of $H_{3,3,b}(z)$ using <i>lena</i> image.	110
8.7	The image analysis algorithm.	111
8.8	The original <i>lena</i> image.	114
8.9	The best reconstructed <i>lena</i> image using Gabor filter bank.	115
8.10	Reconstructed <i>lena</i> image using Coiflet QMF filter bank.	116
8.11	Reconstructed <i>lena</i> image using DB_6 QMF filter bank.	117
8.12	The original <i>girl</i> image.	118
8.13	The original <i>gauss</i> image.	119
8.14	The original <i>burlap</i> image.	120
8.15	The best reconstructed <i>burlap</i> image using Gabor filter bank.	121
8.16	Reconstructed <i>burlap</i> image using Coiflet QMF filter bank.	122

8.17	Reconstructed <i>burlap</i> image using DB_6 QMF filter bank.	123
8.18	The original <i>mandril</i> image.	125
8.19	The best reconstructed <i>mandril</i> image using Gabor filter bank.	126
8.20	Reconstructed <i>mandril</i> image using Coiflet QMF filter bank.	127
8.21	Reconstructed <i>mandril</i> image using DB_6 QMF filter bank.	128
8.22	The original <i>clown</i> image.	129
8.23	The original <i>salesman</i> image.	131
8.24	The best reconstructed <i>salesman</i> image using Gabor filter bank.	132
8.25	Reconstructed <i>salesman</i> image using Coiflet QMF filter bank.	133
8.26	Reconstructed <i>salesman</i> image using DB_6 QMF filter bank.	134
8.27	The original <i>lady</i> image.	135
8.28	The original <i>baby</i> image.	136
A.1	Plot of $\Gamma_{\max}(\lambda)$ of the length 6 filter \mathbf{f} defined in equation (6.46) for $0 \leq \lambda \leq 1$	151
A.2	Plot of $\Gamma_{\min}(\lambda)$ of the length 6 filter \mathbf{f} defined in equation (6.46) for $0 \leq \lambda \leq 1$	151
A.3	Plot of $\Gamma_{\max}(\lambda)$ of the length 8 filter \mathbf{f} defined in equation (6.46) for $0 \leq \lambda \leq 1$	152
A.4	Plot of $\Gamma_{\min}(\lambda)$ of the length 8 filter \mathbf{f} defined in equation (6.46) for $0 \leq \lambda \leq 1$	152
A.5	Plot of $\Gamma_{\max}(\lambda)$ of the length 10 filter \mathbf{f} defined in equation (6.46) for $0 \leq \lambda \leq 1$	153
A.6	Plot of $\Gamma_{\min}(\lambda)$ of the length 10 filter \mathbf{f} defined in equation (6.46) for $0 \leq \lambda \leq 1$	153
A.7	Plot of $\Gamma_{\max}(\lambda)$ of the length 12 filter \mathbf{f} defined in equation (6.46) for $0 \leq \lambda \leq 1$	154
A.8	Plot of $\Gamma_{\min}(\lambda)$ of the length 12 filter \mathbf{f} defined in equation (6.46) for $0 \leq \lambda \leq 1$	154
A.9	Plot of $\Gamma_{\max}(\lambda)$ of the length 14 filter \mathbf{f} defined in equation (6.46) for $0 \leq \lambda \leq 1$	155
A.10	Plot of $\Gamma_{\min}(\lambda)$ of the length 14 filter \mathbf{f} defined in equation (6.46) for $0 \leq \lambda \leq 1$	155
A.11	Plot of $\Gamma_{\max}(\lambda)$ of the length 16 filter \mathbf{f} defined in equation (6.46) for $0 \leq \lambda \leq 1$	156
A.12	Plot of $\Gamma_{\min}(\lambda)$ of the length 16 filter \mathbf{f} defined in equation (6.46) for $0 \leq \lambda \leq 1$	156

A.13 Plot of $\Gamma_{\max}(\lambda)$ of the length 18 filter \mathbf{f} defined in equation (6.46) for $0 \leq \lambda \leq 1$	157
A.14 Plot of $\Gamma_{\min}(\lambda)$ of the length 18 filter \mathbf{f} defined in equation (6.46) for $0 \leq \lambda \leq 1$	157
A.15 Plot of $\Gamma_{\max}(\lambda)$ of the length 20 filter \mathbf{f} defined in equation (6.46) for $0 \leq \lambda \leq 1$	158
A.16 Plot of $\Gamma_{\min}(\lambda)$ of the length 20 filter \mathbf{f} defined in equation (6.46) for $0 \leq \lambda \leq 1$	158

Abstract

AN OPTIMALLY WELL LOCALIZED MULTI-CHANNEL PARALLEL PERFECT RECONSTRUCTION FILTER BANK

Peter C. Tay, Ph.D.
The University of Oklahoma, 2003

Supervisor: Joseph P. Havlicek

This dissertation defines a measure of uncertainty for finite length discrete-time signals. Using this uncertainty measure, a relationship analogous to the well known continuous-time Heisenberg-Weyl inequality is developed. This uncertainty measure is applied to quantify the joint discrete time-discrete frequency localization of finite impulse response filters, which are used in a quadrature mirror filter bank (QMF). A formulation of a biorthogonal QMF where the low pass analysis filter minimizes the newly defined measure of uncertainty is presented. The search algorithm used in the design of the length- N linear phase low pass analysis FIR filter is given for $N = 6$ and 8 . In each case, the other three filters, which constitute a perfect reconstruction QMF, are determined by adapting a method due to Vetterli and Le Gall. From a set of well know QMFs comprised of length six filters, L -channel perfect reconstruction parallel filter banks (PRPFB) are constructed. The Noble identities are used to show that the L -channel PRPFB is equivalent to a $L - 1$ level discrete wavelet

filter bank. Several five-channel PRPFBs are implemented. A separable implementation of a five-channel, one-dimensional filter bank produces twenty-five channel, two-dimensional filter bank. Each non-low pass, two-dimensional filter is decomposed in a novel, nonseparable way to obtain equivalent channel filters that possess orientation selectivity. This results in a forty-one channel, two-dimensional, orientation selective, PRPFB.

Joint uncertainty for the overall L -channel, one-dimensional, parallel filter bank is quantified by a metric which is a weighted sum of the time and frequency localizations of the individual filters. Evidence is presented to show that a filter bank possessing a lower joint filter bank uncertainty with respect to this metric results in a computed multicomponent AM-FM image model that yields lower reconstruction errors. This strongly supports the theory that there is a direct relationship between joint uncertainty as quantified by the measures developed and the degree of local smoothness or “local coherency” that may be expected in the filter bank channel responses. Thus, as demonstrated by the examples, these new measures may be used to construct new filter banks that offer excellent localization properties on par with those of Gabor filter banks.

Chapter 1

Introduction

1.1 Overview

The principle of indeterminacy, first formulated by Heisenberg in 1927, was an idea that is manifested in the physical world of quantum mechanics. At the time of its conception, it was believed that future quantum events could be determined exactly, if the present position and momentum of an electron and all the forces acting on it could be determined exactly. Heisenberg never refuted this concept. His principle of indeterminacy maintains that the conditional is not possible. This notion of uncertainty had implication not just in the scientific society, but also in religion, economics, *etc.* Heisenberg justified uncertainty not with a mathematical proof nor with empirical evidence but rather with a hypothetical experiment. It has been seventy-six year since Heisenberg's first publication on uncertainty and this notion has yet to be disproved. On the contrary, the principle of uncertainty has been supported by empirical evidence and rigorous modern experimentation.

Gabor's application to communication signals is one such example that gives support to Heisenberg's uncertainty principle. Gabor with the aid of wave mechanics and the Schwarz inequality showed that a finite energy, continuous signal can not be arbitrarily and simultaneously localized in both the continuous

time and continuous frequency domains. In addition, Gabor showed that a family of modulated and translated Gaussian functions uniquely attained the minimum area in the time-frequency plane. This gave rise to the notion of the smallest unit or quanta of information possessed by a signal.

In our modern digital world, the signals, which are of most concern, are finite and discrete signals. We rely on sampling theories to connect us to the continuous and analog world. It does not seem unreasonable that truncating and sampling a translated and modulated Gaussian function will lead to minimum finite discrete time and finite discrete frequency localization. Not only does this idea seem reasonable, but it is practiced unquestionably by many researchers.

It is not my intention to refute the work of any research prior to this dissertation. Rather, this dissertation brings mathematical formalism to quantify and conceptualize uncertainty, *i.e.*, localization for a finite discrete signal. This formalism is done in a manner which is consistent with the classical, intuitive, meaningful interpretation of Heisenberg and Gabor. In addition, some of the ideas of modern uncertainty principles are incorporated to define a uncertainty measure for filter banks. This filter bank uncertainty measure is shown to further the science of computer vision in the form of enhancing the AM-FM image modulation model.

1.2 Original Contributions

The original contributions to digital signal and image processing presented in this dissertation are unprecedented. Over the past twenty years, there have been numerous formulations of time and frequency localization used in vari-

ous joint uncertainty measures. These various measures have some unappealing qualities like not based on probability distribution, not directly related to Fourier transform in particular the *DFT*, not translation invariant, not modulation invariant, *etc.* For the first time ever, these problems are solved in the work presented in this dissertation.

I have developed a novel discrete-discrete uncertainty measure that is in direct analogy to the Heisenberg-Weyl uncertainty principle. This measure admits an intuitively satisfying interpretation in terms of energy variances. This new measure is invariant under modulations and translations. In addition, a meaningful extension of this notion of uncertainty is used to quantify uncertainty for a L -channel perfect reconstruction parallel filter bank (PRPFB). The separable implementation of these L -channel PRPFBs are made *orientation selective*. The work in this dissertation produces a design for well-localized *orientation selective* filter banks that result in computed AM-FM models with small reconstruction errors. In general, better joint localization with respect to the new filter bank uncertainty measure directly relates to a lower AM-FM reconstruction error.

1.3 Notation and Nomenclature

\mathbb{N} , \mathbb{Z} , \mathbb{R} , and \mathbb{C} refers, respectively, to the set of natural numbers, the set of integers, the set of real numbers, and the set of complex numbers.

The imaginary unit is denoted $j = \sqrt{-1}$.

Let $z = a + jb \in \mathbb{C}$. Then the complex conjugate of z is $z^* = a - jb$. It is easy to verify that $\{e^{j\Theta}\}^* = e^{-j\Theta}$, $\forall \Theta \in \mathbb{R}$, $\{z_1 z_2\}^* = z_1^* z_2^*$ and $\{z_1 + z_2\}^* = z_1^* + z_2^*$.

For $z \in \mathbb{C}$, the modulus is $|z| = \sqrt{a^2 + b^2}$.

Sequences are represented in several ways. The notation $f(n)$ is used to denote an infinite length sequence, while $f[n]$ denotes a finite length sequence. I use \mathbf{f} to mean a finite length sequence and will also refer to finite length sequences in vector notation according to $\mathbf{f} = [f[0] \ f[1] \ f[2] \ \cdots \ f[N-1]]^T$.

The $\ell^2_{[0, N-1]}$ -norm of \mathbf{f} is denoted

$$\|f[n]\| = \left\{ \sum_{n=0}^{N-1} f[n] f^*[n] \right\}^{\frac{1}{2}}.$$

For $f(n)$ and $g(n)$, linear convolution is defined by

$$f(n) * g(n) = \sum_{l=-\infty}^{\infty} f(l) g(n-l).$$

Mathematical relations are denoted by the symbol \sim . For example, the notation $a \sim b$ indicates that a relation exists between a and b .

- A relation \sim is reflexive if and only if $x \sim x$ for all x in the set on which the relation is defined.
- A relation \sim is symmetric if and only if $x \sim y$ implies $y \sim x$ for all x, y in the set on which the relation is defined.
- A relation \sim is transitive if and only if $x \sim y$ and $y \sim z$ imply $x \sim z$ for all x, y, z in the set on which the relation is defined.
- A relation \sim is an equivalence relation if and only if it is reflexive, symmetric, and transitive.
- I will use the notation $[\mathbf{f}]$ to denote an equivalence class for the sequence \mathbf{f} , *i.e.*, $[\mathbf{f}] = \{\mathbf{g} \mid \mathbf{g} \sim \mathbf{f}\}$.

For $a \in \mathbb{Z}$, the modular notation is $(a)_N = a \bmod N$.

The continuous Fourier transform (*CFT*) of $f(t)$ is defined as

$$F(\omega) = \int_{-\infty}^{\infty} f(t) e^{-j\omega t} dt,$$

where ω is the radian frequency variable. The inverse continuous Fourier transform (*ICFT*) is defined as

$$f(t) = \frac{1}{2\pi} \int_{-\infty}^{\infty} F(\omega) e^{j\omega t} d\omega.$$

The discrete time Fourier transform (*DTFT*) of an infinite sequence $f(n)$ is defined as

$$F(e^{j\omega}) = \sum_{n=-\infty}^{\infty} f(n) e^{-j\omega n}, \quad (1.1)$$

where $\omega \in [-\pi, \pi)$. The inverse discrete time Fourier transform (*IDTFT*) is defined as

$$f(n) = \frac{1}{2\pi} \int_{-\pi}^{\pi} F(e^{j\omega}) e^{j\omega n} d\omega. \quad (1.2)$$

The discrete Fourier transform (*DFT*) of a finite sequence of length- N is defined as

$$F[k] = \sum_{n=0}^{N-1} f[n] e^{-j\frac{2\pi}{N}nk}, \quad (1.3)$$

where $0 \leq k \leq N-1$. The inverse discrete Fourier transform (*IDFT*) is defined as

$$f[n] = \frac{1}{N} \sum_{k=0}^{N-1} F[k] e^{j\frac{2\pi}{N}nk}, \quad (1.4)$$

where $0 \leq n \leq N-1$. The z-transform of sequence $f(n)$ is defined as

$$F(z) = \sum_{n=-\infty}^{\infty} f(n) z^{-n} \quad (1.5)$$

where $z \in \mathbb{C}$. For $f[n]$ a sequence of finite length N , the z -transform of $f[n]$ will be defined as in equation (1.5) where

$$f(n) = \begin{cases} f[n] & \text{for } n = 0, 1, 2, \dots, N - 1 \\ 0 & \text{otherwise.} \end{cases} \quad (1.6)$$

The autocorrelation of a sequence $f(n)$ at lag $l \in \mathbb{Z}$ is defined as

$$r_f(l) = \sum_{n=-\infty}^{\infty} f(n)f^*(n+l). \quad (1.7)$$

For a finite-length sequence, unless otherwise specified, the autocorrelation will be understood to be computed using infinite-length sequences obtained by zero padding as indicated in (1.6).

Additional notations are defined as needed throughout this dissertation. Definitions of some terms already defined may be repeated for the sake of clarity and emphasis.

Chapter 2

Background

2.1 Historical Background

The original formulation of the principle of indeterminacy is credited to Werner Heisenberg (1901-1976) and Hermann Weyl (1885-1955). Along with Erwin Schrödinger (1887-1961, Nobel Prize-Physics: 1933), Albert Einstein (1879-1955, Nobel Prize-Physics: 1921) ¹, and Niels Bohr ² (1885-1962, Nobel Prize-Physics: 1922), Heisenberg is considered to be one of the fathers of modern quantum mechanics. As one biographer has observed “one of the most important developments in quantum theory was Heisenberg’s uncertainty principle...” [1]. Heisenberg’s uncertainty principle (*a.k.a.* the principle of indeterminacy) states that the arbitrarily precise, simultaneous measurement of canonically conjugate variables, such as the position (p) and the momentum (q), or the energy (E) and time (t), of a particle, are excluded in principle. Instead, reciprocal relationships exist between the indeterminacies in the measurements of position (Δp) and momentum (Δq), or energy (ΔE) and time

¹Schrödinger and Einstein held a theory and model of quantum mechanics that rivaled Bohr and Heisenberg’s model. The rival theories were later shown to be equivalent.

²Bohr was Heisenberg’s dissertation advisor.

(Δt). These can be represented by Heisenberg's famous uncertainty relation

$$\Delta p \Delta q \approx \hbar,$$

$$\Delta E \Delta t \approx \hbar,$$

where \hbar is Planck's constant [2]. An English translation of Heisenberg's original 1927 paper is published in [3]. Heisenberg was awarded the Nobel Prize in Physics in 1932 for his formulation of the principle of indeterminacy.

Credit for this uncertainty relation may also be bestowed to Hermann Weyl. Weyl, in *Gruppentheorie and Quantenmechanik* [4], formulated Heisenberg's uncertainty relation, as the more familiar inequality

$$\Delta p \Delta q \geq \frac{1}{2} \hbar. \quad (2.1)$$

The original publication of *Gruppentheorie and Quantenmechanik* was in 1931, while the English translation [4] appeared in 1950.

Dénes Gabor³ (1900-1979) formulated the Heisenberg and Weyl's uncertainty principle (HWUP) in the familiar modern form applicable to finite energy continuous signals. Along with his work in communication theory, Gabor is best known for developing the theory of holography, while trying to improve the resolution of the electron microscope. In 1971, Gabor was awarded the Nobel Prize in Physics for this pioneering work.

In 1946, Gabor realized an example of HWUP in the following: let $h : \mathbb{R} \rightarrow \mathbb{C}$ be a continuous function with $\lim_{t \rightarrow \pm\infty} h(t) = 0$. Then

$$\Delta_t \Delta_f \geq \frac{1}{2}. \quad (2.2)$$

³Commonly known as Dennis Gabor.

In Gabor's formulation, the pulse width Δ_t^2 is defined as

$$\Delta_t^2 = \frac{\int_{-\infty}^{\infty} (t - \bar{t})^2 |h(t)|^2 dt}{\int_{-\infty}^{\infty} |h(t)|^2 dt}, \quad (2.3)$$

where

$$\bar{t} = \frac{\int_{-\infty}^{\infty} t |h(t)|^2 dt}{\int_{-\infty}^{\infty} |h(\tau)|^2 d\tau}.$$

The band width Δ_f^2 is defined as

$$\Delta_f^2 = \frac{\int_{-\infty}^{\infty} (f - \bar{f})^2 |H(f)|^2 df}{\int_{-\infty}^{\infty} |H(f)|^2 df}, \quad (2.4)$$

where

$$\bar{f} = \frac{\int_{-\infty}^{\infty} f |H(f)|^2 df}{\int_{-\infty}^{\infty} |H(f)|^2 df}.$$

This uncertainty relation (2.2) quantifies the fact that continuous time and continuous frequency localization cannot be arbitrarily small simultaneously.

With the aid of the Schwarz inequality, Gabor proved in [5] that the only functions which achieve equality in (2.2) are

$$\psi(t) = e^{-\alpha^2(t-t_0)^2} e^{j2\pi(f_0 t + \phi)}, \quad (2.5)$$

where $\alpha, t_0, f_0, \phi \in \mathbb{R}$ and where j is the imaginary unit. These functions are referred to as the Gabor elementary functions or simply as the Gabor functions.

Since Gabor functions are optimally localized in both continuous time and continuous frequency, they are used in numerous signal and image processing applications which rely on well localized conjoint time-frequency analysis [6]. Their popularity extends even into the finitely supported discrete domain, where Gaussian shaped finite impulse response (FIR) filters are created by sampling continuous Gabor functions, or by various forms of approximation of the continuous Gabor functions.

The current state of digital signal and image processing implementations require filters where only finite computations are allowed. In effect, this requires filters to be finite and discrete. This would include finite impulse response (FIR) and infinite impulse response (IIR) filters, but exclude filters with infinite non-zero terms. Since Gabor functions are Gaussian functions shifted in time and frequency, their supports are infinite in both time and frequency. Creating filters by sampling a Gaussian functions leads to truncations to finite length filters which may result in the loss of the “ideal” joint localization. In addition, since these sampled and truncated Gaussian filters lack orthogonality, perfect reconstruction of these filters is problematic.

2.2 AM-FM Image Models

Gabor’s formulation of HWUP defined the notion of a “quantum” of information. The conjoint time-frequency domain for one dimensional continuous signals is essentially quantized, so that no signal or filter can occupy less than a certain minimal area. This minimal area reflects the inherent trade-off between time resolution and frequency resolution. Gabor showed that his functions yield the best trade-off in terms of achieving the minimal area, and that they are unique in this respect. If we consider that each member of a family of translated and modulated functions carries one quantum of information, then the information bearing capacity of the family is maximized when the family members are Gabor functions, since this choice minimizes the area in the time-frequency plane that is occupied by each member.

A continuous time signal can be expressed as a linear combination of Gabor elementary functions. The coefficients in this linear combination, which are

called the *Gabor Transform*, are computed as inner products between the signal and a biorthogonal family of auxiliary functions. Compared to the Fourier transform, the Gabor transform is better able to represent temporally or spatially local signal features. This is a direct consequence of to the fact that the Gabor functions are optimally and uniquely well localized in the time-frequency plane. The Fourier transform tends to spread localized time features throughout the frequency spectrum. Local transforms such as the Gabor transform tend to reduce transform domain correlations between signal features that are time localized. Thus, local transforms are inherently better for performing time-frequency analysis to determine a signal's local features.

To model a simple cell in the visual cortex, Daugman generalized the Gabor elementary functions to the two-dimensional case [7]. In addition, he showed that the two-dimensional version of HWUP is uniquely minimized by two-dimensional Gabor functions. Daugman's two-dimensional Gabor functions can be expressed as

$$G(x, y) = \frac{1}{2\pi\alpha\beta} e^{-\pi\left(\frac{(x-x_0)^2}{\sigma^2} + \frac{(y-y_0)^2}{\beta^2}\right)} e^{j(\psi_0x + \phi_0y)}, \quad (2.6)$$

where (x_0, y_0) is the spatial centroid of the filter impulse response, (ψ_0, ϕ_0) is the filter center frequency, and σ and β are the standard deviations along the x-axis and y-axis, *resp* [7]. This formulation popularized the use of two-dimensional Gabor functions in image processing techniques where time-frequency analysis is required. One notable example is AM-FM image modeling developed by Havlicek, Bovik, and others. [6, 8–10].

In this dissertation I restrict my attention to the AM-FM image model using the directional 2-D Hilbert transform. To establish a complete back-

ground of the work present in this dissertation, a description of AM-FM image models using Gabor analysis is given. A more concise and detailed description is given in [8,9]. For an n -dimensional complex-valued image $s : \mathbb{R}^n \rightarrow \mathbb{C}$, the K -component AM-FM model of the image is given by

$$s(\mathbf{x}) = \sum_{i=1}^K s_i(\mathbf{x}) = \sum_{i=1}^K a_i(\mathbf{x}) e^{j\varphi_i(\mathbf{x})}, \quad (2.7)$$

where $\mathbf{x} = [x_1 \ x_2 \ \dots \ x_n]^T \in \mathbb{R}^n$, $a_i : \mathbb{R}^n \rightarrow [0, \infty)$ and $\varphi_i : \mathbb{R}^n \rightarrow \mathbb{R}$. The functions $a_i(\mathbf{x})$ and $\nabla\varphi_i(\mathbf{x})$ are called the amplitude and frequency modulations of $s(\mathbf{x})$. The frequency modulation of component $s_i(\mathbf{x})$ is defined as

$$\nabla\varphi_i(\mathbf{x}) = \left[\frac{\partial}{\partial x_1}\varphi_i(\mathbf{x}) \ \frac{\partial}{\partial x_2}\varphi_i(\mathbf{x}) \ \dots \ \frac{\partial}{\partial x_n}\varphi_i(\mathbf{x}) \right]^T. \quad (2.8)$$

For agreement with the model (2.7), a real-valued image $t : \mathbb{R}^n \rightarrow \mathbb{R}$ is extended to a complex image $s(\mathbf{x})$ by adding an imaginary part according to

$$s(\mathbf{x}) = t(\mathbf{x}) + j\mathcal{H}[t(\mathbf{x})], \quad (2.9)$$

where $\mathcal{H}[t(\mathbf{x})]$ is the directional multi-dimensional Hilbert transform [11].

If the component $s_i(\mathbf{x}) = a_i(\mathbf{x})e^{j\varphi_i(\mathbf{x})}$ in (2.7) could somehow be isolated from the other components, then it could be demodulated using the algorithm [6,8–10]

$$\nabla\varphi_i(\mathbf{x}) = \operatorname{Re} \left[\frac{\nabla s_i(\mathbf{x})}{j s_i(\mathbf{x})} \right] \quad (2.10)$$

$$a_i(\mathbf{x}) = |s_i(\mathbf{x})|, \quad (2.11)$$

which is exact at all points where $s_i(\mathbf{x}) \neq 0$. The individual components are not generally available however. Thus, signal processing, often in the form of linear multi-band filtering, must be applied to isolate the components from one another.

The approach devised by Havlicek and Bovik was to apply a linear multi-band filter bank for isolating components and then to modify (2.10) and (2.11) to estimate the component modulating functions directly from the filter bank channel responses. Let $g : \mathbb{R}^n \rightarrow \mathbb{C}$ and $G(\boldsymbol{\Omega})$ be the impulse response and frequency response of one of the filter bank channels. Suppose that, in a neighborhood about a particular point $\mathbf{x} \in \mathbb{R}^n$, the channel response is dominated by component $s_i(\mathbf{x})$ in (2.7), so that

$$y(\mathbf{x}) = s(\mathbf{x}) * g(\mathbf{x}) \approx s_i(\mathbf{x}) * g(\mathbf{x}) \quad (2.12)$$

in the neighborhood. Provided that the modulating functions of $s_i(\mathbf{x})$ are sufficiently smooth in a certain sense [9], the right hand side of (2.12) may be approximated using the quasi-eigenfunction approximation (QEA)

$$\hat{y}(\mathbf{x}) = s_i(\mathbf{x})G[\nabla\varphi_i(\mathbf{x})] \approx s_i(\mathbf{x}) * g(\mathbf{x}) \approx y(\mathbf{x}). \quad (2.13)$$

Applying the frequency demodulation algorithm (2.10) directly to the channel response $y(\mathbf{x})$, the QEA gives

$$\operatorname{Re} \left[\frac{\nabla y(\mathbf{x})}{jy(\mathbf{x})} \right] \approx \operatorname{Re} \left[\frac{\nabla \hat{y}(\mathbf{x})}{j\hat{y}(\mathbf{x})} \right] \quad (2.14)$$

$$= \operatorname{Re} \left[\frac{\nabla s_i(\mathbf{x})G[\nabla\varphi_i(\mathbf{x})]}{js_i(\mathbf{x})G[\nabla\varphi_i(\mathbf{x})]} \right] \quad (2.15)$$

$$= \operatorname{Re} \left[\frac{\nabla s_i(\mathbf{x})}{js_i(\mathbf{x})} \right]. \quad (2.16)$$

Since (2.16) is identical to the right-hand side of (2.10), this motivates the so called “filtered FM” algorithm

$$\nabla \hat{\varphi}_i(\mathbf{x}) = \operatorname{Re} \left[\frac{\nabla y(\mathbf{x})}{jy(\mathbf{x})} \right]. \quad (2.17)$$

A similar QEA application validates the filtered AM algorithm [9]

$$\hat{a}_i(\mathbf{x}) = \left| \frac{y(\mathbf{x})}{G[\nabla\hat{\varphi}_i(\mathbf{x})]} \right| \quad (2.18)$$

$$\approx \left| \frac{\hat{y}(\mathbf{x})}{G[\nabla\hat{\varphi}_i(\mathbf{x})]} \right| \quad (2.19)$$

$$= \left| \frac{y(\mathbf{x})G[\nabla\varphi_i(\mathbf{x})]}{G[\nabla\hat{\varphi}_i(\mathbf{x})]} \right| \quad (2.20)$$

$$\approx a_i(\mathbf{x}). \quad (2.21)$$

Thus, given an appropriately constructed filter bank, (2.17) and (2.18) may be applied to estimate the individual component modulating functions in (2.7) directly from the filter bank channel responses. QEA's were also used to develop equivalent discrete demodulation algorithms in [9].

The filters $G(\Omega)$ should be well localized in frequency so that they have the power to resolve multiple signal components from one another, but also well spatially localized to capture local nonstationary features of the signal structure. To balance these conflicting requirements and also to minimize QEA approximation errors, which are bounded by Sobolev norms of the component modulating functions, Havlicek and Bovik employed discretized Gabor filters [9]. For a Gabor filter bank constructed of channel filters $G_m(\Omega)$, they extracted estimates of the dominant AM and FM functions at each point $\mathbf{x} \in \mathbb{R}^n$ from the filter bank channel that maximized the selection criterion $\Psi_m(\mathbf{x}) = \frac{|y_m(\mathbf{x})|}{\max_{\Omega} |G_m(\Omega)|}$. These dominant modulations have been used to solve a variety of classical computer vision problems. They also computed general AM-FM image representations $\{\hat{a}_i(\mathbf{x}), \nabla\hat{\varphi}_i(\mathbf{x})\}_{i=1,2,\dots,K}$, from which they obtained approximate image reconstructions.

Though the bank of discretized and truncated Gabor filters provided excellent joint localization properties and thereby minimize errors in the QEA,

the fact that it did not provide perfect reconstruction leads to the approximate equalities in (2.12) and (2.13). Thus precludes the possibility of an invertible AM-FM transformation. What is needed to complete this important work is a filter bank design offering both excellent joint time-frequency localization *and* perfect reconstruction.

2.3 Wavelets

The multi-resolution image analysis and synthesis method described by Mallat in [12] requires a quadrature mirror filter bank (QMF). There are a myriad of ways to create QMFs. A few are given in [13–19]. Since wavelets are well suited for this application, they are often chosen to construct QMFs. The use of wavelets to construct filter banks is well documented [12, 20–23]. This dissertation will not focus on formulating the relevance of wavelets and multi-resolution analysis. I refer the reader to [22] as an excellent reference in this area. Rather, this dissertation applies the work already well developed in this area as a guiding framework for the design of filters to be used in a QMF.

To create a binary-tree quadrature mirror FIR filter bank, the low pass analysis, low pass synthesis, high pass analysis, and high pass synthesis filters must be specified. Let \mathbf{f}_a , \mathbf{f}_s , \mathbf{g}_a , and \mathbf{g}_s be the finite-length real-valued low pass analysis, finite-length real-valued low pass synthesis, finite-length real-valued high pass analysis, and finite-length real-valued high pass synthesis filters, *resp.* For a sequence $x(n)$ let

$$\hat{x}_l(n) = \begin{cases} x(n) * f_a(n) & \text{if } n \text{ is even} \\ 0 & \text{if } n \text{ is odd} \end{cases}$$

and

$$\hat{x}_h(n) = \begin{cases} x(n) * g_a(n) & \text{if } n \text{ is even} \\ 0 & \text{if } n \text{ is odd.} \end{cases}$$

Define

$$\tilde{x}_l(n) = \hat{x}_l(n) * f_s(n),$$

$$\tilde{x}_h(n) = \hat{x}_h(n) * g_s(n),$$

and

$$\tilde{x}(n) = \tilde{x}_l(n) + \tilde{x}_h(n).$$

If $x(n) = \tilde{x}(n+D)$ for some $D \in \mathbb{Z}$, then the QMF comprised of \mathbf{f}_a , \mathbf{f}_s , \mathbf{g}_a , \mathbf{g}_s is a *perfect reconstruction* filter bank. Both orthogonal and biorthogonal perfect reconstruction QMFs can be formulated.

2.3.1 Orthogonal Case

The following definitions and properties are stated in a manner relevant to their use in this dissertation. They do not only adhere to FIR filters, but can be adapted to include infinite length filters.

Definition 1. A quadrature mirror filter bank is *orthogonal* if \mathbf{f}_a , \mathbf{f}_s , \mathbf{g}_a , and \mathbf{g}_s are all of equal length N and if

$$f_a[n] = f_s[N-1-n], \quad (2.22)$$

$$g_a[n] = g_s[N-1-n], \quad (2.23)$$

and the following conditions hold:

$$\sum_{m=0}^{N-1} f_a(m) f_a^*(m+2l) = c_1 \delta(l), \quad (2.24)$$

$$\sum_{m=0}^{N-1} g_a(m) g_a^*(m+2l) = c_2 \delta(l), \quad (2.25)$$

$$\sum_{m=0}^{N-1} f_a(m) g_a^*(m+2l) = 0, \quad (2.26)$$

$$\sum_{m=0}^{N-1} f_s(m) g_s^*(m+2l) = 0, \quad (2.27)$$

$$\sum_{m=0}^{N-1} f_a(m) f_s^*(m+2l) = c_3 \delta(l), \quad (2.28)$$

$$\sum_{m=0}^{N-1} g_a(m) g_s^*(m+2l) = c_4 \delta(l), \quad (2.29)$$

for some constants c_1, c_2, c_3, c_4 , where $f_a(m)$, $f_s(m)$, $g_a(m)$, and $g_s(m)$ are $f_a[m]$, $f_s[m]$, $g_a[m]$, and $g_s[m]$ extended infinitely by zeros *resp.* as defined by equation (1.6). The sequence $\delta(l)$ is the Kronecker delta function for $l \in \mathbb{Z}$.

The following properties of orthogonal QMF's are presented for the sake of referencing later in this dissertation. The proofs are omitted since they are well known and have been published elsewhere by others.

Property 1. The $\ell_{[0, N-1]}^2$ -norm of all four filters are equal:

$$\|\mathbf{f}_a\| = \|\mathbf{f}_s\| = \|\mathbf{g}_a\| = \|\mathbf{g}_s\|.$$

Property 2. Let $F_a(e^{j2\pi\phi}) = DTFT\{f_a(n)\}$. Then it has been proved by Vetterli and Herley in [22] and others that equation (2.24) in definition 1 implies

$$|F_a(e^{j2\omega})|^2 + |F_a(e^{j(2\omega+\pi)})|^2 = 2,$$

where $\omega = 2\pi\phi$. I refrain from stating this implication as an equivalence, since the converse statement does not guarantee that $f_a(n)$ is finite length.⁴

⁴ $|F_a(e^{j\omega})|^2 + |F_a(e^{j(\omega+\pi)})|^2 = 2$ does not necessarily imply that $f_a(n) = IDTFT\{F_a(e^{j\omega})\}$ is finite length.

Property 3. Provided the $\ell^2_{[0,N-1]}$ -norm of $f_a[n]$ is unity, The sum of the low pass analysis filter coefficients is equal to $\sqrt{2}$:

$$\sum_{n=0}^{N-1} f_a[n] = \sqrt{2}.$$

Property 4. The sum of the high pass analysis filter coefficients is equal to zero:

$$\sum_{n=0}^{N-1} g_a[n] = 0.$$

Property 5. The high pass analysis filter is obtained by multiplying each element of the low pass analysis filter by $(-1)^n$:

$$g_a[n] = (-1)^n f_a[N - 1 - n].$$

Property 6. The length N must be even.⁵

Property 7. It follows directly from properties 2 and 3 that

$$F_a(e^{j\pi}) = 0,$$

where $F_a(e^{j2\pi\phi}) = DTFT\{f_a(n)\}$.

From equations (2.22) and (2.23) of definition 1 and property 5, specification of just one of the low pass analysis, high pass analysis, low pass synthesis, or high pass synthesis filters is sufficient to completely determine the construction of a orthogonal FIR wavelet QMF.

⁵see [22], pp. 2212

2.3.2 Biorthogonal Case

For a FIR wavelet based filter bank, if the filter bank is to be capable of perfect reconstruction and linear phase, orthogonality is not possible except in the Haar case. Linear phase is sometimes preferred because the filters can be cascaded in pyramidal filter structures without using phase compensation [20].

Definition 2. A filter $f(n)$ with $DTFT\{f(n)\} = F(e^{j\omega})$ has (generalized) linear phase if $\exists a, b \in \mathbb{R}$ such that $\forall \omega \in [-\pi, \pi)$ $F(e^{j\omega}) = |F(e^{j\omega})|e^{j\phi(\omega)}$ or $F(e^{j\omega}) = \text{sgn}\{F(e^{j\omega})\}|F(e^{j\omega})|e^{j\phi(\omega)}$, where $\phi(\omega) = a\omega + b$, up to additions and subtractions of integer multiples of 2π .

To develop real FIR filters whose lengths are greater than two, achieve an perfect reconstruction QMF, and have linear phase, an orthogonal construction is not possible. If perfect reconstruction, linear phase, and length longer than two are all required, it is necessary to construct the QMF in terms of biorthogonal wavelets. A concise and thorough account of biorthogonal wavelets can be found in [24]. The following definition and properties have been reformulated without proof to amplify their practical relevance to the research presented in this dissertation.

Definition 3. Let N_1, N_2 be the lengths of $\mathbf{f}_a, \mathbf{f}_s$, *resp.*. A quadrature mirror filter bank is biorthogonal if

$$g_a[n] = c_1 (-1)^n f_s[N_2 - 1 - n], \quad (2.30)$$

$$g_s[n] = c_2 (-1)^n f_a[N_1 - 1 - n], \quad (2.31)$$

for some constants c_1 and c_2 and the following conditions are met:

$$\sum_{m=0}^{N_1-1} f_a(m)f_s^*(m+2l) = c_3\delta(l), \quad (2.32)$$

$$\sum_{m=0}^{N_2-1} g_a(m)g_s^*(m+2l) = c_4\delta(l), \quad (2.33)$$

for some constants c_3, c_4 , where $g_a(m)$ and $g_s(m)$ are $g_a[m]$ and $g_s[m]$ *resp.* infinitely extended by zeros as defined in equation (1.6).

It is easily deduced from definition 3 that, to construct a biorthogonal QMF, only filters \mathbf{f}_a and \mathbf{f}_s need to be specified. In [22], Vetterli has classified all biorthogonal linear phase perfect reconstruction FIR QMF's into three categories:

1. Both \mathbf{f}_a and \mathbf{g}_a are symmetric and the lengths N_1 and N_2 are odd. These lengths differ by an odd multiple of two.
2. Either \mathbf{f}_a is symmetric and \mathbf{g}_a is antisymmetric or \mathbf{g}_a is symmetric and \mathbf{f}_a is antisymmetric. The lengths N_1 and N_2 are even and equal or differ by an even multiple of two.
3. One filter's length is odd while the other's is even. Both filters have zeros on the unit circle, and neither can be antisymmetric.

In addition to the length considerations, the following properties hold:

Property 8. Analogous to property 2,

$$F_a(e^{j\omega})F_s^*(e^{j\omega}) + F_a(e^{j(\omega+\pi)})F_s^*(e^{j(\omega+\pi)}) = 2,$$

where $F(e^{j\omega}) = DTFT\{f(n)\}$.

Property 9. The low pass analysis and low pass synthesis filters have a zero at -1:

$$F_a(e^{j\pi}) = 0 = F_s(e^{j\pi}),$$

where $F(e^{j\omega}) = DTFT \{f(n)\}$.

Property 10. The sum of the low pass analysis filter and the sum of the low pass synthesis filter are each equal to $\sqrt{2}$:

$$\sum_{n=0}^{N_1-1} f_a[n] = \sum_{n=0}^{N_2-1} f_s[n] = \sqrt{2}.$$

Note as well that when $f_a[n]$ is scaled to attain unit $\ell_{[0, N_a-1]}^2$ -norm, then property 10 may not hold. Regardless, either condition results in the same number of free parameters in determining $f_a[n]$. Restriction to both conditions allows one fewer free parameter compared to an adherence to one.

Property 11. The sum of the high pass analysis filter and the sum of the high pass synthesis filter are each equal to zero:

$$\sum_{n=0}^{N_2-1} g_a[n] = 0 = \sum_{n=0}^{N_1-1} g_s[n].$$

2.4 Time-Bandwidth Measures

In this section I describe several measures that have been proposed for quantifying infinitely and finitely supported sequences.

2.4.1 Uncertainty for Infinite Discrete Time Sequences

This section considers methods that quantify band width for a discrete signal on a continuous frequency domain. Measures for the infinite time support, continuous frequency cases are presented first in this section 2.4.1. Various currently used methods to quantify finite discrete time width and finite discrete band width will be presented in section 2.4.2. The first three measures of

uncertainty can be found in [25]. These measures are relevant to the design of the window to be used in spectral estimation of a signal. Most windows are designed so their values in the time domain are nonnegative or so the negative values are much smaller in absolute value than positive values. Window designs usually center their peak at the origin in both the time and frequency domains. Let

$$\mathbf{d} = [d(-M + 1) \ d(-M + 2), \dots, d(0), \dots, d(M - 2) \ d(M - 1)]^T$$

be some window such that $d(0) \geq |d(k)|$ for $0 < |k| \leq M - 1$. Define the equivalent time width as

$$N_e = \frac{\sum_{k=-M+1}^{M-1} d(k)}{d(0)}. \quad (2.34)$$

The equivalent band width is defined as

$$\beta_e = \frac{\frac{1}{2\pi} \int_{-\pi}^{\pi} D(\omega) d\omega}{D(0)}, \quad (2.35)$$

where $D(\omega) = DTFT \{d(n)\}$. Since

$$D(0) = \sum_{-M+1}^{M-1} d(k)$$

and

$$d(0) = \frac{1}{2\pi} \int_{-\pi}^{\pi} D(\omega) d\omega,$$

we have that

$$N_e \beta_e = 1. \quad (2.36)$$

Equation (2.36) gives us the relation $\beta_e = \frac{1}{N_e}$. This relation shows that $N_e \rightarrow \infty$ as $\beta_e \rightarrow 0$. Thus, the choice of window should be based at least in part on a tradeoff between spectral resolution and temporal variance [25].

The results in equation (2.36) can be generalized to any discrete time sequence. Let $x(n)$ be a discrete time sequence, either real- or complex-valued, and let $X(e^{j\omega}) = DTFT\{x(n)\}$, where $\omega \in [-\pi, \pi]$. Let n_0 be such that $|x(n_0)| \geq |x(n)| \forall n \in \mathbb{Z}$. Let $\omega_0 \in [-\pi, \pi]$ be defined such that $|X(e^{j\omega_0})| \geq |X(e^{j\omega})| \forall \omega \in [-\pi, \pi]$. The time width is defined as

$$\tilde{N}_e = \frac{\sum_{n=-\infty}^{\infty} |x(n)|}{|x(n_0)|}, \quad (2.37)$$

while the frequency band width is defined as

$$\tilde{\beta}_e = \frac{1}{2\pi} \frac{\int_{-\pi}^{\pi} |X(e^{j\omega})| d\omega}{|X(e^{j\omega_0})|}. \quad (2.38)$$

Since $x(n)$ and $X(e^{j\omega})$ are a Fourier transform pair, the following relations hold:

$$\begin{aligned} |X(e^{j\omega_0})| &= \left| \sum_{n=-\infty}^{\infty} x(n) e^{j\omega_0 n} \right| \leq \sum_{n=-\infty}^{\infty} |x(n)|, \\ |x(n_0)| &= \left| \frac{1}{2\pi} \int_{-\pi}^{\pi} X(e^{j\omega}) e^{j\omega n_0} d\omega \right| \leq \frac{1}{2\pi} \int_{-\pi}^{\pi} |X(e^{j\omega})| d\omega. \end{aligned}$$

This gives us the product of the time width and band width of any discrete sequence as

$$\tilde{N}_e \tilde{\beta}_e \geq 1. \quad (2.39)$$

Equation (2.39) shows that a sequence cannot simultaneously be arbitrarily narrow in both the time and frequency domains. Stoica and Moses in [25] state that the inequality does not imply that a signal that is wide in one domain will be narrow in the other domain. It is possible that widening in one domain leads to widening in the other domain.

Since we are restricting our attention to unit $\ell_{\mathbb{Z}}^2$ -norm sequences, Parseval's formula establishes that

$$\sum_{n=-\infty}^{\infty} |x(n)|^2 = \frac{1}{2\pi} \int_{-\pi}^{\pi} |X(e^{j\omega})|^2 d\omega = 1.$$

We can consider $|x(n)|^2$ to be a probability density function on \mathbb{Z} characterizing the distribution of signal energy in time and $\frac{1}{2\pi}|X(\omega)|^2$ to be a probability density function on $(-\pi, \pi]$ characterizing the distribution of signal energy in frequency. The mean and the variance of these two probability functions are given as

$$\mu = \sum_{n=-\infty}^{\infty} n |x(n)|^2, \quad (2.40)$$

$$\sigma^2 = \sum_{n=-\infty}^{\infty} (n - \mu)^2 |x(n)|^2, \quad (2.41)$$

$$\nu = \frac{1}{(2\pi)^2} \int_{-\pi}^{\pi} \omega |X(e^{j\omega})|^2 d\omega, \quad (2.42)$$

and

$$\rho^2 = \frac{1}{(2\pi)^3} \int_{-\pi}^{\pi} (\omega - \nu)^2 |X(e^{j\omega})|^2 d\omega. \quad (2.43)$$

In this way we can define σ and ρ to be the time duration and the band width, *resp.* For $\mu = 0$ and $\nu = 0$, the product of the time duration and band width is

$$\sigma\rho \geq \frac{1}{4\pi}. \quad (2.44)$$

If we let $X(e^{j\omega}) = |X(e^{j\omega})| e^{j\varphi(\omega)}$, then we obtain the bound

$$\sigma\rho \geq \frac{1}{4\pi} \sqrt{1 + 4\gamma^2}, \quad (2.45)$$

where $\gamma = \frac{1}{2\pi} \int_{-\pi}^{\pi} \omega \varphi'(\omega) |X(e^{j\omega})|^2 d\omega$. The bound in (2.45) is tighter than the one given in (2.44). Note that measures similar to (2.41) and (2.43) were given by Ishii and Furukawa in [26] and will be discussed later in this section.

Miloš Doroslovački in [27] defines a measure of uncertainty based on the second moment in time and the second moment in frequency. His measure applies only to discrete time signals that have finite energy. Without loss of

generality, I will describe his measure for unity $\ell_{\mathbb{Z}}^2$ -norm discrete time signals. This is simply defining the energy of the signal to be one. Doroslovački's measure pertains to how localized the signal is about a point (T, Ω) in the time-frequency plane. He defines the second moment in time of a discrete sequence $x(n)$ to be

$$m_2(T, \Omega) = \sum_{n=-\infty}^{\infty} \left(n - \frac{1}{2} - T \right)^2 \left| \frac{f(n) + e^{j\Omega} f(n-1)}{2} \right|^2 \quad (2.46)$$

$$= \frac{1}{2\pi} \int_{-\pi}^{\pi} \left| \left[\cos \left(\frac{\omega - \Omega}{2} \right) e^{j\omega T} F(e^{j\omega}) \right]' \right|^2 d\omega. \quad (2.47)$$

The second moment in frequency is defined as

$$M_2(\Omega) = \frac{1}{2\pi} \int_{-\pi}^{\pi} 4 \sin^2 \left(\frac{\omega - \Omega}{2} \right) |F(e^{j\omega})|^2 d\omega \quad (2.48)$$

$$= \sum_{n=-\infty}^{\infty} |f(n) - e^{j\Omega} f(n-1)|^2. \quad (2.49)$$

His Heisenberg-type uncertainty relation is

$$m_2(T, \Omega) M_2(\Omega) \geq \frac{1}{4}. \quad (2.50)$$

When $f(n)$ is equal to the Kronecker delta function and T is zero, then equation (2.50) achieves equality. Equality is also achieved in equation (2.50) when

$$f(n) = \left(\frac{C}{2^K} \right) \left(\frac{\Gamma(K+1)}{\Gamma\left(\frac{K}{2} + 1 - n\right) \Gamma\left(\frac{K}{2} + 1 + n\right)} \right), \quad (2.51)$$

where $C \in \mathbb{C}$, $\Gamma(\cdot)$ is the gamma function, and $K \geq -\frac{1}{2}$.

In [26], Ishii and Furukawa defined a measure of uncertainty on discrete infinite sequences and their *DTFTs*. These sequences are assumed to be samples from a bandlimited continuous signal. The discrete function is denoted as

$f(n) = f(nT)$. Let $T = \frac{\pi}{\sigma}$ for some $\sigma \in \mathbb{R}$ such that $F(\Omega)$, the continuous-time Fourier transform of the continuous-time (unsampled) signal is zero for $|\Omega| > \sigma$. They defined the pulse width⁶ about an arbitrary point $n_0 \in \mathbb{R}$ as

$$D_n^2 = \sum_{n=-\infty}^{\infty} (n - n_0)^2 |f(n)|^2. \quad (2.52)$$

They defined the band width, which they called (spectral) “*duration*,” by

$$D_\omega^2 = \int_{-\pi}^{\pi} (\omega - \omega_0)^2 |F(e^{j\omega})|^2 d\omega \quad (2.53)$$

for some arbitrary $\omega_0 \in \mathbb{R}$.

Theorem 1. For a unit ℓ_2 -norm sequence $f(n)$, if $F(e^{j\omega})$ is real and $n_0 = \omega_0 = 0$, then $D_n D_\omega > \sqrt{\frac{\pi}{2}}$.

Proof: see [26].

In [28], Calvez and Vilb  generalized Ishii and Furukawa’s results to encompass sequences $f(n)$ for which $F(e^{j\omega})$ might also be complex. I state this generalization in the following theorem.

Theorem 2. Let $f(t)$ be a continuous-time signal bandlimited to some $\sigma \in \mathbb{R}$, so that the *CFT* $F(\Omega) = 0 \forall |\Omega| \geq \sigma$. Let $f(n)$ be a sequence obtained by sampling $f(t)$ and normalizing such that $f(n)$ has unit ℓ_2 -norm. Let $F(e^{j\omega})$ be the *DTFT* of $f(n)$. Then, $\forall n_0, \omega_0 \in \mathbb{R}$, $D_n D_\omega > \sqrt{\frac{\pi}{2}}$.

Proof: see [28].

Note that the inequalities given in Theorem 1 and Theorem 2 are strict. They do not provide *tight* lower bounds on the joint uncertainty. This is in

⁶Specifically, they referred to this quantity as the “*time duration*.”

contrast to the continuous case treated by Gabor: the inequality appearing in the HWUP is not strict and therefore provides a tight, realizable lower bound. Gabor showed that his elementary functions were the only functions that could attain equality on the tight bound imposed by HWUP. Note that the Dirac delta $\delta(t)$ is specifically excluded from consideration as a minimizer of the HWUP because it is not continuous. Likewise, the constant function is excluded because it fails to satisfy the requirement $\lim_{t \rightarrow \pm\infty} h(t) = 0$. If either of these cases were admissible in the Heisenberg/Weyl/Gabor theory, they would result in indeterminate joint uncertainty that would jeopardize the inequality in the HWUP. This problem is exacerbated when one attempts to formulate analogues to the HWUP that can be applied to discrete sequences. Whereas the Dirac delta admits formal interpretation only as a distribution and not as a function. Therefore cannot be considered in quantities such as the pulse width (2.3) and band width (2.4). The Kronecker delta $\delta(n)$ is well defined as a function.

The constant sequence is specifically excluded from consideration in Theorem 1 and Theorem 2 since its ℓ_2 -norm diverges. Moreover, one must assume that the Kronecker delta is also inadmissible, since it would lead to the condition $D_n = 0$ under appropriate choice of n_0 in (2.52). This implies that the Kronecker delta cannot be obtained by sampling a bandlimited signal.⁷

⁷Verification of the implication is outside the scope of this dissertation. Informally, the argument may be stated as follows. Only bandlimited signals may be considered, since an infinite sampling frequency would be required otherwise. Thus, the spectrum of any admissible signal must admit zeros in $[-\pi, \pi]$ on a set of nontrivial Lebesgue measure. However, no signal can admit finite support in both domains. Therefore, all signals under consideration in the Ishii and Furukawa framework must be infinitely supported in time. Therefore, it is impossible to obtain a Kronecker delta from sampling them.

2.4.2 Uncertainty for Finite Discrete Time Sequences

Thus far I have only described measures which concern discrete-time signals defined on \mathbb{Z} and their *DTFT*'s. I now present measures applicable to a finite length sequence and its *DFT*. I will refer to such measures as *discrete-discrete* measures since the sequence domain and its Fourier transform domain are both discrete. For the remainder of this section, let $x[n]$ be a sequence of length N defined for $n \in [0, N - 1]$ and let $X[k]$ be its length- N *DFT* defined for $k \in [0, N - 1]$. A novel measure of uncertainty is presented by Donoho and Stark in [29]. I state their claim in the following theorem.

Theorem 3. *Let N_t be the cardinal number of the set $\{x[n] \mid x[n] \neq 0\}$ and N_ω be the cardinal number of the set $\{X[k] \mid X[k] \neq 0\}$. Then*

$$N_t N_\omega \geq N \tag{2.54}$$

and

$$N_t + N_\omega \geq 2\sqrt{N}. \tag{2.55}$$

Proof: *see [29]*

It is not surprising that the Kronecker delta function attains equality in equation (2.54). It is worth noting that, if N can be factored as a product of two natural numbers p and q , then the picket fence sequence attains equality in (2.54), where the picket fence sequence is defined by

$$III_q^p[n] = \begin{cases} 1, & n = iq \text{ for } i = 0, 1, \dots, p - 1 \\ 0, & \text{otherwise.} \end{cases} \tag{2.56}$$

This sequence has p nonzero samples, all equal to one and spaced q samples apart.

Monro, Bassil, and Dickson in [30] computed time dispersion, Δt , and bandwidth, $\Delta\omega$, of an FIR filter directly from its coefficients. Their measure of band width of a length- N FIR filter is

$$\Delta\omega^2 = \frac{\pi^2}{3} + 4 \sum_{n=0}^{N-2} \sum_{m=n+1}^{N-1} \frac{-1^{m-n}}{P(m-n)^2} h[m]h[n], \quad (2.57)$$

where

$$P = \sum_{n=0}^{N-1} h^2[n].$$

They defined the time dispersion as

$$\Delta t^2 = \sum_{n=0}^{N-1} (n - \tau)^2 h^2[n], \quad (2.58)$$

where

$$\tau = \frac{\sum_{n=0}^{N-1} nh[n]}{\sum_{n=0}^{N-1} h[n]}.$$

They were interested in creating a quadrature mirror filter bank using wavelets. Their proposed measure of uncertainty relates to the QMF filter bank. This measure is defined for the orthogonal filter bank according to

$$M(k) = \Delta\omega^2 + k^2 \Delta t^2, \quad (2.59)$$

where k specifies the relative importance of time verses frequency resolution. In the biorthogonal case as reported in [31] by Monro and Sherlock, the measure of uncertainty of the QMF filter bank is defined as

$$M(k_1, k_2, k_3) = \Delta\omega_a^2 + k_2 \Delta t_a^2 + k_3 \Delta\omega_s^2 + k_4 \Delta t_s^2, \quad (2.60)$$

where the subscripts a and s signify analysis filter and synthesis filter, *resp.*

DeBrunner, Özaydın, and Przebinda in [32] define the spread in time and frequency of a finite length discrete sequence in terms of the entropy of

the sequence in time and the entropy of its *DFT*. To define their measure of uncertainty, let $x[n]$ be a length N sequence whose $\ell_{[0, N-1]}^2$ -norm is one and let $X[k] = \text{DFT}\{x[n]\}$. Their measure of concentration of $x[n]$ in the time domain is defined as

$$H(\mathbf{x}) = - \sum_{n=0}^{N-1} |x[n]|^2 \ln (|x[n]|^2). \quad (2.61)$$

Their measure of concentration of $x[n]$ in the *DFT* domain is defined as

$$H(\mathbf{X}) = - \sum_{k=0}^{N-1} \frac{|X[k]|^2}{N} \ln \left(\frac{|X[k]|^2}{N} \right). \quad (2.62)$$

It is worth noting that the entropy of a sequence is unaffected by arbitrary permutations of the sequence values. So shifting or rotating the sequence does not change the entropy. A joint measure of uncertainty associated with (2.61) and (2.62) may be defined as the weighted sum of the entropy of $x[n]$ and the entropy of its *DFT* according to

$$H_p(\mathbf{x}) = pH(\mathbf{x}) + (1 - p)H(\mathbf{X}), \quad (2.63)$$

where $0 \leq p \leq 1$. In the case $p = \frac{1}{2}$, (2.63) is known as *Hirschmann uncertainty*, and one obtains the inequality

$$H_{\frac{1}{2}}(\mathbf{x}) = \frac{1}{2}H(\mathbf{x}) + \frac{1}{2}H(\mathbf{X}) \geq \frac{1}{2} \ln(N). \quad (2.64)$$

A sequence which attains equality in (2.64) is given by

$$x[n] = \frac{1}{\sqrt{K}} III_K^K[n], \quad (2.65)$$

where $III_K^K[n]$ was defined in (2.56) and $N = K^2$. The relation (2.64) is also minimized by the Kronecker delta and the constant sequence as well as sequences obtained by applying modulations to these two. It should be noted

that the minimizers of the *Hirschmann uncertainty* in equation (2.64) are also minimizers of Donoho's measure in equation (2.54).

Chapter 3

Problem Statement

Computation of the multi-dimensional multi-component AM-FM image model (2.7) by application of the demodulation algorithms (2.17) and (2.18) requires a filter bank where each channel is localized in the joint multi-dimensional time-frequency space. This localization is vital in the estimation of the instantaneous amplitude and frequency of individual AM-FM image components. Gabor's HWUP in one dimension is widely regarded as the best characterization of joint uncertainty for continuous one-dimensional signals. It has been shown that Gabor's elementary functions uniquely optimize the one-dimensional continuous HWUP. Daugman extended the HWUP to the continuous two-dimensional domain [7]. He showed that, as in the one-dimensional case, the two-dimensional continuous Gabor elementary functions uniquely achieve optimal conjoint localization with respect to the two-dimensional HWUP defined on the four dimensional time-frequency hyperplane.¹ This finding is harmonious with the fact that the receptive field profiles of certain simple cells in mammalian visual cortex have been shown to be well described by two-dimensional Gabor functions [7, 33–36].

¹This hyperplane spans two spatial dimensions and two spectral dimensions

In view of the fact that continuous domain Gabor functions have been shown to possess optimal joint localization in both the one- and two-dimensional cases, it is tempting to assume that sampled Gabor filters are also optimal in the discrete domain. Such an assumption would seem to be validated by the idea that the discrete case should converge to the continuous case in the limit as the sampling interval becomes vanishingly small. However, when considering functions such as Gabor functions that are *not* bandlimited, there is no clear notion of what it means to “sample fast enough” to achieve practical agreement between the discrete and continuous optimization problems. Moreover, the meaning of *optimal localization* is clearly dependent on the particular definition of uncertainty that one employs.

DeBrunner, Özaydın, and Przebinda showed that sampled Gabor functions are not optimal when the measure of uncertainty is defined in terms of temporal and spectral entropy as in equation (2.64) [32]. In view of the difficulties inherent in formulating discrete uncertainty relations similar to the HWUP, this casts a shadow of doubt on the idea that sampled Gabor functions are indeed optimal. The formulation of relevant discrete uncertainty measures and the design of discrete filters possessing optimal joint localization is critically important in view of the fact that many if not most modern signal and image processing applications are concerned with discrete rather than continuous signals.

In this dissertation the progression to a finite discrete time/space and finite discrete frequency domain is made. The characterization and conceptualization of uncertainty is vital for time-frequency analysis. A goal of this dissertation is to define a new measure of uncertainty which is analogous to

the one used in HWUP but also is applicable in finite discrete time and finite discrete frequency. The new measure is analogous to HWUP in the sense that it offers intuitively pleasing variance interpretation and is invariant to translations and modulations. Admissibility condition similar to HWUP must be defined to exclude the constant sequence, the Kronecker delta, the alternating sequence, *etc.* The development of the new uncertainty measure is to be used to design filters, which exhibits optimal conjoint localization.

The main concerns of this dissertation are with decomposing an image and faithfully reconstructing the image based on this analysis. This type of analysis and synthesis is relevant in many image processing applications, including Havlicek's AM-FM modeling [9], compression, image segmentation [6], computer vision, *etc.* It will be necessary to extend the notions of localization to multi-channel filter banks. The new filter bank uncertainty measure will be used as a design criteria for a perfect reconstruction parallel filter bank.

As prescribed by the Mallat algorithm, the one-dimensional perfect reconstruction QMF can be cascaded in a pyramid structure to form a multi-channel, one-dimensional, perfect reconstruction filter bank. This cascaded perfect reconstruction filter bank can be implemented using its equivalent parallel structure filter bank. This optimal L -channel perfect reconstruction parallel filter bank (PRPFB) will be determined from a set of well know QMFs and will minimizes the new filter bank uncertainty. A two-dimensional filter bank is created by extending the one dimension parallel filter bank to the two-dimensional case in a separable manner. These separable channels are then decomposed in a novel way to obtain a complete set of nonseparable, orientation selective channels that provide excellent conjoint resolution while still

preserving the perfect reconstruction property.

The AM-FM image demodulation algorithm will produce errors in the image reconstruction. The optimally well localized, multi-channel, orientation selective filter bank results in the best reconstruction based on a quantitative measure.

Chapter 4

Novel Measure of Uncertainty

One highly desirable feature of the HWUP is that the pulse width (2.3), band width (2.4), and uncertainty measure (2.2) admit intuitively appealing interpretations in terms of the statistical variance of signal energy in time and in frequency. Thus, derivation of the uncertainty measure proposed in this section is motivated by statistical considerations and a desire to develop a discrete uncertainty measure that admits interpretation in terms of temporal and spectral variances. Moreover, this dissertation creates a filter for which the uncertainty based on probability distributions in discrete time and discrete frequency is minimized.

4.1 Quantifying Uncertainty and Localization

For the remainder of this chapter, consideration is restricted to finite length discrete sequences with unit $\ell_{[0,N-1]}^2$ -norm. This restriction is not limiting since any finite length discrete non-zero sequence which is not unit $\ell_{[0,N-1]}^2$ -norm can be made into a unit $\ell_{[0,N-1]}^2$ -norm sequence by a simple scaling. So if a finite length non-zero sequence is not unit $\ell_{[0,N-1]}^2$ -norm, then the uncertainty of that sequence is taken to be the uncertainty of the normalized sequence. Let

$h : [0, N - 1] \rightarrow \mathbb{C}$ be a finite length sequence such that

$$\sum_{n=0}^{N-1} |h[n]|^2 = 1 = \frac{1}{N} \sum_{k=0}^{N-1} |H[k]|^2, \quad (4.1)$$

where

$$H[k] = \sum_{n=0}^{N-1} h[n] e^{-j\frac{2\pi}{N}nk}, \quad 0 \leq k \leq N - 1, \quad (4.2)$$

is the N -point *DFT* of $h[n]$. We can consider $|h[n]|^2$ to be a probability density function in discrete time and $\frac{1}{N}|H[k]|^2$ to be a probability density function in discrete frequency. These densities describe, respectively, how the energy of the signal is distributed in time and in frequency. Consider n to be a random variable in $[0, N - 1]$ and k to be a random variable in $[0, N - 1]$ [37]. The *spread* or variance of \mathbf{h} in time is defined by the second central moment

$$\sigma_{n,\mathbf{h}}^2 = \sum_{n=0}^{N-1} (n - \mu)^2 |h[n]|^2, \quad (4.3)$$

where μ is the expected value of n , also known as the mean or first moment, defined by

$$\mu = \sum_{n=0}^{N-1} n |h[n]|^2. \quad (4.4)$$

The band width of $h[n]$ will be computed from $H[k]$ according to

$$\sigma_{\omega,\mathbf{h}}^2 = \frac{1}{N} \sum_{k=0}^{N-1} (k - \nu)^2 |H[k]|^2, \quad (4.5)$$

where the mean in discrete frequency is

$$\nu = \frac{1}{N} \sum_{k=0}^{N-1} k |H[k]|^2. \quad (4.6)$$

The quantities $\sigma_{n,\mathbf{h}}^2$ and $\sigma_{\omega,\mathbf{h}}^2$ are referred to as the variance in time and the variance in frequency, *resp.* It is tempting to simply use the product of these variances as an uncertainty measure to quantify the joint localization of a length- N sequence in discrete time and discrete frequency, i.e.,

$$\gamma_{N,\mathbf{h}}^2 = \sigma_{n,\mathbf{h}}^2 \sigma_{\omega,\mathbf{h}}^2. \quad (4.7)$$

Unfortunately, the quantity in equation (4.7) is neither translation nor modulation invariant.

4.2 Equivalence Classes of Sequences

Uncertainty measures such as $\sigma_{n,\mathbf{h}}^2$ and $\sigma_{\omega,\mathbf{h}}^2$ quantify the concentration, localization, or spread of a signal in time and in frequency. Time or frequency shift invariance are clearly desirable property for any such uncertainty measure to possess: intuitively, shifting a signal in time should not have an effect on how concentrated or localized the signal is in time. Likewise, shifting the spectrum should not have an effect on how concentrated or localized the signal is in frequency. It is worth noting that the HWUP pulse width (2.3), bandwidth (2.4), and uncertainty (2.2) are affected by neither shifts in time nor shifts in frequency.

However, the uncertainty measure $\gamma_{N,\mathbf{h}}^2$ defined in (4.7) is not shift invariant. In precise terms, this means that the statement $f[n] = g[(n - m_t)_N]$ for some $m_t \in \mathbb{Z}$ does not necessarily imply that $\gamma_{N,\mathbf{g}}^2 = \gamma_{N,\mathbf{f}}^2$. Likewise, the statement $F[k] = G[(k - m_f)_N]$ for some $m_f \in \mathbb{Z}$ also does not necessarily imply that $\gamma_{N,\mathbf{g}}^2 = \gamma_{N,\mathbf{f}}^2$. Here, it is understood that shifting for a finite length sequence is defined to be circular shifting (also known as rotation): the values

to be shifted in are taken from the periodic extension of the signal.

Example 1. Let $N = 4$, $\mathbf{f} = \left[\frac{1}{\sqrt{2}} \ \frac{1}{\sqrt{2}} \ 0 \ 0 \right]^T$, and $m = -1$. Then $\mathbf{g} = \left[\frac{1}{\sqrt{2}} \ 0 \ 0 \ \frac{1}{\sqrt{2}} \right]^T = f[(n+1)_N]$. We have that $\gamma_{4,\mathbf{f}}^2 = \frac{1}{8}$ and $\gamma_{4,\mathbf{g}}^2 = \frac{9}{8}$. This is distasteful, since \mathbf{g} is obtained by rotating \mathbf{f} left by one sample or equivalently by rotating \mathbf{f} right by $(m)_N = 3$ samples: $g[n] = f[(n-3)_N]$. Thus, it is desirable for an uncertainty measure to assign the same uncertainty to both \mathbf{f} and \mathbf{g} .

To make the uncertainty measure (4.7) invariant under translations and modulations, the uncertainty measure of a sequence is defined by considering the sequence as an element of an equivalence classes. Let $\mathbb{S} = \{\mathbf{h} \mid \mathbf{h} \text{ is a length } N \text{ sequence}\}$.

Definition 4. Let $\mathbf{f}, \mathbf{g} \in \mathbb{S}$. Define a relation between these two sequences as $\mathbf{f} \sim \mathbf{g}$ if $\exists p, q, r \in \mathbb{Z}$ such that

$$g[n] = e^{j\frac{2\pi}{N}(qn+r)} f[(n-p)_N]. \quad (4.8)$$

Theorem 4. The relation \sim in Definition 4 is an equivalence relation on \mathbb{S} .

Proof: Let $\mathbf{f} \in \mathbb{S}$. Since $f[n] = e^{j\frac{2\pi}{N}(0n+0)} f[(n-0)_N]$, we have that $\mathbf{f} \sim \mathbf{f}$, which establishes that \sim is reflexive.

If $\mathbf{f} \sim \mathbf{g}$, then, by definition, $g[n] = e^{-j\frac{2\pi}{N}(pn+r)} f[(n-q)_N]$ for some $p, q, r \in \mathbb{Z}$. It follows immediately that $f[n] = e^{j\frac{2\pi}{N}(-pn-pq-r)} g[(m+q)_N]$, where $-p, (-pq-r), -q \in \mathbb{Z}$. This establishes that $\mathbf{g} \sim \mathbf{f}$ and that the relation \sim is therefore symmetric.

To show transitivity, let $\mathbf{f} \sim \mathbf{g}$ and $\mathbf{g} \sim \mathbf{h}$, where $g[n] = e^{j\frac{2\pi}{N}(pn+l)} f[(n-q)_N]$ and $h[n] = e^{j\frac{2\pi}{N}(rn+s)} g[(n-t)_N]$ for some $p, q, l, r, s, t \in \mathbb{Z}$. We have that

$$\begin{aligned} h[n] &= e^{j\frac{2\pi}{N}(rn+s)} e^{j\frac{2\pi}{N}[p(n-t)+l]} f[(n-t-q)_N] \\ &= e^{j\frac{2\pi}{N}[(r+p)+s-pt+l]} f[(n-t-q)_N]. \end{aligned}$$

Since $r+p, s-pt+l, t+q \in \mathbb{Z}$, it follows that $\mathbf{f} \sim \mathbf{h}$ and the relation \sim is transitive. Since it is reflexive, symmetric, and transitive, the relation \sim is therefore an equivalence relation on \mathbb{S} . Q.E.D.

Definition 5. For a sequence $\mathbf{f} \in \mathbb{S}$, the equivalence class $[\mathbf{f}]$ is defined by

$$[\mathbf{f}] = \{\mathbf{g} \in \mathbb{S} \mid \mathbf{g} \sim \mathbf{f}\}. \quad (4.9)$$

Theorem 5. Let \mathbf{f} and \mathbf{g} be two length N sequences. Then $\mathbf{f} \sim \mathbf{g}$ if and only if $\mathbf{F} \sim \mathbf{G}$.

Proof: (\implies)

Let $\mathbf{f} \sim \mathbf{g}$. Then $\exists p, q, r \in \mathbb{Z}$ such that $g[n] = e^{j\frac{2\pi}{N}(pn+r)} f[(n-q)_N]$. The *DFT* of $g[n]$ is given by

$$\begin{aligned} G[k] &= \sum_{n=0}^{N-1} g[n] e^{-j\frac{2\pi}{N}nk} \\ &= \sum_{n=0}^{N-1} e^{j\frac{2\pi}{N}(pn+r)} f[(n-q)_N] e^{-j\frac{2\pi}{N}nk}. \end{aligned}$$

Let $m = (n-q)_N$. The *DFT* $G[k]$ may then be expressed as

$$\begin{aligned} G[k] &= e^{j\frac{2\pi}{N}r} \sum_{m=0}^{N-1} f[m] e^{-j\frac{2\pi}{N}(m+q)(k-p)} \\ &= e^{j\frac{2\pi}{N}r} e^{-j\frac{2\pi}{N}q(k-p)} \sum_{m=0}^{N-1} f[m] e^{-j\frac{2\pi}{N}(m)(k-p)} \\ &= e^{j\frac{2\pi}{N}(-qk+qp+r)} \sum_{m=0}^{N-1} f[m] e^{-j\frac{2\pi}{N}(m)(k-p)} \end{aligned}$$

$$= e^{j\frac{2\pi}{N}(-qk+qp+r)} F[(k-p)_N].$$

Since $-q, qp+r, p \in \mathbb{Z}$, this establishes that $\mathbf{F} \sim \mathbf{G}$. A symmetric argument shows (\Leftarrow). Q.E.D.

Theorem 5 establishes that, as an operator, the *DFT* respects equivalence classes under the equivalence relation given in definition 4: every member of $[\mathbf{f}]$ has a *DFT* that is a member of $[\mathbf{F}]$ and every member of $[\mathbf{F}]$ has an *IDFT* that is a member of $[\mathbf{f}]$.

For a given $\mathbf{f} \in \mathbb{S}$, intuition suggests that the spread or variance in time $\sigma_{n,\mathbf{f}}^2$ should not be affected by shifts in time, e.g., that $\sigma_{n,\mathbf{g}}^2$ should be the same $\forall \mathbf{g} \in [\mathbf{f}]$. Note that this intuitive notion is consistent with the fact that the pulse width (2.3) is invariant to time shifts. Therefore, I quantify the time localization of \mathbf{f} by the minimum time variance achieved by any $\mathbf{g} \in [\mathbf{f}]$.

Likewise, I quantify the frequency localization of \mathbf{F} by the minimum frequency variance achieved by any $\mathbf{H} \in [\mathbf{F}]$. According to Theorem 5, this is precisely equivalent to quantifying the frequency localization of \mathbf{f} by the minimum frequency variance achieved by any $\mathbf{h} \in [\mathbf{f}]$. Therefore, the joint localization of \mathbf{f} in time and frequency will be quantified by the measure $\gamma_{N,\mathbf{f}}^2$ defined on $[\mathbf{f}]$ according to

$$\gamma_{N,\mathbf{f}}^2 = \sigma_{n,[\mathbf{f}]}^2 \sigma_{\omega,[\mathbf{f}]}^2 \tag{4.10}$$

where

$$\sigma_{n,[\mathbf{f}]}^2 = \min_{\mathbf{g} \in [\mathbf{f}]} \{ \sigma_{n,\mathbf{g}}^2 \} \tag{4.11}$$

and

$$\sigma_{\omega,[\mathbf{f}]}^2 = \min_{\mathbf{h} \in [\mathbf{f}]} \{ \sigma_{\omega,\mathbf{h}}^2 \}. \tag{4.12}$$

Theorem 6. Let $\mathbf{f} \in \mathbb{S}$. Let $\mathbf{g} \in [\mathbf{f}]$ be such that $g[n] = f[(n - p)_N]$ for some $p \in \mathbb{Z}$. Then

- a) $|F[k]| = |G[k]| \forall k \in [0, N - 1]$.
- b) $\|F[k]\| = \|G[k]\| \forall k \in [0, N - 1]$.
- c) $\sigma_{\omega, \mathbf{f}}^2 = \sigma_{\omega, \mathbf{g}}^2$.

Comment: Part (a) of the theorem follows immediately from the “time shift property” of the *DFT*, which is commonly available in digital signal processing (DSP) textbooks. I provide the proof below only so as to avoid any confusion that might arise from my definition of equivalence classes of sequences.

Proof: Parts (b) and (c) follow immediately from the definition of the $\ell_{[0, N-1]}^2$ norm in Section 1.3, the definition of $\sigma_{\omega, \mathbf{f}}^2$ in (4.5), and part (a).

Part (a): By hypothesis, $\exists m \in \mathbb{Z}$ such that $f[n] = g[(n - m)_N]$. Define $f_p[n] = f[(n - p)_N]$. Then there is a $p \in [0, N - 1]$ such that $g[n] = f_p[n]$. Thus, it is sufficient to show that $|F[k]| = |F_p[k]| \forall 0 \leq p, k \leq N - 1$.

Consider the case $p = 1$ first. We have that

$$\begin{aligned}
 |F(k)| &= \left| \sum_{n=0}^{N-1} f[n] e^{-j \frac{2\pi}{N} nk} \right| \\
 &= \left| \sum_{n=0}^{N-1} f_1[(N - 1 + n)_N] e^{-j \frac{2\pi}{N} nk} \right| \\
 &= \left| f_1[N - 1] + \sum_{n=1}^{N-1} f_1[n - 1] e^{-j \frac{2\pi}{N} nk} \right|, \quad (4.13)
 \end{aligned}$$

where the last line is obtained by pulling the $n = 0$ term out of the sum; modular arithmetic is then no longer required in the indices of the remaining

terms of the sum. We now multiply the term $f_1[N - 1]$ in (4.13) by unity to obtain

$$|F(k)| = \left| f_1[N - 1]e^{-j\frac{2\pi}{N}(N-1)k}e^{-j\frac{2\pi}{N}k} + \sum_{n=1}^{N-1} f_1[n - 1]e^{-j\frac{2\pi}{N}nk} \right|$$

Making the change of variable $q = n - 1$, we have that

$$\begin{aligned} |F(k)| &= \left| f_1[N - 1]e^{-j\frac{2\pi}{N}(N-1)k}e^{-j\frac{2\pi}{N}k} + \sum_{q=0}^{N-2} f_1[q]e^{-j\frac{2\pi}{N}(q+1)k} \right| \\ &= \left| f_1[N - 1]e^{-j\frac{2\pi}{N}(N-1)k}e^{-j\frac{2\pi}{N}k} + \sum_{q=0}^{N-2} f_1[q]e^{-j\frac{2\pi}{N}qk}e^{-j\frac{2\pi}{N}k} \right| \\ &= \left| f_1[N - 1]e^{-j\frac{2\pi}{N}(N-1)k} + \sum_{q=0}^{N-2} f_1[q]e^{-j\frac{2\pi}{N}qk} \right| \\ &= \left| \sum_{q=0}^{N-1} f_1[q]e^{-j\frac{2\pi}{N}qk} \right|. \end{aligned} \quad (4.14)$$

Since (4.14) is precisely the definition of $|F_1[k]|$, this establishes that $|F(k)| = |F_1[k]| \forall k \in [0, N - 1]$. The result (a) is obtained by realizing that analogous arguments may be used to show that $|F_{p-1}[k]| = |F_p[k]| \forall p \in [1, N - 1]$, $0 \leq k \leq N - 1$. Q.E.D.

Theorem 7. Let $\mathbf{F} \in \mathbb{S}$. Let $\mathbf{G} \in [\mathbf{F}]$ be such that $G[k] = F[(k - m)_N]$ for some $m \in \mathbb{Z}$. Then

- a) $|f[n]| = |g[n]| \forall n \in [0, N - 1]$.
- b) $\|f[n]\| = \|g[n]\| \forall n \in [0, N - 1]$.
- c) $\sigma_{n,\mathbf{f}}^2 = \sigma_{n,\mathbf{g}}^2$.

Proof: The proof is symmetric to the proof of Theorem (6). Q.E.D.

Theorem 8. Let $\mathbf{f} \in \mathbb{S}$. Then \exists a single member $\mathbf{y} \in [\mathbf{f}]$ that simultaneously minimizes (4.3) and (4.5) over $[\mathbf{f}]$. In other words, $\sigma_{n,\mathbf{y}}^2 = \min_{\mathbf{h} \in [\mathbf{f}]} \{\sigma_{n,\mathbf{h}}^2\}$ and $\sigma_{\omega,\mathbf{y}}^2 = \min_{\mathbf{h} \in [\mathbf{f}]} \{\sigma_{\omega,\mathbf{h}}^2\}$.

Proof: Let $\mathbf{g} \in [\mathbf{f}]$ be such that $\sigma_{n,\mathbf{y}}^2 = \min_{\mathbf{h} \in [\mathbf{f}]} \{\sigma_{n,\mathbf{h}}^2\}$. By Theorem 5, we have that $\mathbf{G} \in [\mathbf{F}]$. Then either $\sigma_{\omega,\mathbf{g}}^2 = \min_{\mathbf{h} \in [\mathbf{f}]} \{\sigma_{\omega,\mathbf{h}}^2\}$ or $\sigma_{\omega,\mathbf{g}}^2 \neq \min_{\mathbf{h} \in [\mathbf{f}]} \{\sigma_{\omega,\mathbf{h}}^2\}$. If $\sigma_{\omega,\mathbf{g}}^2 = \min_{\mathbf{h} \in [\mathbf{f}]} \{\sigma_{\omega,\mathbf{h}}^2\}$, then $\mathbf{y} = \mathbf{g}$ and the proof is complete.

Otherwise, we have that $\sigma_{\omega,\mathbf{g}}^2 \neq \min_{\mathbf{h} \in [\mathbf{f}]} \{\sigma_{\omega,\mathbf{h}}^2\}$ and there is another element $\mathbf{X} \in [\mathbf{F}]$ such that $\sigma_{\omega,\mathbf{x}}^2 = \min_{\mathbf{h} \in [\mathbf{f}]} \{\sigma_{\omega,\mathbf{h}}^2\}$. Since $\mathbf{X} \in [\mathbf{F}]$ and $\mathbf{G} \in [\mathbf{F}]$, we have that $\mathbf{X} \sim \mathbf{G}$. Then $\exists p, q, r \in \mathbb{Z}$ such that

$$X[k] = e^{j\frac{2\pi}{N}qk} e^{j\frac{2\pi}{N}r} G[(k-p)_N].$$

Let $Y[k] = G[(k-p)_N]$. Then $\mathbf{Y} \sim \mathbf{G}$, so $\mathbf{Y} \in [\mathbf{F}]$ and we have by Theorem 5 that $\mathbf{y} \in [\mathbf{f}]$. Moreover, $|Y[k]| = |X[k]| \forall k \in [0, N-1]$, so $\sigma_{\omega,\mathbf{y}}^2 = \sigma_{\omega,\mathbf{x}}^2 = \min_{\mathbf{h} \in [\mathbf{f}]} \{\sigma_{\omega,\mathbf{h}}^2\}$. But, by Theorem 7 we have that $\sigma_{n,\mathbf{y}}^2 = \sigma_{n,\mathbf{g}}^2 = \min_{\mathbf{h} \in [\mathbf{f}]} \{\sigma_{n,\mathbf{h}}^2\}$ and the theorem is proved. Q.E.D.

In view of Theorem 8, (4.10) can be simplified to

$$\gamma_{N,\mathbf{f}}^2 = \min_{\mathbf{g} \in [\mathbf{f}]} \{\sigma_{n,\mathbf{g}}^2 \sigma_{\omega,\mathbf{g}}^2\}. \quad (4.15)$$

For any $\mathbf{f} \in \mathbb{S}$, the measure $\gamma_{N,\mathbf{f}}^2$ in (4.10) or equivalently in (4.15) is used to quantify the joint localization of all sequences $\mathbf{g} \in [\mathbf{f}]$.

Chapter 5

Application to Scaling Functions

In the wavelet literature, the low pass analysis filter denoted $f_a[n]$ in section 2.3 is often referred to as the *scaling function*, while the high pass analysis filter $g_a[n]$ is called the *wavelet*. In Chapter 3, I stated that a major goal of this dissertation is to construct finite length sequences that have optimal joint uncertainty and are also admissible as wavelet scaling functions so that they can be used to construct a perfect reconstruction quadrature mirror filter banks (QMFs). The restriction to wavelet scaling functions is not unlike HWUP's restriction to continuous functions. It is well known that wavelet scaling functions correspond to continuous functions for which the set of all dilations and shifts constitutes a basis for $L^2(\mathbb{R})$ [21]. The association is that the terms of wavelet scaling functions are the coefficients of the dilation equation. In addition, infinite convolution of a "*regular*" scaling function with itself converges to a continuous function $f(t)$ in which the set of all dilations and integer shifts of $f(t)$ constitute a basis for $L^2(\mathbb{R})$ [16]. The other HWUP restriction that the function approaches zero at negative and positive infinity, is satisfied by compactly supported functions. Thus the two HWUP restrictions are emulated in the discrete domain by applying the uncertainty measure defined in equation (4.10) or equivalently in equation (4.15) to the set of FIR filters, which

are admissible as a low pass analysis filter for a wavelet filter bank.

Orthogonal and biorthogonal wavelet filter banks are perfect construction QMFs, perfect reconstruction QMF's are not necessarily orthogonal nor biorthogonal wavelet filter banks [16]. Since necessary conditions for the two channel orthogonal and biorthogonal wavelet filter banks are readily available in the current literature [13, 16, 20–22, 24, 38], the new uncertainty measure $\gamma_{N, [\mathbf{f}_a]}^2$ defined in (4.15) will be restricted to orthogonal and even length biorthogonal wavelet scaling functions.

Let $\mathcal{A}_N = \{f[n] \mid f[n] \text{ is a real-valued, length } N \text{ where } N \text{ is even, and admissible orthogonal QMF FIR low pass analysis filter with unit } \ell_{[0, N-1]}^2 \text{-norm}\}$. Formulating tight bounds and optimizing the joint uncertainty over the set \mathcal{A}_N is challenging. In this section, the uncertainties of some well known real-valued scaling functions used in orthogonal QMFs are presented. The scaling functions I present are various length zero padded Haar function, the least asymmetric wavelet scaling functions known as the symlet, and the well known Daubechies' wavelet scaling functions. The zero padded Haar function, the symlet, and the Daubechies scaling function possess linear phase, nearly linear phase, and non-linear phase *resp.* These three cases show that linear phase tends to produces the best conjoint localization.

The length two Haar filter is defined as $\mathbf{haar}_2 = \left[\frac{1}{\sqrt{2}} \quad \frac{1}{\sqrt{2}} \right]^T$. The following theorem shows that \mathbf{haar}_2 is the only element of \mathcal{A}_2 .

Theorem 9. For $N = 2$, the only unit $\ell_{[0, N-1]}^2$ -norm length-two sequences satisfying the conditions $\sum_{n=0}^1 h[n] = H[0] = \sqrt{2}$ is the Haar filter.

Proof: For $N = 2$, let $h[0] = a$ and $h[1] = b$. Since the $\ell^2_{[0,1]}$ -norm is one, this means $a^2 + b^2 = 1$. Since $|H[0]| = \sqrt{2}$, thus $a + b = \sqrt{2}$. It follows that

$$\begin{aligned} a &= \sqrt{2} - b, \\ (\sqrt{2} - b)^2 + b^2 &= 1, \\ 2 - 2\sqrt{2}b + 2b^2 &= 1, \\ \frac{1}{2} - \sqrt{2}b + b^2 &= 0. \end{aligned}$$

Applying the quadratic formula to the above, yields

$$\begin{aligned} b &= \frac{\sqrt{2} \pm \sqrt{2 - 4\left(\frac{1}{2}\right)}}{2} = \frac{\sqrt{2}}{2} = \frac{1}{\sqrt{2}}, \\ a + \frac{1}{\sqrt{2}} &= \sqrt{2}, \\ a &= \frac{1}{\sqrt{2}}. \end{aligned}$$

So for $N = 2$ the only element of \mathcal{A}_2 is the Haar filter.

Q.E.D.

The notation \mathbf{haar}_N will be used to denote the haar filter zero padded to length- N . The time variance of the zero padded Haar filter is $\sigma_{n, [\mathbf{haar}_N]}^2 = \frac{1}{4}$.

Theorem 10. The zero padded haar filter \mathbf{haar}_N attains the minimum time variance over elements in \mathcal{A}_N , *i.e.*

$$\frac{1}{4} = \sigma_{n, [\mathbf{haar}_N]}^2 \leq \sigma_{n, [f]}^2$$

for all $f[n] \in \mathcal{A}_N$.

Proof: The proof is by induction on N . From theorem 9 for $N = 2$, since \mathbf{haar}_2 is the only element in \mathcal{A}_2 ,

$$\sigma_{n, [\mathbf{haar}_2]}^2 \leq \sigma_{n, [f]}^2$$

for $f[n] \in \mathcal{A}_2$. To proceed with the induction, let

$$\sigma_{n, [\text{haar}_N]}^2 \leq \sigma_{n, [f]}^2$$

for all $f[n] \in \mathcal{A}_N$. Choose $g[n] \in [\mathbf{h}]$ so that $h[n] \in \mathcal{A}_{N+2}$ and the following equality holds

$$\begin{aligned} \sigma_{n, [\mathbf{h}]}^2 &= \sigma_{n, \mathbf{g}}^2 \\ &= \sum_{n=0}^{N+1} (n - \mu)^2 |g[n]|^2 \\ &\geq \sum_{n=0}^{N-1} (n - \mu)^2 |g[n]|^2. \end{aligned} \tag{5.1}$$

The inequality in equation (5.1) attains equality only in the following cases:

1. $g[N] = g[N + 1] = 0$,¹ or
2. $g[N] = 0$ and $N + 1 = \mu$, or
3. $N = \mu$ and $g[N + 1] = 0$.

Consider case 2,

$$\begin{aligned} \mu = N + 1 &= \sum_{n=0}^{N+1} n |g[n]|^2 \\ &= (N + 1) |g[N + 1]|^2 + \sum_{n=0}^{N-1} n |g[n]|^2 \\ \implies (N + 1)(1 - |g[N + 1]|^2) &= \sum_{n=0}^{N-1} n |g[n]|^2 \\ \implies (N + 1) \sum_{n=0}^{N-1} |g[n]|^2 &= \sum_{n=0}^{N-1} n |g[n]|^2 \end{aligned}$$

¹It could happen that \mathbf{g} was chosen so that $g[0] = g[1] = 0$. If so then a simple circular rotation yields this case.

From the last equation, $g[n] = 0$ for all $n \in [0, N]$ and $g[N + 1] = 1$. Since $g[n] \in [\mathbf{h}]$, hence $h[n] \notin \mathcal{A}_{N+2}$ which is a contradiction.

In case 3,

$$\begin{aligned} \mu = N &= \sum_{n=0}^{N+1} n|g[n]|^2 \\ &= N|g[N]|^2 + \sum_{n=0}^{N-1} n|g[n]|^2 \\ \implies N(1 - |g[N]|^2) &= \sum_{n=0}^{N-1} n|g[n]|^2 \\ \implies N \sum_{n=0}^{N-1} |g[n]|^2 &= \sum_{n=0}^{N-1} n|g[n]|^2 \end{aligned}$$

From the last equation, again $g[n] = 0$ for all $n \in [0, N - 1]$ and $g[N] = 1$. Since $g[n] \in [\mathbf{h}]$, thus $h[n] \notin \mathcal{A}_{N+2}$ which is a contradiction. Thus equality is attain in equation (5.1) if and only if case 1 is satisfied. If case 1 is satisfied, then from the induction hypothesis

$$\sigma_{n, [\mathbf{h}]}^2 = \sum_{n=0}^{N-1} (n - \mu)^2 |g[n]|^2 \geq \sigma_{n, [\mathbf{haar}_N]}^2 = \sigma_{n, [\mathbf{haar}_{N+2}]}^2 = \frac{1}{4}.$$

Therefore the zeros padded Haar scaling function minimizes the time variance for all elements in \mathcal{A}_{N+2} . Q.E.D.

Let \mathbf{HAAR}_N denote the *DFT* of \mathbf{haar}_N . \mathbf{HAAR}_N is easily computed as

$$\begin{aligned} \mathbf{HAAR}_N[k] &= \sum_{n=0}^{N-1} h[n] e^{-\frac{j2\pi}{N}nk}, \quad k = 0, 1, \dots, N-1 \\ &= \frac{1}{\sqrt{2}} + \frac{1}{\sqrt{2}} e^{-\frac{j2\pi}{N}k} \\ &= \sqrt{2} \cos\left(\frac{\pi k}{N}\right) e^{-\frac{j\pi}{N}k}, \end{aligned}$$

with spectral magnitude

$$|HAAR_N[k]| = \sqrt{2} \cos\left(\frac{\pi k}{N}\right). \quad (5.2)$$

The phase response of \mathbf{haar}_N is

$$\varphi[k] = \begin{cases} -\frac{\pi}{N}k & \text{for } k = 0, 1, 2, \dots, \frac{N}{2} \\ \frac{\pi}{N}(N - k) & \text{for } k = \frac{N}{2} + 1, \dots, N - 1. \end{cases} \quad (5.3)$$

The frequency variance, $\sigma_{\omega, [\mathbf{haar}_N]}^2$ can be computed as

$$\sigma_{\omega, [\mathbf{haar}_N]}^2 = \frac{4}{N} \sum_{k=0}^{\frac{N}{2}} k^2 \cos^2\left(\frac{\pi k}{N}\right). \quad (5.4)$$

and is given in second left most column of Table 5.1. Therefore, the uncertainty of the zero padded Haar filter is given by

$$\gamma_{N, \mathbf{haar}_N}^2 = \frac{1}{N} \sum_{k=0}^{\frac{N}{2}} k^2 \cos^2\left(\frac{\pi k}{N}\right). \quad (5.5)$$

The uncertainties $\gamma_{N, \mathbf{haar}_N}^2$ for $N = 2, 4, \dots, 20$ are listed in Table 5.3.

The length- N zero padded Haar filter is the only orthogonal symmetric linear phase scaling function. The symlet scaling functions of I. Daubechies are characterized as the least asymmetric orthogonal nearly linear phase filters. The uncertainties of the symlet scaling functions for lengths two through twenty are given in the second right most column of Table 5.3.

The symlet and Daubechies' orthogonal scaling functions as described in [21] have nearly an ideal magnitude response. The length- N Daubechies orthogonal scaling function will be denoted as \mathbf{db}_N .

To make clear the comparison of the frequency variances of the symlet and \mathbf{db}_N with frequency variance of the ideal half-band filter, a brief description of the magnitude response of the ideal half-band filter is given.

The magnitude response for a ideal half-band filter with length- N not divisible by 4 is

$$|D_N[k]| = \begin{cases} \sqrt{2} & \text{for } k = 0, 1, \dots, \frac{N-2}{4} \\ 0 & \text{for } k = \frac{N+2}{4}, \dots, \frac{N}{2} \\ |D_N[N-k]| & \text{for } k = \frac{N}{2} + 1, \frac{N}{2} + 2, \dots, N-1. \end{cases} \quad (5.6)$$

For a half-band ideal filter with length- N that is divisible by 4, the magnitude response is

$$|D_N[k]| = \begin{cases} \sqrt{2} & \text{for } k = 0, 1, \dots, \frac{N}{4} - 1, \\ 1 & \text{for } k = \frac{N}{4}, \\ 0 & \text{for } k = \frac{N}{4} + 1, \dots, \frac{N}{2}. \\ |D_N[N-k]| & \text{for } k = \frac{N}{2} + 1, \frac{N}{2} + 2, \dots, N-1. \end{cases} \quad (5.7)$$

Let $d_N[n]$ be the real-valued length- N impulse response of a half-band ideal filter with *DFT* $D_N[k]$. Since $d_N[n] \in \mathbb{R}$, $|D_N[k]|$ is real and even symmetric in the sense that $|D_N[k]| = |D_N[N-k]| \forall k \in [0, N-1]$. Thus, $\sigma_{\omega, \mathbf{d}_N}^2$ could alternatively be defined in terms of the discrete Fourier series (*DFS*) $\tilde{D}_N[k]$, which is the periodic extension of $D_N[k]$, according to

$$\sigma_{\omega, \mathbf{d}_N}^2 = \frac{1}{N} \sum_{k=-\frac{N}{2}+1}^{\frac{N}{2}} (k - \xi)^2 |\tilde{D}_N[k]|^2, \quad (5.8)$$

where

$$\xi = \frac{1}{N} \sum_{k=-\frac{N}{2}+1}^{\frac{N}{2}} k |\tilde{D}_N[k]|^2. \quad (5.9)$$

It follows from the fact that $|D_N[\frac{N}{2}]| = 0$ and properties 7 and 9 in Section 2.3 that the first moment of discrete frequency ξ in (5.9) is equal to zero and that

$$\sigma_{\omega, \mathbf{d}_N}^2 = \frac{2}{N} \sum_{k=0}^{\frac{N}{2}} k^2 |D_N[k]|^2.$$

Filter Length N	haar $_N$ Frequency Variance	Symlet and db $_N$ Frequency Variance	Ideal Frequency Variance
2	0.0000	0.0000	0.0000
4	0.5000	0.5000	0.5000
6	1.6667	0.8737	0.6667
8	2.0858	1.5444	1.5000
10	3.2639	2.3327	2.0000
12	4.7026	3.3042	3.1667
14	6.4022	4.4371	4.0000
16	8.3629	5.7382	5.5000
18	10.5849	7.2055	6.6667
20	13.0683	8.8395	8.5000

Table 5.1: Frequency variance of **haar** $_N$, symlet and **db** $_N$, and the ideal magnitude response for lengths 2 – 20.

Therefore,

$$\sigma_{\omega, [\mathbf{d}_N]}^2 = \frac{2}{N} \sum_{k=0}^{\frac{N}{2}} k^2 |D_N[k]|^2. \quad (5.10)$$

We get the band width as

$$\sigma_{\omega, [\mathbf{d}_N]}^2 = \frac{4}{N} \sum_{k=1}^{\lfloor \frac{N}{4} \rfloor} k^2 \quad (5.11)$$

for N not divisible by 4 and

$$\sigma_{\omega, [\mathbf{d}_N]}^2 = \frac{4}{N} \sum_{k=1}^{\frac{N}{4}-1} k^2 + \frac{N}{8} \quad (5.12)$$

for N divisible by 4. The frequency variances of the ideal magnitude response for lengths two to twenty are given in the right most column of Table 5.1.

The length- N symlet and **db** $_N$ differ in the fact that the phase response of the symlet is nearly linear while the **db** $_N$ phase response is far from linear. The near linear phase response of the symlet accounts for the better symmetry in the impulse response when compared with **db** $_N$. Since the magnitude

Filter Length N	Linear Phase Time Variance	Symlet Time Variance	\mathbf{db}_N Time Variance
2	0.2500	0.2500	0.2500
4	0.2500	0.3036	0.3036
6	0.3458	0.4412	0.4412
8	0.4154	0.4427	0.5930
10	0.4560	0.5596	0.7664
12	0.5026	0.5314	0.9565
14	0.5409	0.6570	1.1583
16	0.5780	0.6318	1.3800
18	0.6126	0.7195	1.6177
20	0.6453	0.7250	1.8708

Table 5.2: Time variance of a symmetric filter with phase given in equation (5.3), symlet, and \mathbf{db}_N for lengths 2 – 20. All three types of filters have the same magnitude $|F[k]|$.

Filter Length N	\mathbf{haar}_N Uncertainty	Symlet Uncertainty	\mathbf{db}_N Uncertainty
2	0.0000	0.0000	0.0000
4	0.1250	0.1518	0.1518
6	0.2917	0.3958	0.3958
8	0.5214	0.6529	0.9117
10	0.8160	1.3053	1.7877
12	1.1756	1.7559	3.1606
14	1.6005	2.9152	5.1395
16	2.0907	3.6252	7.9187
18	2.6462	5.1842	11.6561
20	3.2671	6.4086	16.5378

Table 5.3: Uncertainty measure of \mathbf{haar}_N , symlet, and \mathbf{db}_N for lengths 2 – 20.

response of both the symlet and \mathbf{db}_N are equal and close to the magnitude response of the ideal half-band filter, the frequency variances of \mathbf{db}_N and the symlet filters are less than the frequency variances of \mathbf{haar}_N for $N > 4$. The frequency variances of \mathbf{haar}_N and \mathbf{db}_N are shown in the middle two columns of Table 5.1. Table 5.2 shows the time variance of a symmetric filter attained by taking the inverse discrete Fourier transform of $F[k] = |DB_N[k]|e^{j\varphi[k]}$ where $k = 0, 1, 2, \dots, N - 1$ and $\varphi[k]$ is given in Equation (5.3). The time variance of the length- N symlet, and \mathbf{db}_N are also given in Table 5.2 for comparison. It is shown in Table 5.2 that the nearly linear phase $N > 6$ length symlet exhibits better time localization than \mathbf{db}_N . Since the length- N symlet and \mathbf{db}_N share the same frequency variance, the uncertainty of the least asymmetric symlet is less than or equal to the uncertainty of the Daubechies non-linear phase filter. Table 5.3 shows the uncertainty of \mathbf{haar}_N , symlet, and \mathbf{db}_N . The linear phase filter \mathbf{haar}_N is shown to exhibit poor frequency localization and the best time localization yielding the minimum uncertainty of the three different types of filters. This comparison strongly supports that symmetric, *i.e.* linear phase, yield better conjoint discrete time-discrete frequency localization.

Chapter 6

Optimal Scaling Function

6.1 A Best In Time and Best In Frequency Lower Bound

A nonattainable lower bound for $\gamma_{N,\mathbf{f}}^2$ for all $f[n] \in \mathcal{A}_N$ can be given as

$$\begin{aligned}
 \gamma_{N,\mathbf{f}}^2 &\geq \sigma_{n, [\mathbf{haar}_N]}^2 \sigma_{\omega, [\mathbf{d}_N]}^2 \\
 &\geq \begin{cases} \frac{1}{N} \sum_{k=1}^{\frac{N-2}{4}} k^2 & \text{for } N \text{ not divisible by } 4 \\ \frac{1}{N} \sum_{k=1}^{\frac{N-1}{4}} k^2 + \frac{N}{32} & \text{for } N \text{ divisible by } 4 \end{cases} \\
 &\geq \begin{cases} \frac{(N^2 - 4)}{192} & \text{for } N \text{ not divisible by } 4 \\ \frac{(N^2 + 8)}{192} & \text{for } N \text{ divisible by } 4. \end{cases} \tag{6.1}
 \end{aligned}$$

The lower bound in equation (6.1) is unattainable for $N \geq 6$ since it is the product of the minimum time variance given by \mathbf{haar}_N and the minimum frequency variance given by \mathbf{d}_N . The bounds given in equation (6.1) for filters length two through twenty are computed in the second leftmost column of Table 6.1.

To attain a tighter lower bound, better conjoint localized scaling function than \mathbf{haar}_N and still maintain perfect reconstruction, it is necessary to relax the orthogonal condition to favor linear phase and seek a biorthogonal

solution. Further insight into the nature and behavior of joint uncertainty on \mathcal{A}_N can be made by considering, for N even, the larger set $\mathcal{B}_N = \{f[n] \mid f[n]$ is a real-valued length- N sequence with unit ℓ_2 -norm such that $F[0] = \sqrt{2}$ and $|F[l]|^2 + |F[\frac{N}{2} - l]|^2 = 2$ for $l \in [0, \frac{N}{2}]$ \}. Justifications for the conditions $F[0] = \sqrt{2}$ and $|F[l]|^2 + |F[\frac{N}{2} - l]|^2 = 2$ for $l \in [0, \frac{N}{2}]$ of \mathcal{B}_N are given. These conditions of \mathcal{B}_N are derived from necessary conditions of a length- N orthogonal scaling function, hence $\mathcal{A}_N \subset \mathcal{B}_N$. It is noted that the conditions of the set \mathcal{B}_N are not sufficient for membership to be in \mathcal{A}_N , hence in general $\mathcal{B}_N \neq \mathcal{A}_N$. The set \mathcal{B}_N also contains some elements $f[n]$ that are admissible biorthogonal QMF FIR low pass analysis filters and some $f[n]$ that are not admissible as FIR low pass analysis filters for any QMF. To find a good lower bound for the uncertainty $\gamma_{N,\mathbf{f}}^2$ for all $\mathbf{f} \in \mathcal{A}_N$, it is my strategy to implement a search for \mathbf{f}^{opt} such that $\gamma_{N,\mathbf{f}^{opt}}^2 \leq \gamma_{N,\mathbf{g}}^2$ for some $\mathbf{f}^{opt} \in \mathcal{B}_N$ and for all $\mathbf{g} \in \mathcal{B}_N$. Since \mathcal{A}_N is contained in \mathcal{B}_N , $\gamma_{N,\mathbf{f}^{opt}}^2$ would provide a lower bound for the uncertainty of elements in \mathcal{A}_N . In this chapter, some results on optimizing the joint uncertainty obtained for the set \mathcal{B}_N are presented.

It is well understood that the magnitude and phase terms are not independent of each other in order to achieve certain properties. For example, the Paley-Wiener condition for causality [39] claims that given a magnitude response $|F(\omega)|$ there is a phase response $\Theta(\omega)$ so that $f(t) = ICFT \{|F(\omega)|e^{j\Theta(\omega)}\} \in L^2(\mathbb{R})$ is causal if and only if

$$\int_{-\infty}^{\infty} \frac{|\ln(|F(\omega)|)|}{1 + \omega^2} d\omega < \infty.$$

The interdependence between the magnitude and phase terms that minimizes time localization is not known. I do not claim any condition like the existence of

a certain phase sequence yielding better time localization for a given magnitude sequence. Rather, a strong justification for using a generalized linear phase in all cases is made.

6.2 Magnitude of an Orthogonal Scaling Function

The conditions $F[0] = \sqrt{2}$ and $|F[l]|^2 + |F[\frac{N}{2} - l]|^2 = 2$ of \mathcal{B}_N are based on necessary conditions for a real-valued length- N orthogonal scaling functions, where N is even with unit $\ell_{[0, N-1]}^2$ -norm, *i.e.*, necessary conditions for an element of \mathcal{A}_N . These conditions immediately follow from the definition and properties found in Section 2.3.

From property 3 of Section 2.3 it is easy to deduce $F[0] = \sum_{n=0}^{N-1} f[n] = \sqrt{2}$. If the condition $|F[l]|^2 + |F[\frac{N}{2} - l]|^2 = 2$ of \mathcal{B}_N can be verified as a necessary condition of an orthogonal scaling function, then $F[\frac{N}{2}] = 0$ and $|F[\frac{N}{2} - k]| = \sqrt{2 - |F[k]|^2} \leq \sqrt{2}$.

For $f[n] \in \mathcal{B}_N$ a real-valued length- N filter, where N is even, the *DFT* $F[k]$ must be conjugate symmetric and the following must hold:

$$F\left[\frac{N}{2} - k\right] = F\left[\frac{N}{2} + k\right]^* \quad (6.2)$$

for all $k \in [0, \frac{N}{2} - 1]$. Thus the magnitude terms of $f[n]$ satisfy:

$$\left|F\left[\frac{N}{2} - k\right]\right| = \left|F\left[\frac{N}{2} + k\right]\right| \quad (6.3)$$

for all $k \in [0, \frac{N}{2} - 1]$. Restricting to filters whose $\ell_{[0, N-1]}^2$ -norm is one, the following condition is satisfied:

$$2 + 2 \sum_{k=1}^{\frac{N}{2}} |F[k]|^2 = N. \quad (6.4)$$

It would seem that there are $\frac{N}{2}-2$ independent terms of the magnitude sequence of $f[n]$ to be determined. The condition $|F[l]|^2 + |F[\frac{N}{2}-l]|^2 = 2$ reduces the number of independent terms to $\lceil \frac{N}{4} \rceil - 1$. This condition is justified by the following application of equation (2.24) of definition 1 in Section 2.3.

To show that the condition $|F[l]|^2 + |F[\frac{N}{2}-l]|^2 = 2$ is a necessary condition of orthogonal length- N scaling functions, it is necessary to interpret the magnitude $|F[k]|$ via the autocorrelation of $f[n]$ infinitely extended by zeros. To do this let $f[n]$ be any complex-valued finite length sequence of length- N and extend $f[n]$ infinitely by zeros to get

$$f(n) = \begin{cases} f[n] & \text{for } n = 0, 1, 2, \dots, N-1, \\ 0 & \text{otherwise.} \end{cases} \quad (6.5)$$

The autocorrelation of $f(n)$ is defined as

$$r_f(l) = \sum_{n=-\infty}^{\infty} f(n)f^*(n+l) \quad (6.6)$$

$$= \sum_{n=\max\{0,-l\}}^{\min\{N-1-l,N-1\}} f[n]f^*[n+l]. \quad (6.7)$$

The limits of the summation in equation (6.7) is expressed in such a way that if $\max\{0,-l\} = 0$, then $\min\{N-1-l,N-1\} = N-1-l$ and if $\max\{0,-l\} = -l$, then $\min\{N-1-l,N-1\} = N-1$. For $|l| \geq N$, the autocorrelation of $f(n)$ at lag l is zero, *i.e.* $r_f(l) = 0$. Regardless of the lag l the autocorrelation of $f(n)$ is computed as

$$\begin{aligned} r_f(l) &= \sum_{n=0}^{N-1} f(n)f^*(n+l) \\ &= \sum_{n=0}^{N-1} f[n]f^*(n+l) \end{aligned} \quad (6.8)$$

A very nice property of the autocorrelation of $f(n)$ is given in the following theorem.

Theorem 11. The autocorrelation of $f(n)$ is conjugate symmetric, *i.e.* $r_f(l) = r_f^*(-l)$.

The proof of Theorem 11 is well know and not included.

Before proceeding to the justification of the last condition of \mathcal{B}_N , I will state and prove a theorem that will be used in the justification.

Theorem 12. Let $g(n) \in \mathbb{C}$ be any discrete sequence. If $g(n) = g^*(-n)$ for all $n \in [-M + 1, M - 1]$ where $M \in \mathbb{N} \setminus \{0\}$, then

$$\sum_{\substack{n=-M+1 \\ n \neq 0}}^{M-1} g(n)e^{-j\frac{2\pi}{M}nk} = 2\text{Re} \left\{ \sum_{n=1}^{M-1} g(n)e^{-j\frac{2\pi}{M}nk} \right\} \quad (6.9)$$

for some $k \in \mathbb{Z}$.

Proof:

$$\begin{aligned} \sum_{\substack{n=-M+1 \\ n \neq 0}}^{M-1} g(n)e^{-j\frac{2\pi}{M}nk} &= \sum_{n=-M+1}^{-1} g(n)e^{-j\frac{2\pi}{M}nk} + \sum_{n=1}^{M-1} g(n)e^{-j\frac{2\pi}{M}nk} \\ &= \sum_{n=1}^{M-1} g(-n)e^{j\frac{2\pi}{M}nk} + \sum_{n=1}^{M-1} g(n)e^{-j\frac{2\pi}{M}nk} \end{aligned}$$

We have $g^*(n) = \{g^*(-n)\}^* = g(-n)$.

$$\begin{aligned} \sum_{\substack{n=-M+1 \\ n \neq 0}}^{M-1} g(n)e^{-j\frac{2\pi}{M}nk} &= \sum_{n=1}^{M-1} g^*(n)e^{j\frac{2\pi}{M}nk} + \sum_{n=1}^{M-1} g(n)e^{-j\frac{2\pi}{M}nk} \\ &= \left\{ \sum_{n=1}^{M-1} g(n)e^{-j\frac{2\pi}{M}nk} \right\}^* + \sum_{n=1}^{M-1} g(n)e^{-j\frac{2\pi}{M}nk} \\ &= 2\text{Re} \left\{ \sum_{n=1}^{M-1} g(n)e^{-j\frac{2\pi}{M}nk} \right\}. \quad \text{Q.E.D.} \end{aligned}$$

We have $f[n] \in \mathbb{C}$ a length N sequence. To define a length N sequence from $r_f(l) \in \mathbb{C}$ let

$$\psi[l] = \begin{cases} r_f(0) & \text{for } l = 0 \\ 2r_f(-l) & \text{for } l = 1, 2, 3, \dots, N-1 \end{cases} \quad (6.10)$$

and denote the N -point DFT of $\psi[l]$ as $\Psi[k]$ for $k \in [0, N-1]$.

Theorem 13. For every length- N sequence $f[n] \in \mathbb{C}$, $Re\{\Psi[k]\} = |F[k]|^2$ where $F[k]$ is the DFT of $f[n]$ and $|F[k]|^2 = F[k]F^*[k]$.

Proof:

$$\begin{aligned} Re\{\Psi[k]\} &= Re\left\{\sum_{l=0}^{N-1} \psi[l]e^{-j\frac{2\pi}{N}lk}\right\} \\ &= Re\left\{\psi[0] + \sum_{l=1}^{N-1} \psi[l]e^{-j\frac{2\pi}{N}lk}\right\} \end{aligned}$$

The autocorrelation at lag $l = 0$ is a real number, *i.e.* $\psi[0] \in \mathbb{R}$.

$$\begin{aligned} Re\{\Psi[k]\} &= \psi[0] + Re\left\{\sum_{l=1}^{N-1} \psi[l]e^{-j\frac{2\pi}{N}lk}\right\} \\ &= \psi[0] + Re\left\{2\sum_{l=1}^{N-1} r_f(-l)e^{-j\frac{2\pi}{N}lk}\right\} \\ &= \psi[0] + 2Re\left\{\sum_{l=1}^{N-1} r_f(-l)e^{-j\frac{2\pi}{N}lk}\right\} \end{aligned}$$

Since $r_f(l) = r_f^*(-l)$ for $l \in [-N+1, N-1]$, by Theorem 12 we get the following.

$$\begin{aligned} Re\{\Psi[k]\} &= r_f[0] + \sum_{\substack{l=-N+1 \\ l \neq 0}}^{N-1} r_f(-l)e^{-j\frac{2\pi}{N}kl} \\ &= \sum_{l=-N+1}^{N+1} r_f(-l)e^{-j\frac{2\pi}{N}kl} \\ &= \sum_{l=-N+1}^{N+1} \sum_{n=-\infty}^{\infty} f(n)f^*(n-l)e^{-j\frac{2\pi}{N}kl} \end{aligned}$$

$$\begin{aligned}
&= \sum_{l=-N+1}^{N+1} \sum_{n=0}^{N-1} f[n] f^*(n-l) e^{-j \frac{2\pi}{N} kl} \\
&= \sum_{n=0}^{N-1} f[n] \sum_{l=-N+1}^{N+1} f^*(n-l) e^{-j \frac{2\pi}{N} kl}
\end{aligned}$$

Let $m = n - l \implies l = n - m$ and the last equation becomes

$$\begin{aligned}
\text{Re} \{ \Psi[k] \} &= \sum_{n=0}^{N-1} f[n] \sum_{m=n-N+1}^{n-N+1} f^*(m) e^{-j \frac{2\pi}{N} k(n-m)} \\
&= \sum_{n=0}^{N-1} f[n] e^{-j \frac{2\pi}{N} kn} \sum_{m=n-N+1}^{n+N-1} f^*(m) e^{j \frac{2\pi}{N} km}
\end{aligned}$$

Since for every $n \in [0, N-1]$, we have $[0, N-1] \subset [n-N+1, n+N-1]$, $f(m) = 0$ for $m \in \mathbb{Z} \setminus [0, N-1]$,

$$\begin{aligned}
\text{Re} \{ \Psi[k] \} &= \left\{ \sum_{n=0}^{N-1} f[n] e^{-j \frac{2\pi}{N} kn} \right\} \left\{ \sum_{m=0}^{N-1} f[m] e^{-j \frac{2\pi}{N} km} \right\}^* \\
&= |F[k]|^2. \qquad \text{Q.E.D.}
\end{aligned}$$

For every $f[n] \in \mathcal{A}_N$, since $f[n]$ has unit $\ell_{[0, N-1]}^2$ -norm, its autocorrelation at lag zero must be one, *i.e.* $r_f(0) = 1$. In addition equation (2.24) of Definition 1 in Section 2.3 requires the autocorrelation to be zero for every even nonzero lags. For every $f[n] \in \mathcal{A}_N$, equation (6.10) becomes

$$\psi[l] = \begin{cases} 1 & \text{for } l = 0 \\ 0 & \text{for } l = 2, 4, 6, \dots, N-2 \\ 2r_f(-l) & \text{for } l = 1, 3, 5, \dots, N-1 \end{cases} \quad (6.11)$$

Theorem 14. If $f[n] \in \mathcal{A}_N$, then $|F[k]|^2 + |F[\frac{N}{2} - k]|^2 = 2$ for $k \in [0, \frac{N}{2}]$.

Proof: For $f[n] \in \mathcal{A}_N$ and from Theorem 13, we get

$$\begin{aligned}
|F[k]|^2 &= \text{Re} \{ \Psi[k] \} \\
&= \text{Re} \left\{ \sum_{l=0}^{N-1} \psi[l] e^{-j \frac{2\pi}{N} lk} \right\}
\end{aligned}$$

$$\begin{aligned}
&= \psi[0] + \operatorname{Re} \left\{ \sum_{l=1}^{N-1} \psi[l] e^{-j \frac{2\pi}{N} l k} \right\} \\
&= 1 + \operatorname{Re} \left\{ \sum_{m=1}^{\frac{N-2}{2}} \psi[2m] e^{-j \frac{2\pi}{N} (2m) k} + \sum_{m=1}^{\frac{N-2}{2}} \psi[2m+1] e^{-j \frac{2\pi}{N} (2m+1) k} \right\} \\
&= 1 + \operatorname{Re} \left\{ \sum_{m=1}^{\frac{N-2}{2}} \psi[2m+1] e^{-j \frac{2\pi}{N} (2m+1) k} \right\} \\
&= 1 + \sum_{m=1}^{\frac{N-2}{2}} \psi[2m+1] \cos \left(\frac{2\pi}{N} (2m+1) k \right) \tag{6.12}
\end{aligned}$$

$$\begin{aligned}
\left| F\left[\frac{N}{2} - k\right] \right|^2 &= 1 + \operatorname{Re} \left\{ \sum_{m=1}^{\frac{N-2}{2}} \psi[2m+1] e^{-j \frac{2\pi}{N} (2m+1) \left(\frac{N}{2} - k\right)} \right\} \\
&= 1 + \operatorname{Re} \left\{ \sum_{m=1}^{\frac{N-2}{2}} \psi[2m+1] e^{-j \pi (2m+1)} e^{j \frac{2\pi}{N} (2m+1) k} \right\} \\
&= 1 - \sum_{m=1}^{\frac{N-2}{2}} \psi[2m+1] \cos \left(\frac{2\pi}{N} (2m+1) k \right). \tag{6.13}
\end{aligned}$$

Summing equations (6.12) and (6.13), we get $|F[k]|^2 + |F[\frac{N}{2} - k]|^2 = 2$. Q.E.D.

From Theorem 14, the condition $|F[k]|^2 + |F[\frac{N}{2} - k]|^2 = 2$ for $k \in [0, \frac{N}{2}]$ is a necessary condition for any filter to be a unit $\ell_{[0, N-1]}^2$ -norm orthogonal scaling function. To determine an element $f[n] \in \mathcal{B}_N$, it is only necessary to specify $|F[k]|$ for $k \in [1, \lceil \frac{N}{4} - 1 \rceil]$, since $|F[\frac{N}{2} - k]| = \sqrt{2 - |F[k]|^2}$ for $k \in [1, \frac{N}{2}]$.

6.3 A Linear Phase Response

To specify a particular $f[n] \in \mathcal{B}_N$, it is sufficient to specify the *DFT* $F[k]$. To specify $F[k]$, it is sufficient to specify the phase sequence $\varphi[k]$ and magnitude

sequence $|F[k]|$ such that $F[k] = |F[k]|e^{j\varphi[k]}$ for $k = 1, 2, \dots, \frac{N}{2} - 1$. The finite time sequence is then the *IDFT* of $F[k]$. Before I proceed to describe the method used for determining the terms of the magnitude sequence, *viz.*, $|F[0]|, |F[1]|, \dots, |F[N-1]|$, it is necessary to formulate the finite discrete phase sequence.

Tables 5.1 and 5.3 strongly suggests that symmetry, *i.e.*, linear phase, decreases the uncertainty measure γ_N^2 . In particular the length- N symlet and \mathbf{db}_N have identical magnitude response, thus their frequency variances are equal. The length- N symlet has a phase sequence that is nearly linear. The symlet time sequence exhibits better symmetry than the time sequence of \mathbf{db}_N for $N > 6$ and the symlet yields a smaller uncertainty measure. Though \mathbf{haar}_N has poor frequency localization, it is shown in Table 5.3 to have smaller uncertainty measure than the symlet or \mathbf{db}_N for $N > 2$. It is my argument that this is because the linear phase of \mathbf{HAAR}_N results in a smaller time uncertainty for \mathbf{haar}_N . It is desirable in many signal and image processing algorithm for the phase sequence to be linear (in the generalized sense). Except for the Haar case, linear phase and orthogonality are not compatible for N even and $N > 2$. For the purpose of minimizing the uncertainty measure γ_N^2 , linear phase is preferred over orthogonality.

Definition 2 in Section 2.3 describes linear phase response as follows: $F(e^{j\omega}) = |F(e^{j\omega})|e^{j\varphi(\omega)}$ or $F(e^{j\omega}) = \text{sgn}\{F(e^{j\omega})\}|F(e^{j\omega})|e^{j\varphi(\omega)}$, where, up to additions and subtractions of integer multiples of 2π , $\varphi(\omega) = a\omega + b$ for some $a, b \in \mathbb{R}$. Since $F[k]$, the *DFT* of $f[n]$, is a uniform sampling of $F(e^{j\omega}) = \text{DTFT}\{f[n]\}$, and since $F(e^{j\omega})$ is 2π periodic, $F[k]$ is related to $F(e^{j\omega})$ simply

as

$$\begin{aligned} F[k] &= F(e^{j\omega}) \Big|_{\omega=\frac{2\pi}{N}k} \\ &= |F(e^{j\frac{2\pi}{N}k})| e^{j\varphi(\frac{2\pi}{N}k)} \end{aligned}$$

for $k \in [0, N - 1]$. Up to additions and subtractions of integer multiples of 2π , the discrete phase sequence attained from sampling a linear phase response *DTFT* is

$$\varphi[k] = \frac{2\pi}{N} \left(\lambda k + \rho + \pi \left(\frac{1}{2} - \frac{1}{2} \operatorname{sgn} \left\{ F(e^{j\frac{2\pi}{N}k}) \right\} \right) \right), \quad (6.14)$$

where $\lambda \in \mathbb{R}$, $\rho \in \mathbb{Z}$, and $k \in [0, N - 1]$. Since the measure of uncertainty defined in (4.15) is determined over the equivalence class of all integer shifts in time and frequency, we may assume without loss of generality that $0 \leq \lambda \leq 1$ in (6.14).

Note that the term ρ in (6.14) has no effect whatsoever on the joint uncertainty; I have therefore assumed $\rho = 0$ for the remainder of this dissertation. If we assume further that the phase $\varphi[k]$ takes the special form

$$\varphi[k] = \begin{cases} -\frac{2\pi}{N}\lambda k & \text{for } k = 0, 1, 2, \dots, \frac{N}{2}, \\ \frac{2\pi}{N}\lambda(N - k) & \text{for } k = \frac{N}{2} + 1, \frac{N}{2} + 2, \dots, N - 1, \end{cases} \quad (6.15)$$

then the discrete phase sequence given in equation (6.14) coincides with the phase sequence ¹ of the Haar scaling function when $\lambda = \frac{1}{2}$. Except in the Haar case, the phase sequence in equation (6.15) will not lead to a scaling function of an orthogonal QMF.

Theorem 15. Let N be even and let $f[n]$ be a real-valued length- N sequence with *DFT* $F[k] = |F[k]| e^{j\varphi[k]}$, where $\varphi[k]$ is given by (6.15) with $\lambda = \frac{1}{2}$. Then

¹Up to a time shift.

there exists a real-valued $\mathbf{g} \in [\mathbf{f}]$ such that $g[n] = g[N-1-n]$ for $n = 0, 1, 2, \dots, N-1$.

Proof: Since $\lambda = \frac{1}{2}$, we have that

$$f[n] = \frac{1}{N} \left\{ \sum_{k=0}^{\frac{N}{2}} |F[k]| e^{-j\frac{\pi}{N}k} e^{j\frac{2\pi}{N}nk} + \sum_{k=\frac{N}{2}+1}^{N-1} |F[k]| e^{j\frac{\pi}{N}(N-k)} e^{j\frac{2\pi}{N}nk} \right\}. \quad (6.16)$$

In the second summation of (6.16), let $l = k - \frac{N}{2}$, so that $l = 1, 2, \dots, \frac{N}{2} - 1$.

We then have

$$\begin{aligned} f[n] &= \frac{1}{N} \left\{ \sum_{k=0}^{\frac{N}{2}} |F[k]| e^{j\frac{\pi}{N}(2n-1)k} \right. \\ &\quad \left. + \sum_{l=1}^{\frac{N}{2}-1} \left| F \left[N - \frac{N}{2} - l \right] \right| e^{j\frac{\pi}{N}(N-\frac{N}{2}-l)} e^{j\frac{2\pi}{N}(\frac{N}{2}+l)n} \right\} \\ &= \frac{1}{N} \left\{ \sum_{k=0}^{\frac{N}{2}} |F[k]| e^{j\frac{\pi}{N}(2n-1)k} + \sum_{l=1}^{\frac{N}{2}-1} \left| F \left[\frac{N}{2} - l \right] \right| e^{j\frac{\pi}{N}(\frac{N}{2}-l)} e^{j\frac{2\pi}{N}nl} e^{j\pi n} \right\} \\ &= \frac{1}{N} \left\{ \sum_{k=0}^{\frac{N}{2}} |F[k]| e^{j\frac{\pi}{N}(2n-1)k} + \sum_{l=1}^{\frac{N}{2}-1} \left| F \left[\frac{N}{2} - l \right] \right| e^{j\frac{\pi}{N}(\frac{N}{2}-l+2nl)} e^{j\pi n} \right\} \\ &= \frac{1}{N} \left\{ \sum_{k=0}^{\frac{N}{2}} |F[k]| e^{j\frac{\pi}{N}(2n-1)k} \right. \\ &\quad \left. + \sum_{l=1}^{\frac{N}{2}-1} \left| F \left[\frac{N}{2} - l \right] \right| e^{j\frac{\pi}{N}(\frac{N}{2}+(2n-1)l)} e^{j\pi n} \right\} \quad (6.17) \\ &= \frac{1}{N} \left\{ \sum_{k=0}^{\frac{N}{2}} |F[k]| e^{j\frac{\pi}{N}(2n-1)k} e^{-j\frac{2\pi}{N}Nk} \right. \\ &\quad \left. + \sum_{l=1}^{\frac{N}{2}-1} \left| F \left[\frac{N}{2} - l \right] \right| e^{j\frac{\pi}{N}(\frac{N}{2}+(2n-1)l)} e^{-j\frac{2\pi}{N}Nl} e^{j\pi n} \right\} \end{aligned}$$

$$\begin{aligned}
&= \frac{1}{N} \left\{ \sum_{k=0}^{\frac{N}{2}} |F[k]| e^{j\frac{\pi}{N}(2n-1-2N)k} \right. \\
&\quad \left. + \sum_{l=1}^{\frac{N}{2}-1} \left| F\left[\frac{N}{2}-l\right] \right| e^{j\frac{\pi}{N}\left(\frac{N}{2}+(2n-1)l-2Nl\right)} e^{j\pi n} \right\} \\
&= \frac{1}{N} \left\{ \sum_{k=0}^{\frac{N}{2}} |F[k]| e^{j\frac{\pi}{N}(-2N+2n-1-1+1)k} \right. \\
&\quad \left. + \sum_{l=1}^{\frac{N}{2}-1} \left| F\left[\frac{N}{2}-l\right] \right| e^{j\frac{\pi}{N}\left(\frac{N}{2}+(-2N+2n-1-1+1)l\right)} e^{j\pi n} \right\} \\
&= \frac{1}{N} \left\{ \sum_{k=0}^{\frac{N}{2}} |F[k]| e^{j\frac{\pi}{N}(-2(N-n+1)+1)k} \right. \\
&\quad \left. + \sum_{l=1}^{\frac{N}{2}-1} \left| F\left[\frac{N}{2}-l\right] \right| e^{j\frac{\pi}{N}\left(\frac{N}{2}+(-2(N-n+1)+1)l\right)} e^{j\pi n} \right\} \\
&= \frac{1}{N} \left\{ \sum_{k=0}^{\frac{N}{2}} |F[k]| e^{-j\frac{\pi}{N}(2(N-n+1)-1)k} \right. \\
&\quad \left. + \sum_{l=1}^{\frac{N}{2}-1} \left| F\left[\frac{N}{2}-l\right] \right| e^{j\frac{\pi}{N}\left(\frac{N}{2}-(2(N-n+1)-1)l\right)} e^{j\pi n} \right\} \\
&= \frac{1}{N} \left\{ \sum_{k=0}^{\frac{N}{2}} \text{“ ”} \right. \\
&\quad \left. + \sum_{l=1}^{\frac{N}{2}-1} \left| F\left[\frac{N}{2}-l\right] \right| e^{-j\frac{\pi}{N}N} e^{j\frac{\pi}{N}\left(\frac{N}{2}-(2(N-n+1)-1)l\right)} e^{j\pi n} e^{-j\pi(N+1)} \right\} \\
&= \frac{1}{N} \left\{ \sum_{k=0}^{\frac{N}{2}} \text{“ ”} + \sum_{l=1}^{\frac{N}{2}-1} \left| F\left[\frac{N}{2}-l\right] \right| e^{j\frac{\pi}{N}\left(-\frac{N}{2}-(2(N-n+1)-1)l\right)} e^{j\pi(n-N-1)} \right\} \\
&= \frac{1}{N} \left\{ \sum_{k=0}^{\frac{N}{2}} |F[k]| e^{-j\frac{\pi}{N}(2(N-n+1)-1)k} \right.
\end{aligned}$$

$$+ \sum_{l=1}^{\frac{N}{2}-1} \left| F \left[\frac{N}{2} - l \right] \right| e^{-j\frac{\pi}{N}(\frac{N}{2} + (2(N-n+1)-1)l)} e^{-j\pi(N-n+1)} \left. \right\} \quad (6.18)$$

$$= f^*[(N+1-n)_N]. \quad (6.19)$$

The last equality (6.19) is gotten by noticing that (6.18) is equivalent to (6.17), where the argument is $N+1-n$ instead of n . Since $f[n]$ is real-valued, (6.19) becomes $f[n] = f[(N+1-n)_N]$. Computing the first $\frac{N}{2}$ terms of $f[n]$ yields:

$$\begin{aligned} f[0] &= f[(N+1-0)_N] = f[1] \\ f[1] &= f[(N+1-1)_N] = f[0] \\ f[2] &= f[N+1-2] = f[N-1] \\ f[3] &= f[N+1-3] = f[N-2] \\ &\vdots \\ f\left[\frac{N}{2}\right] &= f\left[N+1-\frac{N}{2}\right] = f\left[\frac{N}{2}+1\right]. \end{aligned}$$

A desired symmetric sequence $g[n]$ such that $g[n] = g[N-1-n] \forall n \in [0, N-1]$ can now be obtained by applying either of two circular shifts to $f[n]$. The first shift is given by $g[n] = f[(n - \frac{N}{2} + 1)_N]$, while the second is given by $g[n] = f[(1+n)_N]$. To see that $g[n]$ is symmetric in the first case, let $g[n] = f[(n - \frac{N}{2} + 1)_N]$. Then

$$\begin{aligned} g[N-1-n] &= f\left[\left(N-1-n-\frac{N}{2}+1\right)_N\right] \\ &= f\left[\left(\frac{N}{2}-n\right)_N\right] \\ &= f\left[\left(N+1-\frac{N}{2}+n\right)_N\right] \\ &= f\left[\left(n-\frac{N}{2}+1\right)_N\right] = g[n]. \end{aligned}$$

To see that $g[n]$ is also symmetric in the second case, let $g[n] = f[(1+n)_N]$. We have then that

$$\begin{aligned} g[N-1-n] &= f[(1+N-1-n)_N] \\ &= f[(N-n)_N] \end{aligned}$$

$$\begin{aligned}
&= f[(N + 1 - N + n)_N] \\
&= f[(n + 1)_N] = g[n].
\end{aligned}$$

Therefore, both shifts construct a $\mathbf{g} \in [\mathbf{f}]$ that has the desired symmetry property. Q.E.D.

Let $F[k] = |F[k]| e^{j\psi[k]}$ be the *DFT* of a real-value sequence $f[n]$ for $n = 0, 1, \dots, N - 1$ and $\Gamma : \mathbb{R}^{\frac{N}{2}-1} \rightarrow \mathbb{R}$ where $\Gamma(\psi[1], \psi[2], \dots, \psi[\frac{N}{2} - 1]) = \sigma_{n,\mathbf{f}}^2$. Clearly Γ is continuous. It is well known from [40] that the global maximum/minimum of Γ is a local maximum/minimum, thus must be a critical point.

Definition 6. A point $\vec{\psi}_0 \in \mathbb{R}^{\frac{N}{2}-1}$ is a local minimum of Γ , if

$$\Gamma\left(\psi_0[1], \psi_0[2], \dots, \psi_0\left[\frac{N}{2} - 1\right]\right) \leq \Gamma\left(\psi[1], \psi[2], \dots, \psi\left[\frac{N}{2} - 1\right]\right) \quad (6.20)$$

for all $\vec{\psi}$ such that $\sqrt{\sum_{k=1}^{\frac{N}{2}-1} (\psi_0[k] - \psi[k])^2} < \epsilon$ for some real number $\epsilon > 0$.

The definition for local maximum is analogous to definition 6 except the inequality in equation (6.20) is reversed.

Definition 7. A point $\vec{\psi}_0 \in \mathbb{R}^{\frac{N}{2}-1}$ is a critical point of Γ , if

$$\left. \frac{\partial \Gamma}{\partial (\psi[k])} \right|_{\psi[k]=\psi_0[k]} = 0 \quad (6.21)$$

for all $k = 1, 2, \dots, \frac{N}{2} - 1$.

Theorem 16. Let $\lambda = \frac{1}{2}$, so that

$$\varphi[k] = \begin{cases} -\frac{\pi}{N}k & \text{for } k = 0, 1, 2, \dots, \frac{N}{2}, \\ \frac{\pi}{N}(N - k) & \text{for } k = \frac{N}{2} + 1, \frac{N}{2} + 2, \dots, N - 1. \end{cases} \quad (6.22)$$

For fixed magnitude terms $|F[k]|$ such that $F[0] = \sqrt{2}$, $F[\frac{N}{2}] = 0$, and

$$\frac{1}{N} \sum_{k=0}^{N-1} |F[k]|^2 = 1,$$

$$\psi[k] = \varphi[k] + \frac{2\pi}{N}k \quad (6.23)$$

and

$$\psi[k] = \varphi[k] - \frac{2\pi}{N} \left(\frac{N}{2} - 1 \right) k \quad (6.24)$$

are critical points for $\Gamma(\psi[1], \psi[2], \dots, \psi[\frac{N}{2} - 1]) = \sigma_{n,f}^2$ where

$$f[n] = \frac{1}{N} \sum_{k=0}^{N-1} |F[k]| e^{j\psi[k]} e^{j\frac{2\pi}{N}nk} \text{ and } f[n] \in \mathbb{R}.$$

Proof: Before proceeding to the proof, it is worthwhile to make a few notes.

1. Since $|f[n]|^2 = f[n]f^*[n]$,

$$|f[n]|^2 = \frac{1}{N^2} \left\{ \sum_{k=0}^{N-1} |F[k]| e^{j(\psi[k] + \frac{2\pi}{N}nk)} \right\} \left\{ \sum_{k=0}^{N-1} |F[k]| e^{-j(\psi[k] + \frac{2\pi}{N}nk)} \right\}. \quad (6.25)$$

2. The partial derivative of $|f[n]|^2$ with respect to $\psi[k]$ is

$$\frac{\partial (|f[n]|^2)}{\partial (\psi[k])} = 2f[n] \frac{\partial (f[n])}{\partial (\psi[k])}. \quad (6.26)$$

3. The partial derivative of $f[n]$ with respect to $\psi[k]$ is

$$\begin{aligned} \frac{\partial (f[n])}{\partial (\psi[k])} &= \frac{j}{N} |F[k]| e^{j(\psi[k] + \frac{2\pi}{N}nk)} - \frac{j}{N} |F[N-k]| e^{j(-\psi[k] + \frac{2\pi}{N}n(N-k))} \\ &= -\frac{2}{N} |F[k]| \sin \left(\psi[k] + \frac{2\pi}{N}nk \right). \end{aligned} \quad (6.27)$$

4. When $\psi[k] = \varphi[k] + \frac{2\pi}{N}k$, we get

$$\psi[k] + \frac{2\pi}{N}nk = \frac{\pi}{N}k(2n+1). \quad (6.28)$$

5. When $\psi[k] = \varphi[k] - \frac{2\pi}{N} \left(\frac{N}{2} - 1\right) k$, we get

$$\psi[k] + \frac{2\pi}{N} nk = \frac{\pi}{N} k (2n - N + 1). \quad (6.29)$$

To show that the phase terms in equation (6.23) and (6.24) are critical points of Γ , it is necessary to show that

$$\left. \frac{\partial \Gamma}{\partial (\psi[k])} \right|_{\psi[k]=\varphi[k]+\frac{2\pi}{N}k} = 0 \quad (6.30)$$

and

$$\left. \frac{\partial \Gamma}{\partial (\psi[k])} \right|_{\psi[k]=\varphi[k]-\frac{2\pi}{N}(\frac{N}{2}-1)k} = 0. \quad (6.31)$$

Taking the first derivative of Γ with respect to $\psi[k]$, we get

$$\frac{\partial \Gamma}{\partial (\psi[k])} = \sum_{n=0}^{N-1} 2(n - \mu_{\mathbf{f}}) \frac{\partial \mu_{\mathbf{f}}}{\partial (\psi[k])} |f[n]|^2 + \sum_{n=0}^{N-1} (n - \mu_{\mathbf{f}})^2 \frac{|f[n]|^2}{\partial (\psi[k])}. \quad (6.32)$$

The first summation of equation (6.32) is zero, thus

$$\begin{aligned} \frac{\partial \Gamma}{\partial (\psi[k])} &= \sum_{n=0}^{N-1} (n - \mu_{\mathbf{f}})^2 \frac{|f[n]|^2}{\partial (\psi[k])} \\ &= 2 \sum_{n=0}^{N-1} (n - \mu_{\mathbf{f}})^2 g[n] \frac{\partial (g[n])}{\partial (\psi[k])} \\ &= -\frac{4}{N} |F[k]| \sum_{n=0}^{N-1} (n - \mu_{\mathbf{f}})^2 g[n] \sin \left(\psi[k] + \frac{2\pi}{N} nk \right). \end{aligned} \quad (6.33)$$

The last two equalities are obtained from equations (6.26) and (6.27). When equation (6.33) is evaluated at $\psi[k] = \varphi[k] + \frac{2\pi}{N} k$ and using equation (6.28), we get

$$\left. \frac{\partial \Gamma}{\partial (\psi[k])} \right|_{\psi[k]=\varphi[k]+\frac{2\pi}{N}k} = -\frac{4}{N} |F[k]| \sum_{n=0}^{N-1} (n - \mu_{\mathbf{f}})^2 g[n] \sin \left(\frac{2\pi}{N} (2n + 1) k \right). \quad (6.34)$$

From Theorem 15, we have

$$f[n] = f[N - 1 - n] \quad (6.35)$$

thus

$$\mu_f = \frac{N - 1}{2}. \quad (6.36)$$

It is easily shown that

$$(n - \mu_f)^2 = (N - 1 - n - \mu_f)^2. \quad (6.37)$$

To show that equation (6.30) holds for $F[k] \neq 0$ it is enough to show that

$$\sin\left(\frac{\pi}{N}(2n + 1)k\right) = -\sin\left(\frac{\pi}{N}(2(N - 1 - n) + 1)k\right). \quad (6.38)$$

Starting with the right hand side of equation (6.38), we get

$$\begin{aligned} -\sin\left(\frac{\pi}{N}(2(N - 1 - n) + 1)k\right) &= -\sin\left(\frac{\pi}{N}(2N - 2n - 1)k\right) \\ &= -\sin\left(2\pi k - \frac{\pi}{N}(2n + 1)k\right) \\ &= -\sin(2\pi k) \cos\left(\frac{\pi}{N}(2n + 1)k\right) \\ &\quad + \cos(2\pi k) \sin\left(\frac{\pi}{N}(2n + 1)k\right) \\ &= \sin\left(\frac{\pi}{N}(2n + 1)k\right). \end{aligned}$$

Thus equation (6.30) holds and $\psi[k] = \varphi[k] + \frac{2\pi}{N}k$ is a critical point for Γ .

If $\psi[k]$ is defined as in equation (6.24), then the first partial derivative of Γ with respect to $\psi[k]$ evaluated at $\psi[k] = \varphi[k] - \frac{2\pi}{N}(\frac{N}{2} - 1)k$ is

$$\begin{aligned} \frac{\partial \Gamma}{\partial (\psi[k])} \Big|_{\psi[k] = \varphi[k] - \frac{2\pi}{N}(\frac{N}{2} - 1)k} &= -\frac{4}{N} |F[k]| \sum_{n=0}^{N-1} (n - \mu_f)^2 g[n] \sin\left(\frac{2\pi}{N}(2n - N + 1)k\right) \quad (6.39) \end{aligned}$$

and equations (6.35) and (6.36) follow from Theorem 15. Since

$$\begin{aligned} \sin\left(\frac{2\pi}{N}(2n - N + 1)k\right) &= -\sin\left(\frac{2\pi}{N}(N - 2n - 1)k\right) \\ &= -\sin\left(\frac{2\pi}{N}(2N - N - 2n - 2 + 1)k\right) \\ &= -\sin\left(\frac{2\pi}{N}(2(N - 1 - n) - N + 1)k\right), \end{aligned}$$

equation (6.39) is equal to zero. Thus equation (6.31) holds and $\psi[k] = \varphi[k] - \frac{2\pi}{N}\left(\frac{N}{2} - 1\right)k$ is also a critical point of Γ . Q.E.D.

To determine if the critical points in equations (6.23) and (6.24) are local minimums, it is necessary to determine whether the second order partial derivatives of Γ are continuous and the Hessian matrix of Γ evaluated at these points are positive definite. For continuous second partial derivatives of Γ , the critical points are local maximums if the Hessian matrix of Γ evaluated at these points are negative definite. If the Hessian of Γ evaluated at a critical point is neither positive definite nor negative definite, then it is indeterminate whether Γ is a local minimum or local maximum at this point [40] and can be considered a saddle point on a hypersurface.

Definition 8. Let $\mathcal{H}_\Gamma(\vec{\psi})$ denote the Hessian matrix of Γ evaluated at $\vec{\psi}$.

Then

$$\mathcal{H}_\Gamma(\vec{\psi}) = \begin{pmatrix} \frac{\partial^2 \Gamma}{\partial(\psi[1])\partial(\psi[1])} & \cdots & \frac{\partial^2 \Gamma}{\partial(\psi[\frac{N}{2}-1])\partial(\psi[1])} \\ \vdots & & \vdots \\ \frac{\partial^2 \Gamma}{\partial(\psi[1])\partial(\psi[\frac{N}{2}-1])} & \cdots & \frac{\partial^2 \Gamma}{\partial(\psi[\frac{N}{2}-1])\partial(\psi[\frac{N}{2}-1])} \end{pmatrix}. \quad (6.40)$$

It is obvious that $\mathcal{H}_\Gamma(\vec{\psi})$ is symmetric, *i.e.* $\frac{\partial^2 \Gamma}{\partial(\psi[l])\partial(\psi[k])} = \frac{\partial^2 \Gamma}{\partial(\psi[k])\partial(\psi[l])}$.

Definition 9. For all $\vec{x} \in \mathbb{R}^{\frac{N}{2}-1} \setminus \{\vec{0}\}$ the Hessian matrix of Γ evaluated at $\vec{\psi}$ is positive definite if

$$\vec{x}^T \mathcal{H}_\Gamma(\vec{\psi}) \vec{x} = \sum_{l=1}^{\frac{N}{2}-1} \sum_{k=1}^{\frac{N}{2}-1} \frac{\partial^2 \Gamma}{\partial(\psi[l]) \partial(\psi[k])} x_l x_k > 0 \quad (6.41)$$

The Hessian matrix of Γ evaluated at $\vec{\psi}$ is negative definite, if

$$\vec{x}^T \mathcal{H}_\Gamma(\vec{\psi}) \vec{x} = \sum_{l=1}^{\frac{N}{2}-1} \sum_{k=1}^{\frac{N}{2}-1} \frac{\partial^2 \Gamma}{\partial(\psi[l]) \partial(\psi[k])} x_l x_k < 0. \quad (6.42)$$

The use of the Hessian matrix to show whether the phase terms defined in equations (6.23) and (6.24) are local minimums or local maximums results in an indeterminate conclusion. In other words, the Hessian matrix of Γ evaluated at equations (6.23) and (6.24) are neither positive definite nor negative definite. Since the admissibility condition cannot be fully accounted for in this analysis, it cannot be determined if Γ at these critical points are local minimums, local maximums, or points of inflection.

To determine whether the phase terms in equation (6.23) produces a local minimum, a local maximum, or a point of inflection, define a function $\Gamma_{\max}(\lambda) : [0, 1] \rightarrow \mathbb{R}$ as

$$\Gamma_{\max}(\lambda) = \max_{\mathbf{g} \in \{f\}} \{ \sigma_{n, \mathbf{g}}^2 \}, \quad (6.43)$$

where $D[k]$ is the ideal magnitude sequence specified in equations (5.6) and (5.7). The sequence $f[n]$ is defined as

$$f[n] = \sum_{k=0}^{N-1} D[k] e^{j\varphi[k]} e^{j\frac{2\pi}{N}nk}, \quad (6.44)$$

where $\varphi[k]$ is defined in equation (6.15). Fig. 6.1 is a plot of $\Gamma_{\max}(\lambda)$ verses λ for the length four filters defined in equation (6.44). Fig. 6.1 clearly shows that

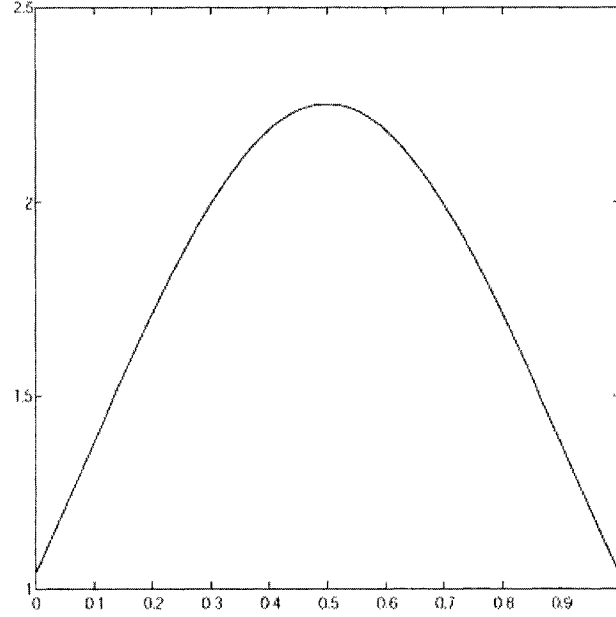


Figure 6.1: Plot of $\Gamma_{\max}(\lambda)$ of the length four filter \mathbf{f} defined in equation (6.44) for $0 \leq \lambda \leq 1$.

the maximum of Γ_{\max} is achieved at $\lambda = \frac{1}{2}$. In addition, if $\mathbf{g} \in [\mathbf{f}]$ such that $\Gamma_{\max}(\frac{1}{2}) = \sigma_{n,\mathbf{g}}^2$, the phase terms of \mathbf{g} corresponds to the function described in equation (6.23). To illustrate this point, in the length four case, we have $\Gamma_{\max}(\frac{1}{2}) = 2.25$, $\mathbf{f} = \left[\frac{1}{\sqrt{2}} \ \frac{1}{\sqrt{2}} \ 0 \ 0 \right]$, and $\mathbf{g} = \left[\frac{1}{\sqrt{2}} \ 0 \ 0 \ \frac{1}{\sqrt{2}} \right]$.

The plots of $\Gamma_{\max}(\lambda)$ of the filters defined in equation (6.44) for $0 \leq \lambda \leq 1$ and length $N = 6, 8, 10, 12, 14, 16, 18, 20$ can be found in the Appendix A. In all cases investigated $\Gamma_{\max}(\lambda)$ achieved a maximum at $\lambda = \frac{1}{2}$. The element $\mathbf{g} \in [\mathbf{f}]$ that achieves this maximum has a phase which correspond to the function in equation (6.23). This suggests that the critical point of Γ in equation (6.23) is a local maximum and possibly a global maximum of Γ_{\max} .

In the case when the phase terms are defined as in equation (6.24), a

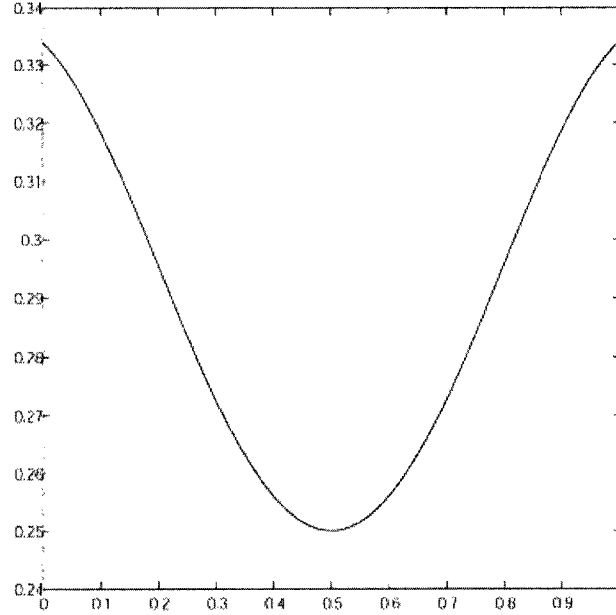


Figure 6.2: Plot of $\Gamma_{\min}(\lambda)$ of the length four filter \mathbf{f} defined in equation (6.44) for $0 \leq \lambda \leq 1$.

function $\Gamma_{\min} : [0, 1] \rightarrow \mathbb{R}$ is defined as

$$\Gamma_{\min}(\lambda) = \min_{\mathbf{g} \in [\mathbf{f}]} \{ \sigma_{n, \mathbf{g}}^2 \} \quad (6.45)$$

where $D[k]$ is the ideal magnitude sequence, $f[n]$ is defined in equation (6.44), and $\varphi[k]$ defined in equation (6.15). Fig. 6.2 is a plot of $\Gamma_{\min}(\lambda)$ verses λ for the length four filters defined in equation (6.44). Fig. 6.2 clearly shows that the minimum of Γ_{\min} is achieved at $\lambda = \frac{1}{2}$. In addition, if $\mathbf{g} \in [\mathbf{f}]$ such that $\Gamma_{\min}(\frac{1}{2}) = \sigma_{n, \mathbf{g}}^2$, the phase terms of \mathbf{g} corresponds to the function described in equation (6.24). To illustrate this point, in the length four case, we have $\Gamma_{\min}(\frac{1}{2}) = 0.25$, $\mathbf{f} = \left[\frac{1}{\sqrt{2}} \quad \frac{1}{\sqrt{2}} \quad 0 \quad 0 \right]$, and $\mathbf{g} = \left[0 \quad \frac{1}{\sqrt{2}} \quad \frac{1}{\sqrt{2}} \quad 0 \right]$.

The plots of $\Gamma_{\min}(\lambda)$ of the filters defined in equation (6.44) for $0 \leq \lambda \leq 1$ and for $N = 6, 8, 10, 12, 14, 16, 18, 20$ can be found in Appendix A. In all cases

investigated a minimum is achieved at $\lambda = \frac{1}{2}$. The element $\mathbf{g} \in [\mathbf{f}]$ that achieves this minimum has a phase which corresponds to the function in equation (6.24). This suggests that the critical point of Γ in equation (6.24) is a local minimum and possibly a global minimum of Γ_{\min} .

If $F[k] = |F[k]| e^{j\varphi[k]}$ where $\varphi[k]$ is defined in equation (6.22) and $G[k] = |F[k]| e^{j\psi[k]}$ where $\psi[k]$ is defined as in equations (6.23) or (6.24), then $\mathbf{g} \in [\mathbf{f}]$ where \mathbf{g} and \mathbf{f} are the *IDFT* of \mathbf{G} and \mathbf{F} , *resp.* For $f[n]$ that are admissible as a FIR scaling function for a biorthogonal QMF, the results of this subsection provide strong evidence that the phase given in equation (6.22) minimizes $\sigma_{n,[\mathbf{f}]}^2$.

6.4 A Search Algorithm to Determine the Lower Bound

6.4.1 Orthogonal Case

Let $\mathcal{B}'_N = \{\mathbf{f} \in \mathcal{B}_N \mid F[k] \text{ has phase } \varphi[k] \text{ given by (6.22)}\}$. It is evident that $\mathbf{haar}_N \in \mathcal{B}'_N$. The following conjecture asserts that there is an $\mathbf{f}^{opt} \in \mathcal{B}'_N$ that minimizes the joint uncertainty over \mathcal{B}_N .

Conjecture 1. There exists an $\mathbf{f}^{opt} \in \mathcal{B}'_N$ such that $\gamma_{N,\mathbf{f}^{opt}}^2 = \min_{\mathbf{h} \in \mathcal{B}_N} \{\gamma_{N,\mathbf{h}}^2\}$.

Although this conjecture has not been proven, the evidences described in the previous section strongly suggests that it holds. The lower bound for \mathcal{B} , which will provide a lower bound for \mathcal{A} , as the evidence suggest will come from an element in \mathcal{B}' . To attain a lower bound for $\gamma_{N,\mathbf{f}}^2$ for all $f[n] \in \mathcal{A}_N$, I will describe a numerical search algorithm used to find an optimal low pass analysis filter $f^{opt}[n]$ that minimize $\gamma_{N,\mathbf{f}}^2$ over \mathcal{B}'_N for a variety of even N . The algorithm decreases the frequency variance $\sigma_{\omega,[\mathbf{f}]}^2$ and in effect increases the time variance

$\sigma_{n,[f]}^2$ in order to minimize the uncertainty $\gamma_{N,f}^2$.

To be concise in defining the search algorithm used for finding $f^{\text{opt}}[n]$, I will list the constraints used for the search space. It should be noted that these constraints do not necessarily lead to filters which will constitute an orthogonal QMF. The search space consists of all $f[n]$ satisfying the following:

1. The filter $f[n]$ is real valued.
 - This condition implies $F[k] = F^*[N - 1 - k]$ where $k \in [0, N - 1]$ and $F[k] = DFT\{f[n]\}$.
2. The length N is even.
3. The filter $f[n]$ has unity ℓ_2 -norm.
4. $F[0] = \sqrt{2}$.
5. $|F[\frac{N}{2} - k]| = \sqrt{2 - |F[k]|^2}$ for $k \in [0, \frac{N}{2}]$.
6. $|F[k]| \leq \sqrt{2}$.
7. The phase response of $f[n]$ is given in equation (6.22).

The only real-valued scaling functions which meet all the restrictions for $N = 2$ and 4 are the Haar filters. The Haar filter zero padded to length six gives a starting point to find a length six filter with optimal conjoint localization. To find an optimal length six real-valued scaling function, I have only to specify the terms of the magnitude response $|F[1]|$ and $|F[2]|$. To fulfill the requirement of equation (6.4) and derive a unit ℓ^2 ($[0, N - 1]$) norm filter, I let $|F[2]| = \sqrt{2 - |F[1]|^2}$. Let $|HAAR_6[k]|$ and $|DB_6[k]|$ be the magnitude response of the

Haar filter zero padded to length six and Daubechies length six scaling function. The search varies the $|F[1]|$ term in such a way that

$$|HAAR_6[1]| \leq |HAAR_6[1]| + \Omega i = |F[1]| \leq |DB_6[1]|,$$

where i indexes the iteration and Ω is a fixed incremental change. The incrementation stops at $|DB_6[1]|$, since it is known that the Daubechies have maximally flat passband for orthogonal scaling functions. At each iteration, using the phase response defined in equation (6.15), the impulse response is determined and the joint uncertainty is calculated. The iteration repeats until $|F[1]| > |DB_6[1]|$. The filter that produces the minimum uncertainty is saved.

To find the optimal length eight filter, only the $|F[1]|$ term of the magnitude response needs to be determined, since $|F[0]| = \sqrt{2}$, $|F[2]| = 1$, $|F[3]| = \sqrt{2 - |F[1]|^2}$, and $|F[4]| = 0$. The search algorithm begins at $|HAAR_8[1]|$ and increments $|F[1]|$ by Ω until $|F[1]| > |DB_8[1]|$. This incrementation decreases the frequency variance $\sigma_{\omega,[f]}^2$ while increasing the time variance $\sigma_{n,[f]}^2$. The filter which minimizes the uncertainty $\gamma_{8,f}^2$ is saved. Precisely, the search varies $|F[1]|$ such that

$$|HAAR_8[1]| \leq |F_{6,8}[1]| + \Omega i = |F[1]| \leq |DB_8[1]|. \quad (6.46)$$

and where $F_{6,8}[k]$ is the *DFT* of the optimal length six filter zero padded to length eight and Ω is a fixed increment. At each iteration, using the phase response given in equation (6.15), the inverse *DFT* of $F[k]$ yields the impulse response and the joint uncertainty can be calculated. The iterations continue until equations (6.46) is no longer satisfied. The length eight filter which minimizes the uncertainty is saved.

For $N = 10$ there are two terms $|F[1]|$ and $|F[2]|$ to be determined, since $|F[0]| = \sqrt{2}$, $|F[3]| = \sqrt{2 - |F[2]|^2}$, $|F[4]| = \sqrt{2 - |F[1]|^2}$, and $|F[5]| = 0$. The search consist of two nested “for” loops in which

$$|HAAR_{10[1]}| \leq |HAAR_{10}[1]| + \Omega i = |F[1]| \leq |DB_{10}[1]| \quad (6.47)$$

and

$$|F[1]| \geq |F[1]| - \Omega k = |F[2]| \geq |HAAR_{10}[2]| \quad (6.48)$$

where Ω is the increment and the search is indexed by (i, k) . Again the search moves toward $|DB_{10}[k]|$ for $k = 1, 2$, since this decreases the frequency variance at the expense of increasing the time variance. The search determines the best trade off.

The search algorithm for $N = 12$ is very similiar to the previous search for $N = 10$ except $|F[3]| = 1$, $|F[4]| = \sqrt{2 - |F[2]|^2}$, $|F[5]| = \sqrt{2 - |F[1]|^2}$, and $|F[6]| = 0$. There are still two nested “for” loops that are implemented as described in equation (6.47) and (6.48).

In general, for N not divisible by four there are $\lfloor \frac{N}{4} \rfloor$ nested “for” loops so that

$$\begin{aligned} |HAAR_N[1]| &\leq |HAAR_N[1]| + \Omega i_1 = |F[1]| &\leq |DB_N[1]| \\ |F[1]| &\geq |F[1]| - \Omega i_2 = |F[2]| &\geq |HAAR_N[2]| \\ |F[2]| &\geq |F[2]| - \Omega i_3 = |F[3]| &\geq |HAAR_N[3]| \\ &\vdots \\ |F[\lfloor \frac{N}{4} \rfloor - 1]| &\geq |F[\lfloor \frac{N}{4} \rfloor - 1]| - \Omega i_{\lfloor \frac{N}{4} \rfloor} = |F[\lfloor \frac{N}{4} \rfloor]| &\geq |HAAR_N[\lfloor \frac{N}{4} \rfloor]| \end{aligned}$$

where the iterations of the search are indexed by $(i_1, i_2, i_3, \dots, i_{\lfloor \frac{N}{4} \rfloor})$ and Ω is some small incremental amount. The other terms necessarily follow, *i.e.*, $|F[0]| = \sqrt{2}$, $|F[\frac{N}{2} - k]| = \sqrt{2 - |F[k]|^2}$ for $k \in [1, \lfloor \frac{N}{4} \rfloor]$, and $|F[\frac{N}{2}]| = 0$.

The magnitude terms of the optimal length- N filter zero padded to length $N + 2$ denoted $|F_{N,N+2}[k]|$ for $k \in [1, \lfloor \frac{N}{4} \rfloor]$ give the search algorithm a starting point. If N is not divisible by four, then $N + 2$ is divisible by four. The search for the length $N + 2$ filter $\mathbf{f}^{\text{opt}} \in \mathcal{B}'_{N+2}$ implements $\lfloor \frac{N}{4} \rfloor$ nested “for” loops as just described. The following terms must necessarily follow: $|F[0]| = \sqrt{2}$, $|F[\frac{N+2}{2} - k]| = \sqrt{2 - |F[k]|^2}$ for $k \in [1, \frac{N+2}{4}]$, $|F[\frac{N+2}{4}]| = 1$, and $|F[\frac{N+2}{2}]| = 0$.

The results of this search produce a symmetric filter different from \mathbf{HAAR}_N , thus for $N > 4$ these filters are not orthogonal. They exhibit better conjoint localization than the zero padded Haar filter. Their uncertainty provides a good lower bound for $\gamma_{N,\mathbf{f}}^2$ for all $f[n] \in \mathcal{A}_N$. Since the lower bounds are produced by symmetric filters different from the zero padded Haar filter, these lower bounds are not attainable by any elements in \mathcal{A}_N . Table 6.1 list the uncertainty measures found by this search algorithm for $N = 6, 8, 10, \dots, 20$ and using an incremental amount $\Omega = 0.001$ for $N = 6, 8, 10, 12, 14, 16$ and $\Omega = 0.01$ for $N = 18, 20$.

The best localized filter $\mathbf{f}^{\text{opt}} \in \mathcal{B}'_6$ is

$$\begin{aligned} f^{\text{opt}}[0] &= -0.03085567563131 &= f^{\text{opt}}[5] \\ f^{\text{opt}}[1] &= 0.03226648753395 &= f^{\text{opt}}[4] \\ f^{\text{opt}}[2] &= 0.70569596928391 &= f^{\text{opt}}[3]. \end{aligned} \tag{6.49}$$

The time variance for this filter is

$$\sigma_{n, [\mathbf{f}^{\text{opt}}]}^2 = 0.2656$$

and the frequency variance is

$$\sigma_{\omega, [\mathbf{f}^{\text{opt}}]}^2 = 1.0391.$$

Filter Length	Equation 6.1 Lower Bound	$f^{opt} \in \mathcal{B}'_N$ Uncertainty	\mathbf{haar}_N Uncertainty
2	0.0000	0.0000	0.0000
4	0.1250	0.1250	0.1250
6	0.1667	0.2760	0.2917
8	0.3750	0.4937	0.5214
10	0.5000	0.7717	0.8160
12	0.7917	1.1116	1.1756
14	1.0000	1.5178	1.6005
16	1.3750	1.9857	2.0907
18	1.6667	2.5041	2.6462
20	2.1250	3.0915	3.2671

Table 6.1: Lower bounds for uncertainty measure for filter lengths 2 – 20 given by $\sigma_{n, \{\mathbf{haar}_N\}}^2 \sigma_{\omega, \{d_N\}}^2$ in the second leftmost column and as determined by the search algorithm in subsection 6.4.1 in the second rightmost column.

The joint uncertainty is

$$\gamma_{6, f^{opt}}^2 = 0.2760.$$

The best localized filter $f^{opt} \in \mathcal{B}'_8$ is

$$\begin{aligned} f^{opt}[0] &= 0.00119212710431 &= f^{opt}[7] \\ f^{opt}[1] &= -0.02900930872082 &= f^{opt}[6] \\ f^{opt}[2] &= 0.02900930872082 &= f^{opt}[5] \\ f^{opt}[3] &= 0.70591465408224 &= f^{opt}[4]. \end{aligned}$$

The time variance for this filter is

$$\sigma_{n, \{f^{opt}\}}^2 = 0.2635$$

and the frequency variance is

$$\sigma_{\omega, \{f^{opt}\}}^2 = 1.8735.$$

The joint uncertainty is

$$\gamma_{8, f^{opt}}^2 = 0.4937.$$

The scaling function $f^{opt}[n]$ for $N = 10, 12, 14, 16, 18, 20$ are given in Appendix B.

6.4.2 Biorthogonal Case

A better conjointly localized scaling function can be attained by reducing the conditions of \mathcal{B}_N . Define this larger set as $\mathcal{C}_N = \{ \mathbf{f} \mid \mathbf{f} \text{ is an even length-}N \text{ real-value sequence, } F[0] = \sqrt{2}, \text{ and } F[\frac{N}{2}] = 0 \}$. The set relations are as follow

$$\mathcal{A}_N \subseteq \mathcal{B}_N \subseteq \mathcal{C}_N.$$

Let $\mathcal{C}'_N = \{ \mathbf{f} \in \mathcal{C}_N \mid F[k] \text{ has phase } \varphi[k] \text{ given by equation (6.22)} \}$. The evidence of Section 6.3 suggests that there exists a $f^{opt}[n] \in \mathcal{C}'_N$ such that $\gamma_{N, f^{opt}}^2 \leq \gamma_{N, \mathbf{f}}^2$ for all $f[n] \in \mathcal{C}_N$. To be concise in defining the search algorithm used for finding $f^{opt}[n] \in \mathcal{C}'_N$, I will list the constraints used for the search space. It should be noted that these constraints do not necessarily lead to filters which will constitute an biorthogonal QMF. The search space consists of all $f[n]$ satisfying the following:

1. The filter $f[n]$ is real valued.
2. The length N is even.
3. The filter $f[n]$ has unity ℓ_2 -norm.
4. $F[0] = \sqrt{2}$ where $F[k] = DFT\{f[n]\}$.
5. $F[\frac{N}{2}] = 0$.

6. $|F[k]| \leq \sqrt{2}$.
7. The phase terms of $f[n]$ are given in equation (6.22).

It was noted in Section 2.3.2 that items three and four do not both need to be met to constitute a low pass scaling function for a biorthogonal QMF. Both constraints are adopted in this section to reduce the number of free parameters and keep the search algorithm from becoming too cumbersome. Indeed, better conjointly localized biorthogonal scaling functions can be realized by requiring to either item three or item four but not both at the cost of increasing the search space. Even accepting both constraints, there are more free parameters in the biorthogonal case than in the orthogonal case. Thus, the biorthogonal search is expected to yield smaller lower bounds on the uncertainty measure verses the more restrictive orthogonal case. The search will produce filters that constitute a perfect reconstruction biorthogonal QMF. Therefore I consider the uncertainty measures produced by this search as a upper bound on the lower bound for even length biorthogonal scaling functions.

The only real-valued scaling functions which meets all the restrictions for $N = 2$ and 4 are the Haar filters. The search for the length six $f^{opt}[n] \in \mathcal{C}'_N$ is the same as in the previous Section 6.4.1.

To find the optimal length eight filter, only the $|F[1]|$ and $|F[2]|$ terms of the magnitude response need to be determined, since $|F[0]| = \sqrt{2}$, $|F[4]| = 0$ and $|F[3]| = \sqrt{3 - |F[1]|^2 - |F[2]|^2}$. To specify a starting point for the search algorithm, define $f_{6,8}[n]$ to be the filter obtained by zero padding the optimal length six filter $f^{opt}[n]$ to length $N = 8$. Let $F_{6,8}[k]$ be the *DFT* of $f_{6,8}[n]$. The

search varied $|F[1]|$ and $|F[2]|$ such that

$$|F_{6,8}[1]| \leq |F_{6,8}[1]| + \Omega i = |F[1]| \leq \sqrt{2} \quad (6.50)$$

and

$$|F_{6,8}[2]| \geq |F_{6,8}[2]| + \Omega k = |F[2]| \geq 0, \quad (6.51)$$

where the iterations are now indexed by (i, k) and Ω is a fixed increment. At each iteration, using the phase response given in equation (6.15), the inverse *DFT* of $F[k]$ yields the impulse response and the joint uncertainty can be calculated. The iterations continue until equations (6.50) and (6.51) are no longer satisfied. The length eight filter which minimizes the uncertainty is saved.

For $N = 8$, a search was implemented using a search increment of $\Omega = 0.001$. The following low pass filter was found:

$$\begin{aligned} f^{\text{opt}}[0] &= -0.01315882031237 = f^{\text{opt}}[7] \\ f^{\text{opt}}[1] &= -0.02843832297817 = f^{\text{opt}}[6] \\ f^{\text{opt}}[2] &= 0.04364111877368 = f^{\text{opt}}[5] \\ f^{\text{opt}}[3] &= 0.70506280570341 = f^{\text{opt}}[4]. \end{aligned} \quad (6.52)$$

The time variance for this filter is

$$\min_{\mathbf{h} \in \{\mathbf{f}^{\text{opt}}\}} \{\sigma_{n,\mathbf{h}}^2\} = 0.27147875680532$$

and the frequency variance is

$$\min_{\mathbf{h} \in \{\mathbf{f}^{\text{opt}}\}} \{\sigma_{\omega,\mathbf{h}}^2\} = 1.78386055920144.$$

The joint uncertainty is

$$\gamma_{8,\mathbf{f}^{\text{opt}}}^2 = 0.48428024692605.$$

In both the $N = 6$ and $N = 8$ cases, a smoothing of the Haar filter increased the time variance but decreased the frequency variance. It is evident that sensibly increasing the time variance of the Haar filter to achieve improved frequency localization leads to minimizing the joint uncertainty measure. Since the filters found in the search algorithm are symmetric in time, they cannot be used in a orthogonal QMF. Yet construction of a biorthogonal QMF is possible. Given the low pass analysis filter, *i.e.*, the scaling function, to determine a biorthogonal QMF it is necessary to specify the high pass analysis filter, *i.e.*, the wavelet. To do this a technique by M. Vetterli and D. Le Gall as described in [16] is employed.

Let $H_0(z)$ and $H_1(z)$ be the z -transforms of the scaling function and wavelet *resp.* The synthesis low pass filter, $G_0(z)$, and synthesis high pass filter $G_1(z)$, are obtained by $G_0(z) = sH_1(-z)$ and $G_1(z) = -sH_0(-z)$, where $s \in \mathbb{R}$ is a scaling factor. In [16], polynomials of the even and odd terms of the scaling function and the wavelets are expressed in the matrix form

$$\mathbf{H}_p(z) = \begin{pmatrix} H_{0,0}(z) & H_{0,1}(z) \\ H_{1,0}(z) & H_{1,1}(z) \end{pmatrix} \quad (6.53)$$

where $H_{0,0}(z)$, $H_{0,1}(z)$, $H_{1,0}(z)$, $H_{1,1}(z)$ are the z -transforms of the even terms of the scaling function, the odd terms of the scaling function, the even terms of the wavelet, the odd terms of the wavelet, *resp.* A possible method to obtain an even length $N = 2K$ linear phase perfect reconstruction QMF is to express the matrix $\mathbf{H}_p(z)$ as

$$\mathbf{H}_p(z) = \begin{pmatrix} 1 & 1 \\ 1 & -1 \end{pmatrix} \prod_{k=1}^{K-1} \begin{pmatrix} 1 & 0 \\ 0 & z^{-1} \end{pmatrix} \begin{pmatrix} 1 & \alpha_k \\ \alpha_k & 1 \end{pmatrix} \quad (6.54)$$

where $\alpha_k \in \mathbb{R}$ and the scaling factor is $s = \left(2 \prod_{k=1}^{K-1} (1 - \alpha_k^2) \right)^{-1}$.

For $N = 6 = 2 \cdot 3$, equation (6.54) becomes

$$\mathbf{H}_p(z) = \begin{pmatrix} 1 + (\alpha_1 + \alpha_1\alpha_2)z^{-1} + \alpha_2z^{-2} & \alpha_2 + (\alpha_1 + \alpha_1\alpha_2)z^{-1} + z^{-2} \\ 1 + (-\alpha_1 + \alpha_1\alpha_2)z^{-1} - \alpha_2z^{-2} & \alpha_2 + (\alpha_1 - \alpha_1\alpha_2)z^{-1} - z^{-2} \end{pmatrix}$$

where $s = (2(1 - \alpha_1^2)(1 - \alpha_2^2))^{-1}$. The z-transforms of the scaling function can be derived as

$$H_0(z) = 1 + \alpha_2z^{-1} + (\alpha_1 + \alpha_1\alpha_2)z^{-2} + (\alpha_1 + \alpha_1\alpha_2)z^{-3} + \alpha_2z^{-4} + z^{-5}. \quad (6.55)$$

The z-transform of the high pass analysis wavelet is

$$H_1(z) = 1 + \alpha_2z^{-1} + (-\alpha_1 + \alpha_1\alpha_2)z^{-2} + (\alpha_1 - \alpha_1\alpha_2)z^{-3} - \alpha_2z^{-4} - z^{-5}. \quad (6.56)$$

Since $f^{opt}[0] \neq 0$ let $f_0[n] = \frac{f^{opt}[n]}{f^{opt}[0]}$ where $f^{opt}[n]$ is defined in equation (6.49). The z-transform of $f_0[n]$ is

$$F_0(z) = 1 + f_0[1]z^{-1} + f_0[2]z^{-2} + f_0[2]z^{-3} + f_0[1]z^{-4} + z^{-5}. \quad (6.57)$$

Set $H_0(z)$ in equation (6.55) equal to $F_0(z)$ in equation (6.57), to get a solvable linearly dependent set of two equations with two unknowns

$$f_0[1] = \alpha_2 \quad (6.58)$$

$$f_0[2] = \alpha_1 + \alpha_1\alpha_2. \quad (6.59)$$

Since $f^{opt}[0] \neq -f^{opt}[1]$, we get $f_0[1] \neq -1$ and we can solve equation (6.59) for α_2 to get

$$\alpha_2 = \frac{f_0[2]}{f_0[1] + 1}.$$

The low pass analysis scaling function and the high pass analysis wavelet can be determined by equations (6.55) and (6.56), *resp.* Since $\alpha_1 = 499.3580330364305$ and $\alpha_2 = -1.04576258295054$, the low pass and high pass synthesis filters can

n	$H_0[n]$	$H_1[n]$	$G_0[n]$	$G_1[n]$
0	1.00000000000000	0.00000100000000	0.0000214181474	-0.0000214181474
1	-1.045762582950	-0.0000010457625	0.0000223982972	-0.0000223982972
2	-22.851913408846	-0.0001021567979	-0.0218800936362	0.0004894456513
3	-22.851913408846	0.00010215679794	-0.0218800936362	-0.0004894456513
4	-1.045762582950	0.0000010457625	0.0000223982972	0.0000223982972
5	1.00000000000000	-0.00000100000000	0.0000214181474	0.0000214181474

Table 6.2: Length-six biorthogonal QMF

be determined by $G_0(z) = sH_1(-z)$ and $G_1(z) = -sH_0(-z)$, *resp.* The terms of the length six biorthogonal QMF are given in Table 6.2.

To check that this is a perfect reconstruction QMF, it is only necessary to check that $\det \{H_p(z)\} = cz^{-n}$ for some $n \in \mathbb{Z}$ and $c \in \mathbb{R} \setminus \{0\}$ [16]. The determinant of $H_p(z)$ is computed as

$$\begin{aligned}
\det \{H_p(z)\} &= 2(\alpha_1^2 - \alpha_1^2\alpha_2^2 + \alpha_2^2 - 1)z^{-2} \\
&= -2(1 - \alpha_1^2)(1 - \alpha_2^2)z^{-2} \\
&= -s^{-1}z^{-2}.
\end{aligned} \tag{6.60}$$

Since $\alpha_1 \neq \pm 1$ and $\alpha_2 \neq \pm 1$, the constant $s^{-1} \neq 0$ and the four filters in Table 6.2 constitute a perfect reconstruction QMF.

For $N = 8 = 2 \cdot 4$, let $f^{opt}[n]$ be defined in equation (6.52). Since $f^{opt}[0] \neq 0$, define $f_0[n] = \frac{f^{opt}[n]}{f^{opt}[0]}$. The z-transform of $f_0[n]$ is

$$\begin{aligned}
F_0(z) &= 1 + f_0[1]z^{-1} + f_0[2]z^{-2} + f_0[3]z^{-3} + f_0[3]z^{-4} + f_0[2]z^{-5} \\
&\quad + f_0[1]z^{-6} + z^{-7}.
\end{aligned} \tag{6.61}$$

The matrix $H_p(z)$ defined in equation (6.53) becomes

$$\begin{pmatrix}
1 + (\alpha_2\alpha_3 + \alpha_1\alpha_2 + \alpha_1)z^{-1} + (\alpha_1\alpha_3 + \alpha_1\alpha_2\alpha_3 + \alpha_2)z^{-2} + \alpha_3z^{-3} \\
\alpha_3 + (\alpha_1\alpha_3 + \alpha_1\alpha_2\alpha_3 + \alpha_2)z^{-1} + (\alpha_2\alpha_3 + \alpha_1\alpha_2 + \alpha_1)z^{-2} + z^{-3} \\
1 + (\alpha_2\alpha_3 + \alpha_1\alpha_2 - \alpha_1)z^{-1} + (\alpha_1\alpha_3 - \alpha_1\alpha_2\alpha_3 - \alpha_2)z^{-2} - \alpha_3z^{-3} \\
\alpha_3 + (-\alpha_1\alpha_3 + \alpha_1\alpha_2\alpha_3 + \alpha_2)z^{-1} + (-\alpha_2\alpha_3 - \alpha_1\alpha_2 + \alpha_1)z^{-2} - z^{-3}
\end{pmatrix}.$$

The low pass analysis scaling function can be determined as

$$\begin{aligned}
H_0(z) = 1 &+ \alpha_3 z^{-1} + (\alpha_2 \alpha_3 + \alpha_1 \alpha_2 + \alpha_1) z^{-2} + (\alpha_1 \alpha_3 + \alpha_1 \alpha_2 \alpha_3 + \alpha_2) z^{-3} \\
&+ (\alpha_1 \alpha_3 + \alpha_1 \alpha_2 \alpha_3 + \alpha_2) z^{-4} + (\alpha_2 \alpha_3 + \alpha_1 \alpha_2 + \alpha_1) z^{-5} \\
&+ \alpha_3 z^{-6} + z^{-7}.
\end{aligned} \tag{6.62}$$

The high pass analysis wavelet is

$$\begin{aligned}
H_1(z) = 1 &+ \alpha_3 z^{-1} + (\alpha_2 \alpha_3 + \alpha_1 \alpha_2 - \alpha_1) z^{-2} - (\alpha_1 \alpha_3 - \alpha_1 \alpha_2 \alpha_3 - \alpha_2) z^{-3} \\
&+ (\alpha_1 \alpha_3 - \alpha_1 \alpha_2 \alpha_3 - \alpha_2) z^{-4} - (\alpha_2 \alpha_3 + \alpha_1 \alpha_2 - \alpha_1) z^{-5} \\
&- \alpha_3 z^{-6} - z^{-7}.
\end{aligned} \tag{6.63}$$

Set equation (6.61) equal to equation (6.62) to get the following set of non-linearly dependent equations

$$f_0[1] = \alpha_3 \tag{6.64}$$

$$f_0[2] = \alpha_2 \alpha_3 + \alpha_1 \alpha_2 + \alpha_1 \tag{6.65}$$

$$f_0[3] = \alpha_1 \alpha_3 + \alpha_1 \alpha_2 \alpha_3 + \alpha_2. \tag{6.66}$$

Solving this system of non-linearly dependent equations for α_1 and α_2 gives

$$\begin{aligned}
\alpha_1 &= \frac{f_0[1]f_0[3] - f_0[2]}{f_0^2[1] + f_0[1]f_0[2] - f_0[3] - 1}, \\
\alpha_2 &= \frac{f_0[2] - \alpha_1}{f_0[1] + \alpha_1}.
\end{aligned}$$

Since $f_0^2[1] + f_0[1]f_0[2] - f_0[3] - 1 = 50.08414794378206 \neq 0$, we get $\alpha_1 = -2.24583353786622$. We can solve for α_2 , since $\alpha_1 \neq -f_0[1] = -2.16116052222708$, to get $\alpha_2 = 12.64462103327462$, and $\alpha_3 = 2.16116052222708$. The low pass analysis and the high pass analysis filters can be determined by equations (6.62) and (6.63), *resp.*, where $s =$

n	$H_0[n]$	$H_1[n]$	$G_0[n]$	$G_1[n]$
0	1.0000000000000	1.0000000000000	-0.0002120108533	0.0002120108533
1	2.1611605222270	2.1611605222270	0.0004581894865	-0.0004581894865
2	-3.3164917323676	1.1751753433648	-0.0002491499273	-0.0007031322423
3	-53.5810041452346	-43.8737905821746	-0.0093017197811	0.0113597544122
4	-53.5810041452346	43.8737905821746	-0.0093017197811	-0.0113597544122
5	-3.3164917323676	-1.1751753433648	-0.0002491499273	0.0007031322423
6	2.1611605222270	-2.1611605222270	0.0004581894865	0.0004581894865
7	1.0000000000000	-1.0000000000000	-0.0002120108533	-0.0002120108533

Table 6.3: Length-eight biorthogonal QMF

$(2(1 - \alpha_1^2)(1 - \alpha_2^2)(1 - \alpha_3^2))^{-1}$. The terms of all four filters of the length eight biorthogonal QMF are given in Table 6.3. To check that the four filters in Table 6.3 constitute a perfect reconstruction QMF, the determinant of $H_p(z)$ is computed as

$$\begin{aligned}
\det \{H_p(z)\} &= 2(-1 - \alpha_2^2\alpha_3^2 - \alpha_1^2\alpha_2^2 + \alpha_1^2 - \alpha_1^2\alpha_3^2 + \alpha_1^2\alpha_2^2\alpha_3^2 + \alpha_2^2 + \alpha_3^2) \\
&= -2(1 - \alpha_1^2)(1 - \alpha_2^2)(1 - \alpha_3^2)z^{-3} \\
&= -s^{-1}z^{-3}.
\end{aligned} \tag{6.67}$$

Since $\alpha_1 \neq \pm 1$, $\alpha_2 \neq \pm 1$, and $\alpha_3 \neq \pm 1$, the constant $s^{-1} \neq 0$ in equation (6.67) and the four filters in Table 6.3 constitute a perfect reconstruction QMF.

Chapter 7

Multi-Channel Parallel Filter Bank Realizations

7.1 $L - 1$ Level Discrete Wavelet Transform

The rigors of signal and image processing generally require a multi-channel filter bank such as in Gabor analysis. A multi-channel filter bank can easily be created using Mallat's algorithm of [12]. Mallat's analysis algorithm consists of successively cascading a perfect reconstruction QMF's analysis filters to the output of the low pass analysis filter. A typical three level cascaded filter bank is shown in Fig. 7.1. This method is commonly referred to as the discrete

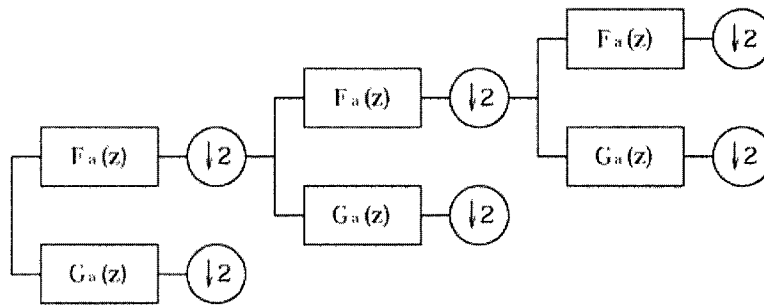


Figure 7.1: The three level discrete wavelet transform cascaded filter bank.

wavelet transform (DWT). The number of channels produced by the DWT is one more than the number of levels of decomposition, *i.e.*, if the DWT consist of $L - 1$ levels then there are L channels in the filter bank. The original signal or

image can be perfectly reconstructed by reversing the DWT with the synthesis filters of the QMF as shown in Fig. 7.2. This is generally known as the inverse

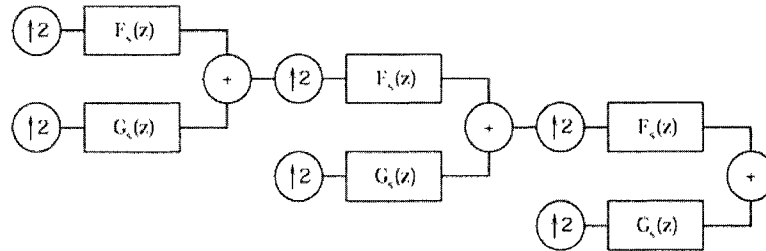


Figure 7.2: The three level inverse discrete wavelet transform cascaded filter bank.

discrete wavelet transform (IDWT).

The DWT and IDWT can be implemented as a parallel filter bank via the Noble Identities. The Noble Identities are shown pictorially in Fig. 7.3 and are stated as:

1. Down-sampling by M then filtering by $G(z)$ is equivalent to filtering by $G(z^M)$ then down-sampling by M .
2. Filtering by $G(z)$ then up-sampling by M is equivalent of up-sampling by M then filtering by $G(z^M)$.

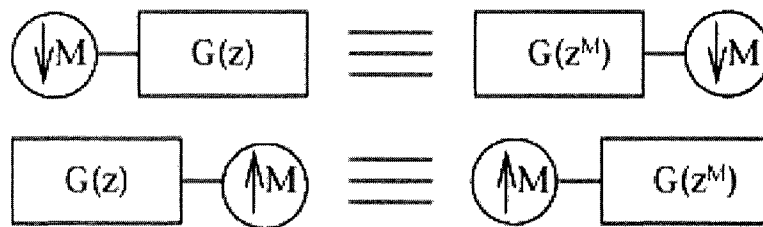


Figure 7.3: The Noble identities.

To create an L -channel PRPFB as shown in Fig. 7.4, $L - 1$ level DWT and IDWT perfect reconstruction filter banks are employed. The filter bank

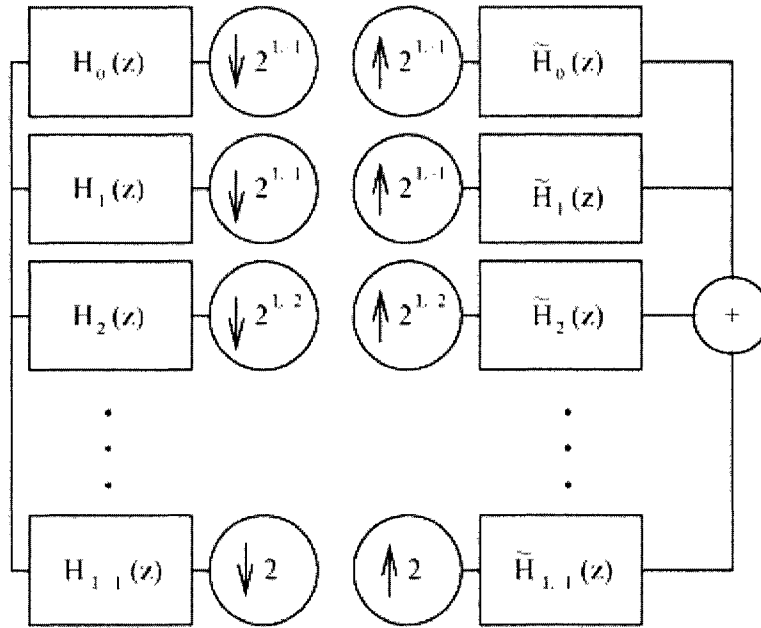


Figure 7.4: A L channel parallel filter bank.

in Fig. 7.4 consists of L analysis filters, $H_0(z)$, $H_1(z)$, \dots , $H_{L-1}(z)$ and L synthesis filters, $\tilde{H}_0(z)$, $\tilde{H}_1(z)$, \dots , $\tilde{H}_{L-1}(z)$. The analysis filters in Fig. 7.4 are determined by applying the first Noble identity to the filters in the DWT. The synthesis filters are the results of applying the second Noble identity to the filters used in the IDWT.

For $L = 2$ the filter bank in Fig. 7.4 is simply the familiar QMF. The analysis filters are

$$\begin{aligned} H_0(z) &= F_a(z) \\ H_1(z) &= G_a(z). \end{aligned}$$

The synthesis filters are

$$\begin{aligned} \tilde{H}_0(z) &= F_s(z) \\ \tilde{H}_1(z) &= G_s(z). \end{aligned}$$

When $L = 3$ the analysis and synthesis filter banks in Fig. 7.4 are equivalent to a two-level DWT and a two-level IDWT filter banks, *resp.* The analysis filters are determined as

$$\begin{aligned} H_0(z) &= F_a(z)F_a(z^2) \\ H_1(z) &= F_a(z)G_a(z^2) \\ H_2(z) &= G_a(z). \end{aligned}$$

The synthesis filters are

$$\begin{aligned} \tilde{H}_0(z) &= F_s(z^2)F_s(z) \\ \tilde{H}_1(z) &= G_s(z^2)F_s(z) \\ \tilde{H}_2(z) &= G_s(z). \end{aligned}$$

A $L = 4$ channel analysis and synthesis parallel filter bank is equivalent to a three level DWT and IDWT filter bank as shown in Fig. 7.1 and Fig. 7.2, *resp.* The four analysis filters are determined as

$$\begin{aligned} H_0(z) &= F_a(z)F_a(z^2)F_a(z^4) \\ H_1(z) &= F_a(z)F_a(z^2)G_a(z^4) \\ H_2(z) &= F_a(z)G_a(z^2) \\ H_3(z) &= G_a(z). \end{aligned}$$

The four synthesis filters of the PRPFB are

$$\begin{aligned} \tilde{H}_0(z) &= F_s(z^4)F_s(z^2)F_s(z) \\ \tilde{H}_1(z) &= G_s(z^4)F_s(z^2)F_s(z) \\ \tilde{H}_2(z) &= G_s(z^2)F_s(z) \\ \tilde{H}_3(z) &= G_s(z). \end{aligned}$$

For five-channel PRPFB, the five analysis filters are

$$\begin{aligned}
 H_0(z) &= F_a(z)F_a(z^2)F_a(z^4)F_a(z^8) \\
 H_1(z) &= F_a(z)F_a(z^2)F_a(z^4)G_a(z^8) \\
 H_2(z) &= F_a(z)F_a(z^2)G_a(z^4) \\
 H_3(z) &= F_a(z)G_a(z^4) \\
 H_4(z) &= G_a(z).
 \end{aligned}$$

The five synthesis filters are

$$\begin{aligned}
 \tilde{H}_0(z) &= F_s(z^8)F_s(z^4)F_s(z^2)F_s(z) \\
 \tilde{H}_1(z) &= G_s(z^8)F_s(z^4)F_s(z^2)F_s(z) \\
 \tilde{H}_2(z) &= G_s(z^4)F_s(z^2)F_s(z) \\
 \tilde{H}_3(z) &= G_s(z^2)F_s(z) \\
 \tilde{H}_4(z) &= G_s(z).
 \end{aligned}$$

It is possible to create PRPFBs with more than five channels in the preceding manner. This chapter stops at five channels because a five channel filter bank implemented separably for image processing produces a twenty-five channel two dimensional filter bank. This quantity is adequate for the work presented in the next chapter.

7.2 Uncertainty of a Multi-Channel Filter Bank

In this section, a novel uncertainty measure will be defined for multi-channel parallel filter banks described in Section 7.1. This measure will quantify the conjoint localization of an L -channel parallel filter bank as the weighted arith-

metric mean of the conjoint localizations in time/space and frequency of the analysis filters which comprise the filter bank.

The formulation of uncertainty in HWUP is the product of a signal's time/space variance and frequency variance. This can be considered as an area of a tile defined on the time-frequency plane. In considering a quantification of uncertainty of a multi-channel filter bank, the geometric mean of the modified uncertainty of each analysis filters can be considered as an area defined on a hyperplane. One could thus argue that this formulation is analogous with the quantification and conceptualization of uncertainty used in the HWUP extended to the time-frequency hyperplane. Then achieving small geometric mean would only require one of the filters in the bank to possess small localization in the either time or the frequency domain. Therefore quantifying uncertainty as the geometric mean of the conjoint localization of each filter in the bank does not prove adequate time or frequency resolution for the purpose of the image analysis given in the next chapter.

The arithmetic mean of the time and frequency variances can be considered as the length of the diagonal of a tile in the time-frequency plane. It is clear that the length of this diagonal attains a minimum when the sides are equal. The weighting of the time and frequency localization is based on the frequency domain partitioning of the filter bank construction given in Section 7.1 and will be explained in greater detail later in this section.

Since the filters used in this dissertation are all real-valued, it is necessary to modify the frequency variances of the mid-frequency pass band analysis filters. Since this dissertation is concerned with directly extracting conjoint local features from a signal or image, only the analysis filters are considered. The

synthesis filters are not considered to be directly related to the time-frequency localization, though this will be a topic for future work. Rationale for the modification is easily understood by considering the following theorem.

Theorem 17. The band pass filters $H_1(z), H_2(z), \dots, H_{L-2}(z)$ of an L channel parallel filter bank shown in Fig. 7.4 exhibit zeros at $z = \pm 1$.

Proof: The construction of $H_i(z)$ for $i = 1, 2, \dots, L - 2$ can be described as

$$H_i(z) = G_a(z^{2(L-1-i)}) \prod_{k=1}^{i-1} F_a(z^{2(L-2-i)}).$$

Since $H_i(z)$ is a FIR filter, there are no poles to consider that may cancel out a zero. Since $F_a(z)$ has a zero at $z = -1$, the filter $H_i(z) = (z + 1)p(z)$ for some polynomial $p(z)$ and $z = -1$ is a root of $H_i(z)$. The filter $G_a(z)$ has a zero at $z = 1$, thus $G_a(z) = (z - 1)q(z)$ for some polynomial $q(z)$. The band pass filter can be factored as $H_i(z) = (z^{2(L-1-i)} - 1)\hat{q}(z)$ for some polynomial $\hat{q}(z)$. Thus $H_i(z)$ has a root at $z = 1$. Q.E.D.

Fig. 7.5 shows the magnitude terms of $H_1(z)$ for a four channel parallel filter bank when a Daubechies length six orthogonal QMF is used. The length of the filter is thirty-six¹. Since the filter is real-valued, a conjugate symmetry relationship exists between the *DFT* terms $H_1[k]$ and $H_1[35 - k]$, *i.e.*, $H_1[k] = H_1^*[35 - k]$, where $k = 1, 2, \dots, 16$. Thus the magnitude terms $|H_1[k]|$ and $|H_1[35 - k]|$ for $k = 1, 2, \dots, 16$ are equal. From Fig. 7.5, the term which corresponds to $z = 1$ is $H_1[0]$ and is equal to zero. The term that corresponds to $z = -1$ is $H_1[16]$ and is also zero.

¹The length of each filter in the filter bank will be discussed in the following section.

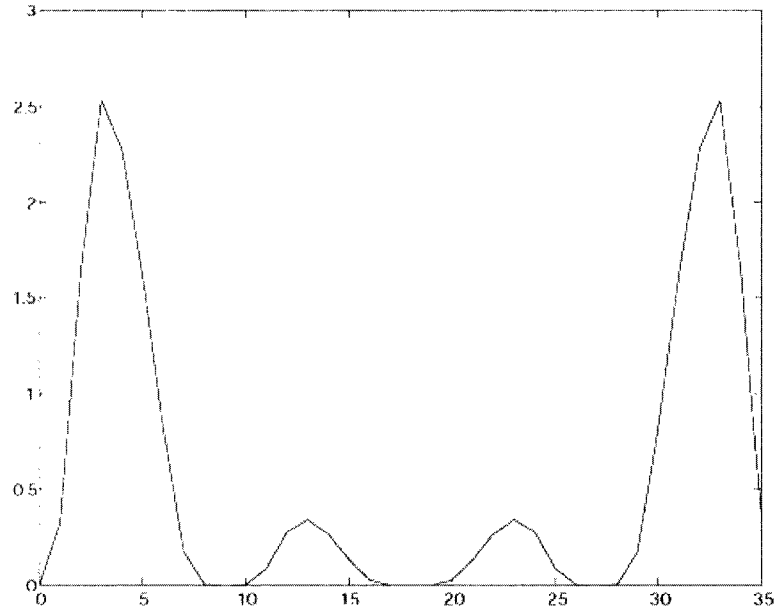


Figure 7.5: The magnitude terms of $H_1(z)$ using a Daubechies length 6 QMF to implement a four-channel parallel filter bank.

In light of Theorem 17 and the fact that the filters will be restricted to be real-value, which will imply conjugate symmetry in the DFT domain, it is only necessary to consider the DFT on the discrete values $0, 1, \dots, \frac{N}{2}$ where $H_i(z)$ is a length- N sequence. To characterize conjoint localization of a L -channel filter bank, let $\langle h \rangle$ be the set of appropriately zeros padded analysis filters in an L -channel parallel filter bank and $\Gamma_L(\langle h \rangle)$ be the weighted arithmetic mean of the modified uncertainty of each analysis filters, *i.e.*,

$$\begin{aligned} \Gamma_L(\langle h \rangle) &= \frac{1}{2} \sigma_{n, [\tilde{\mathbf{h}}_0]}^2 + \frac{1}{2^{L-1}} \sigma_{\omega, [\tilde{\mathbf{h}}_0]}^2 + \frac{1}{2^{L-1}} \sigma_{n, [\tilde{\mathbf{h}}_{L-1}]}^2 + \frac{1}{2} \sigma_{\omega, [\tilde{\mathbf{h}}_{L-1}]}^2 \\ &+ \sum_{i=1}^{L-2} \left(\frac{1}{2^i} \sigma_{n, [\tilde{\mathbf{h}}_i]}^2 + \frac{1}{2^{L-i}} \hat{\sigma}_{\omega, [\tilde{\mathbf{h}}_i]}^2 \right), \end{aligned} \quad (7.1)$$

where $\tilde{h}[n] = \frac{1}{\|\tilde{\mathbf{h}}\|} h[n]$, $\sigma_{n, [\tilde{\mathbf{h}}]}^2$ and $\sigma_{\omega, [\tilde{\mathbf{h}}]}^2$ are defined in equation (4.11) and (4.12),

resp. The quantity $\widehat{\sigma}_{\omega, [\tilde{\mathbf{h}}]}$ is defined as

$$\widehat{\sigma}_{\omega, [\tilde{\mathbf{h}}]}^2 = \min_{l \in [0, \frac{N}{2}]} \left\{ \frac{2}{N} \sum_{k=0}^{\frac{N}{2}} (k - \widehat{\mu}_l)^2 \left| \widehat{H} \left[(k - l) \frac{N}{2} \right] \right|^2 \right\}, \quad (7.2)$$

$$\widehat{H}[k] = \begin{cases} \widetilde{H}[k] & \text{for } k = 0, 1, \dots, \frac{N}{2} \\ 0 & \text{for } k = \frac{N}{2} + 1, \frac{N}{2} + 2, \dots, N - 1, \end{cases} \quad (7.3)$$

$$\widehat{\mu}_l = \sum_{k=0}^{\frac{N}{2}} k \left| \widetilde{H} [(k - l)] \right|^2, \quad (7.4)$$

and $\widetilde{H}[k]$ is the *DFT* of $\widetilde{h}[n]$.

The weighting of the frequency variance is induced by the partitioning of the frequency domain. For example, in the four-channel case, assuming that one-half period of the frequency domain is the unit interval $[0, 1]$, then, using real-valued filters, the three-level wavelet transform partitions the unit interval into $[0, \frac{1}{8}]$, $[\frac{1}{8}, \frac{1}{4}]$, $[\frac{1}{4}, \frac{1}{2}]$, and $[\frac{1}{2}, 1]$ that the pass band of \mathbf{h}_0 , \mathbf{h}_1 , \mathbf{h}_2 , and \mathbf{h}_3 resp., occupies. Thus the frequency variance of $\sigma_{\omega, [\tilde{\mathbf{h}}_0]}^2$ and $\sigma_{\omega, [\tilde{\mathbf{h}}_1]}^2$ are weighted by $\frac{1}{8}$, $\sigma_{\omega, [\tilde{\mathbf{h}}_2]}^2$ is weighted by $\frac{1}{4}$, and $\sigma_{\omega, [\tilde{\mathbf{h}}_3]}^2$ by $\frac{1}{2}$. Since reciprocal relations hold between the time variance and frequency variance, the weightings for the time variances are the exact reverse of the frequency variance weights. Thus the time variances $\sigma_{n, [\tilde{\mathbf{h}}_0]}^2$ and $\sigma_{n, [\tilde{\mathbf{h}}_1]}^2$ are weighted by $\frac{1}{2}$, $\sigma_{n, [\tilde{\mathbf{h}}_2]}^2$ is weighted by $\frac{1}{4}$, and $\sigma_{n, [\tilde{\mathbf{h}}_3]}^2$ is weighted by $\frac{1}{8}$. In general, for an L -channel parallel filter bank, the frequency variances $\sigma_{\omega, [\tilde{\mathbf{h}}_0]}^2$ and $\sigma_{\omega, [\tilde{\mathbf{h}}_1]}^2$ are weighted by $\frac{1}{2^{L-1}}$, $\sigma_{\omega, [\tilde{\mathbf{h}}_2]}^2$ is weighted by $\frac{1}{2^{L-2}}$, $\sigma_{\omega, [\tilde{\mathbf{h}}_3]}^2$ is weighted by $\frac{1}{2^{L-3}}$, \dots , and $\sigma_{\omega, [\tilde{\mathbf{h}}_{L-1}]}^2$ weighted by $\frac{1}{2}$. The time variances $\sigma_{n, [\tilde{\mathbf{h}}_0]}^2$ and $\sigma_{n, [\tilde{\mathbf{h}}_1]}^2$ are weighted by $\frac{1}{2}$, $\sigma_{n, [\tilde{\mathbf{h}}_2]}^2$ is weighted by $\frac{1}{4}$, $\sigma_{n, [\tilde{\mathbf{h}}_3]}^2$ is weighted by $\frac{1}{8}$, \dots , and $\sigma_{n, [\tilde{\mathbf{h}}_{L-1}]}^2$ is weighted by $\frac{1}{2^{L-1}}$.

7.3 Optimal Multi-Channel Filter Bank

In this section optimal L -channel parallel filter banks for $L = 2, 3, 4, 5$ will be determined. The objective function used to define optimal will be to minimize the filter bank uncertainty $\Gamma_L(\langle h \rangle)$ as defined in equation (7.1). These filter banks will be created from a perfect reconstruction QMF. Thus the L -channel parallel filter bank will possess the perfect reconstruction property. Though there are many QMF's, this section will focus on five well known QMF's. They are the length six orthogonal Daubechies QMF (DB_6), the biorthogonal length three low pass analysis with a length five high pass analysis QMF (BO3/5) by Daubechies², the biorthogonal length six low pass analysis with a length two high pass analysis QMF (B06/2), the biorthogonal length four low pass analysis and length four high pass analysis (BO4/4) QMF, and the length six coiflet QMF (Coif). If necessary, the filters which compose the QMF are zero padded to length six for the sake of fair comparison. The four filters that constitute DB_6 , B03/5, B06/2, B04/4, and the Coif QMF are listed in Appendix C.

For a three channel PRPFB, the filters $h_0[n]$ and $h_1[n]$ are longer than $h_2[n]$. In this case the length- N used to determine localization for each filter is the length of $h_0[n]$, which is equal to the length of $h_1[n]$. The filter $h_2[n]$ is zero padded to achieve the proper length. Since I am restricting to QMF's which consist of length six filters, the value N for a three channel filter bank is sixteen. In the four channel case the length of $h_0[n]$ and $h_1[n]$ is thirty-six. The

²This QMF is used in the JPEG 2000 compression standard and is commonly referred to as the biorthogonal 5/3. The analysis and synthesis filters of the biorthogonal 5/3 are respectively the synthesis and analysis filters of the biorthogonal 3/5. The uncertainty measure of the latter is reported, since it yield, a larger weighted arithmetic mean in every case than the former.

analysis filters $h_2[n]$ and $h_3[n]$ are zero padded to length thirty-six. In the five channel case the length of $h_0[n]$ and $h_1[n]$ is seventy-six. The analysis filters $h_2[n]$, $h_3[n]$, and $h_4[n]$ are zero padded to length seventy-six. The appropriately zero padded filters are used to determine the filter bank uncertainty $\Gamma_L(\cdot)$ given in equation (7.1).

Table 7.1 lists the filter bank uncertainties for the two, three, four, and five channel cases. In all cases the Coiflet QMF exhibits the lowest filter bank uncertainty measure. The biorthogonal $B04/4$ yielding the worst filter bank uncertainty.

The length six biorthogonal QMF found in Chapter 6 that minimized $\gamma_{6,\mathbf{f}_a}^2$ does not minimize $\Gamma_L(\langle h \rangle)$. Since I want to show that smaller filter bank weighted uncertainty measure leads to small cumulative reconstruction errors, I do not include the evaluation of the QMF's given in Chapter 6 in this dissertation.

The reconstruction error evaluation in this dissertation is restricted to QMF's composed of length six filters. It is published in [41] that all length six scaling functions of an orthogonal QMF can be defined by two variables, α and β in the following way:

$$\begin{aligned} f_a[0] &= \frac{[(1 + \cos \alpha + \sin \alpha)(1 - \cos \beta - \sin \beta) + 2 \cos \alpha \sin \beta]}{\sqrt{32}}, \\ f_a[1] &= \frac{[(1 - \cos \alpha + \sin \alpha)(1 + \cos \beta - \sin \beta) - 2 \cos \alpha \sin \beta]}{\sqrt{32}}, \\ f_a[2] &= \frac{[1 + \cos(\alpha - \beta) + \sin(\alpha - \beta)]}{\sqrt{8}}, \\ f_a[3] &= \frac{[1 + \cos(\alpha - \beta) - \sin(\alpha - \beta)]}{\sqrt{8}}, \\ f_a[4] &= \frac{1}{\sqrt{2}} - f_a[0] - f_a[2], \end{aligned}$$

	Coif	DB₆	BO6/2	BO3/5	BO4/4
$\Gamma_2(\cdot)$	1.2746	1.3148	1.327	1.3575	1.7666
$\Gamma_3(\cdot)$	5.9007	6.3985	6.5831	7.1363	10.8768
$\Gamma_4(\cdot)$	26.4128	28.6159	30.1205	33.6001	52.664
$\Gamma_5(\cdot)$	113.549	122.1118	130.2016	146.1098	230.0551

Table 7.1: Two, three, four, five channel filter bank uncertainties using the length 6 Coiflet (Coif), Daubechies length 6 (DB_6), the biorthogonal 6/2 (BO6/2), the biorthogonal 3/5 (BO3/5), and the biorthogonal 4/4 (BO4/4), QMFs.

$$f_a[5] = \frac{1}{\sqrt{2}} - f_a[1] - f_a[3].$$

An exhaustive search, where α and β were allowed to vary from $-\pi$ to π was performed with the objective to minimize $\Gamma_5(\cdot)$. The search determined an orthogonal QMF that was nearly exactly equal to the length six Coiflet. The filter bank uncertainty $\Gamma_5(\cdot)$ differed by only one-tenth less than the uncertainty using the length six Coiflet QMF. Since the filter bank uncertainty of the QMF found in the search is nearly equal to the length six Coiflet QMF, I proclaim the Coiflet QMF the optimal five channel PRPFB from the set of the five QMFs in consideration.

Chapter 8

Image Analysis

The final goal of this dissertation is to recover a real value image from its amplitude and frequency modulations. To accomplish this, the real valued image \mathbf{I} and the directional two dimensional Hilbert transform of the image \mathbf{H} multiplied by the imaginary unit j are summed to produce the analytic image \mathbf{S} . The analytic image \mathbf{S} is defined as

$$S[n, m] = I[n, m] + jH[n, m] \quad (8.1)$$

where $I[n, m]$ is the original image and $H[n, m]$ is the directional two dimensional Hilbert transform of $I[n, m]$. This dissertation does not cover the details of the discrete version of the directional two dimensional Hilbert transform. The discrete theory of the directional two dimensional Hilbert transform is treated comprehensively in [11].

8.1 Analysis and Synthesis Algorithm

The analytic image \mathbf{S} is passed through a multi-channel analysis filter bank to separate spectral components. The filter bank needs spectral localization to residue components and needs spatial localization to capture local image features. In gist, the filter bank must be conjointly well-localized in the spatial

and spectral domains to capture the local features inherent to the image. It is desirable to be able to recreate the original image from the outputs of the analysis filter bank so that no information is lost. The filter bank must provide an adequate number of subband channels to resolve the frequency contents of the image. These considerations justify the use of the L -channel filter banks constructed from the Coiflet QMF. Since in Section 7.3, the filter bank constructed using the Coiflet QMF attained smaller filter bank uncertainty $\Gamma_L(\cdot)$. Eventhough the L -channel PRPFB were constructed to render perfect reconstruction, regardless of their uncertainty measure, it is expected and is shown that the filter bank constructed using the length six Coiflet QMF results in smaller reconstruction errors. In the evaluation used in this dissertation, the original image \mathbf{I} is reproduced as the real part of the sum of the analytic subband images at the output of the synthesis filter bank,

$$\begin{aligned} I[n, m] &= \operatorname{Re} \left[\sum_{l,k=0}^{L-1} S_{l,k}[n, m] \right] \\ &= \operatorname{Re} \left[\sum_{l,k=0}^{L-1} (I_{l,k}[n, m] + jH_{l,k}[n, m]) \right] \\ &= \sum_{l,k=0}^{L-1} I_{l,k}[n, m] \end{aligned}$$

where $\mathbf{S}_{l,k}$ is the output image of channel $C_{l,k}$. Channel $C_{l,k}$ is defined to be filtering the rows of the input image \mathbf{S} by $H_l(z)$, followed by filtering the columns of \mathbf{S} by $H_k(z)$. After the appropriate downsampling and upsampling, the columns are filtered by $\tilde{H}_k(z)$ then filtering the rows by $\tilde{H}_l(z)$ produces the output $\mathbf{S}_{l,k} = \mathbf{I}_{l,k} + j\mathbf{H}_{l,k}$.

Though the real part of the sum of all the $\mathbf{S}_{l,k}$ produces the the original real-valued image \mathbf{I} , the down sampling and up sampling between the analysis

filter bank and the synthesis filter bank are not shift invariant and dramatically changes the spectrum at the output of the analysis filter bank. The dramatic and unpredictable change to the spectrum occurs when down sampling. It is difficult, if not impossible, to determine the *DFT* of the down sampled signal/image from the *DFT* of the signal/image prior to down sampling. The *DFT* of the upsampled signal/image is easily determined as multiple periods of the *DFT* of the signal/image post down sampling and prior to up sampling. In turn, the frequency resolution at the output of the synthesis filter bank is inadequate for determining instantaneous amplitudes and frequencies.

Let $\widehat{\mathbf{S}}_{l,k}$ be the output image of the analysis filter bank prior to down-sampling. If transient stages are ignored, this image is the same dimension as the original image. Since the goal is to describe an image in terms of its instantaneous amplitudes and frequencies, attaining a full resolution image is important. The five channel filter bank created by the Coiflet QMF as described in Chapter 7 provides the best trade off not only for the conjoint localization of each filter in the analysis filter bank but also inter-filter relationships within the analysis filter bank are accounted for by $\Gamma_L(\cdot)$ given in equation (7.1). The images immediately at the output of the analysis filter bank prior to downsampling achieves the best time-frequency resolution. In addition, perfect reconstruction is still possible.

The implementation of the analysis filter bank is performed in the *DFT* domain. Precisely the impulse response of the separable analysis filter is zero padded to the dimensions of the original image. The filter is transformed into the *DFT* domain. The *DFT* of the non-low pass filters $\mathbf{H}_{l,k}$ where $l \neq 0$ and $k \neq 0$ are split to provide orientation selectivity. This is required to separate

image features which reside in the same subband but are perpendicular into different channels. This separation is necessary, otherwise, it would result in components with poor local coherency, causing large demodulation errors. The result of the split produces filters $\mathbf{H}_{l,k,t}$ and $\mathbf{H}_{l,k,b}$. The support of $\mathbf{H}_{l,k,t}$ consists of quadrants I and III of the two dimensional DFT domain. The support of $\mathbf{H}_{l,k,b}$ is quadrants II and IV of the two dimensional DFT domain. To illustrate, Fig. 8.1 shows the log magnitude spectrum ¹ of the channel $H_{3,3}(z)$. The spectrum has been shifted so that the origin is in the center of the image. Fig. 8.2 show the output of the $H_{3,3}(z)$ using the *lena* image. It is quite notice-

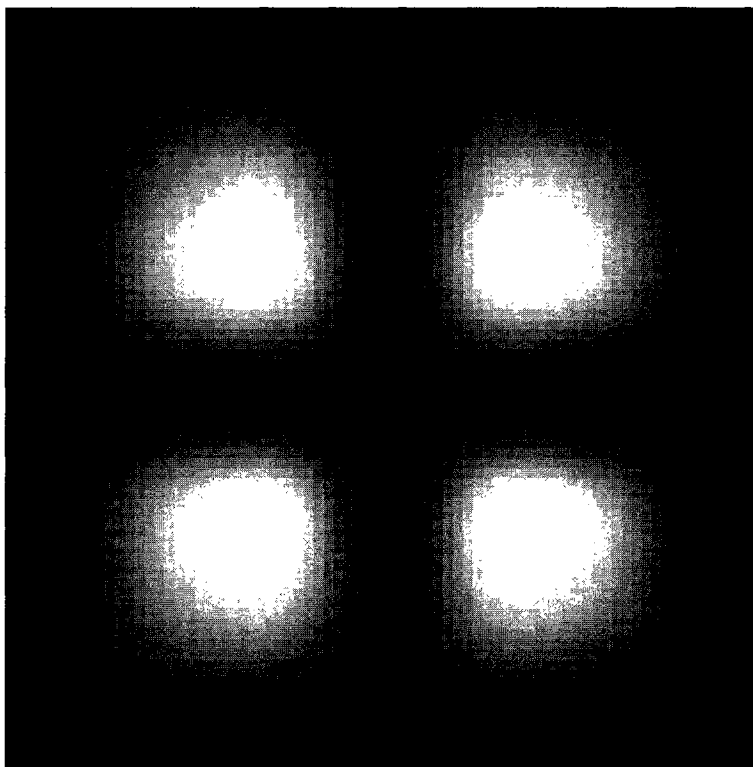


Figure 8.1: Log magnitude spectrum of $H_{3,3}(z)$.

¹The log magnitude spectrum of channel $H_{i,j}(z)$ is defined as $\log(1 + |H_{k,l}[n, m]|)$.

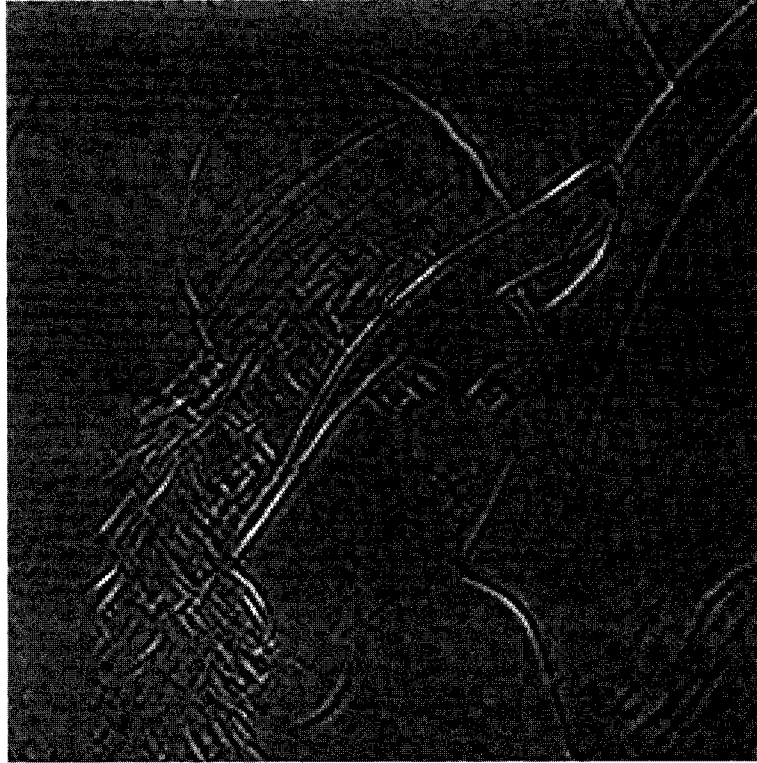


Figure 8.2: Output of $H_{3,3}(z)$ using the *lena* image.

able even to the untrained that the image consists of perpendicular edges and features, which results in poor local coherency and eventually large demodulation errors in the reconstruction. This problem is easily remedied, since the non-low pass channels, *i.e.*, $H_{k,l}(z)$ for $k \neq 0$ and $l \neq 0$, is zero on the axis of the shifted spectrum. This is due to Theorem 17 and the separable construction of the filter bank. The non-low pass channel can be split in two separate channels each with different orientation. This split is illustrated in Figs 8.3 and 8.4 which shows the shifted log magnitude spectrum of channel $H_{3,3,t}(z)$ and $H_{3,3,b}(z)$, *resp.* The channel $H_{3,3}(z)$ can be recreated by adding $H_{3,3,t}(z)$ with $H_{3,3,b}(z)$. It is evident from Figs 8.5 and 8.6 that splitting the channel into orientation selective channels separates perpendicular edges and features.

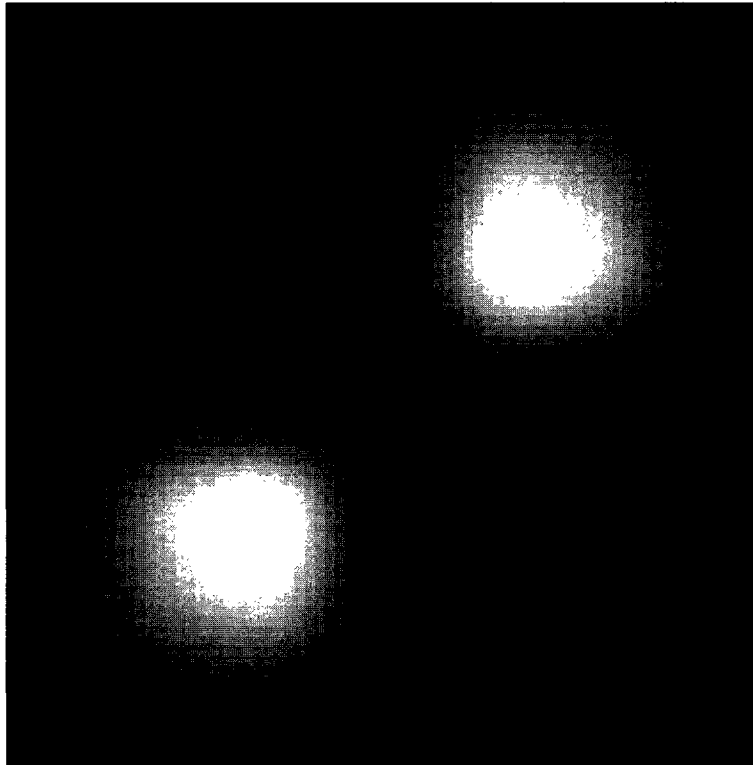


Figure 8.3: Log magnitude spectrum of $H_{3,3,t}(z)$.

For example, the top edge of *lena*'s hat and the edge on the brim of her hat, which are perpendicular edges, are separated into different channels. Thus the non-low pass channels are made orientation selective in this manner. It should be pointed out that the orientation selective channels are no longer separable. Most importantly, the splitting did not effect the localization of the channel.

Splitting the non-low pass filters in this manner produces a filter bank of forty-one channels in which the non-low pass channels are non-separable. The complex output of the forty-one channel filter bank is determined by multiplying the two dimensional *DFT* of the analytic image \mathbf{S} with the two dimensional *DFT* of filter $\mathbf{H}_{l,k,x}$ where $l, k \in [1, 4]$, $x \in \{t, b\}$ or to the filter $\mathbf{H}_{l,k}$, if either

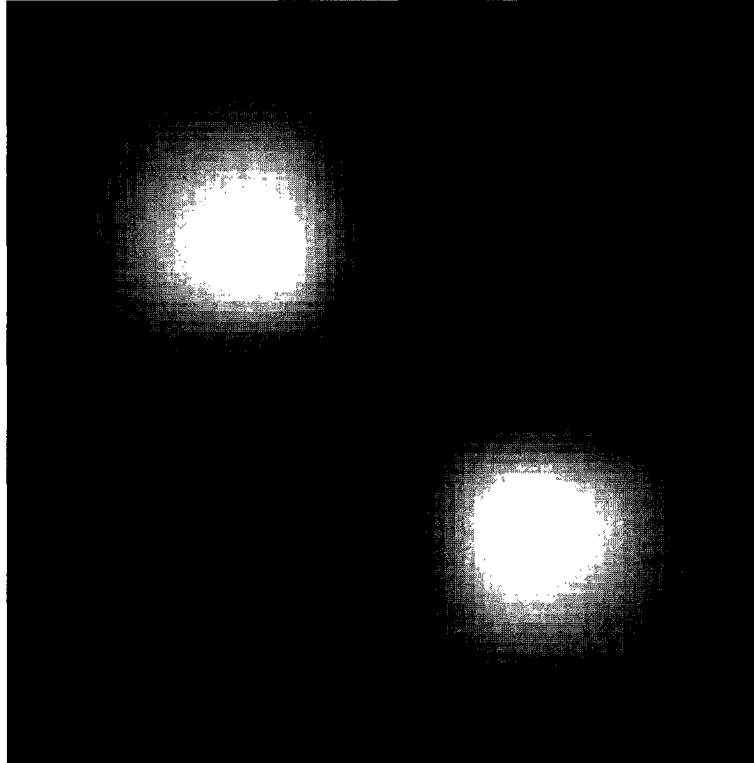


Figure 8.4: Log magnitude spectrum of $H_{3,3,b}(z)$.

l or k is equal to zero. The complex images $\widehat{\mathbf{S}}_{l,k,x}$ and $\widehat{\mathbf{S}}_{l,k}$ are the outputs of the forty-one channel analysis filter bank.

The analysis filter bank complex output images $\widehat{\mathbf{S}}_{l,k,x}$ and $\widehat{\mathbf{S}}_{l,k}$ are used to determine the amplitude and frequency modulation components of the original image \mathbf{I} . The method used to determine frequency component of each pixel from the frequency modulation component of $\widehat{\mathbf{S}}_{l,k,x}$ and $\widehat{\mathbf{S}}_{l,k}$ is given in [10]. Let $\mathbf{A}_{l,k,x}$ and $\mathbf{A}_{l,k}$ be the images after AM-FM demodulation. If $\mathbf{A}_{l,k,x} = \widehat{\mathbf{S}}_{l,k,x}$ and $\mathbf{A}_{l,k} = \widehat{\mathbf{S}}_{l,k}$ for all $l, k = 0, 1, 2, 3, 4$ and $x = t, b$ then this algorithm produces a perfect reconstruction of the original image \mathbf{I} . Generally this is not the case. Rather $\mathbf{A}_{l,k,x} \approx \widehat{\mathbf{S}}_{l,k,x}$ and $\mathbf{A}_{l,k} \approx \widehat{\mathbf{S}}_{l,k}$ and the AM-FM demodulation

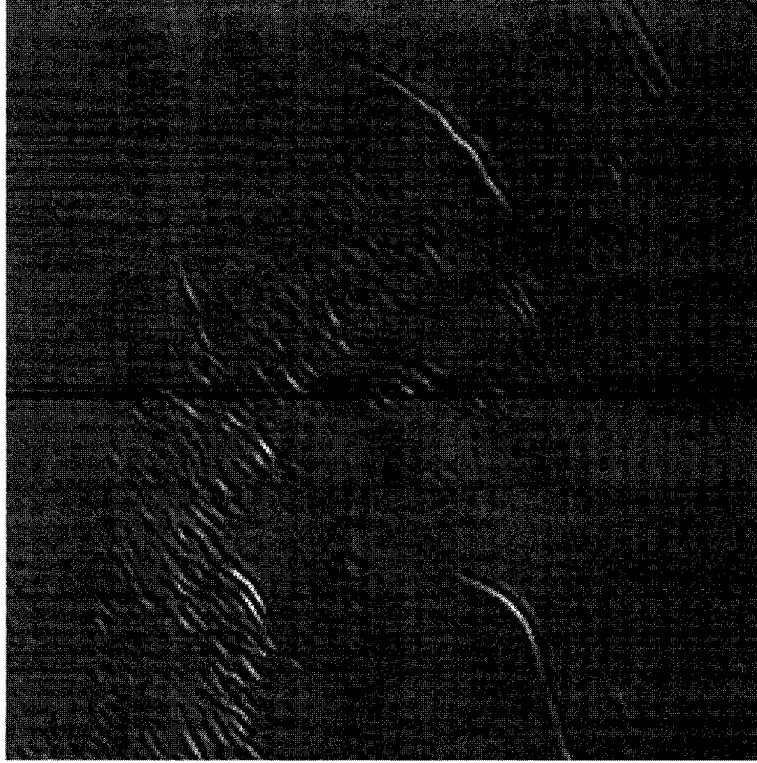


Figure 8.5: Output of $H_{3,3,t}(z)$ using *lena* image.

of Havlicek, Harding, and Bovik introduces errors in the reconstruction. To prevent large reconstruction errors, I allow $A_{l,k,x}[4m, 4n] = \widehat{S}_{l,k,x}[4m, 4n]$ and $A_{l,k}[4m, 4n] = \widehat{S}_{l,k}[4m, 4n]$. This ensure that errors do not propropagate pass a four by four grid.

The error compensation stage of this algorithm does not account for errors associated with the AM-FM demodulation. The error compensation stage is needed to correct errors associated with the implementation of the analysis and synthesis filter banks. The five channel parallel analysis filter bank is equivalent to cascading a QMF at four levels via the Noble identities. This equivalence holds for linear convolution. The implementation of the analysis

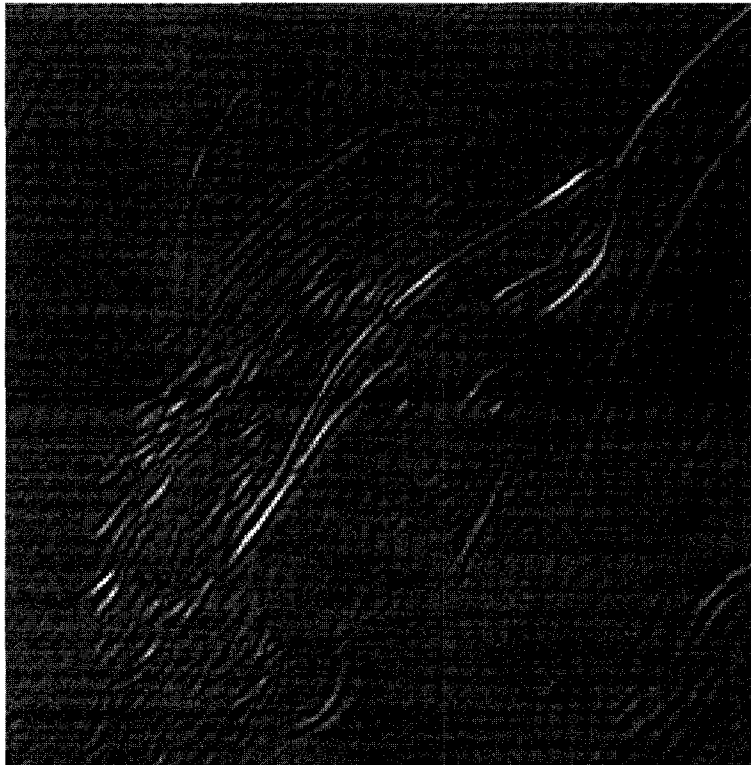


Figure 8.6: Output of $H_{3,3,b}(z)$ using *lena* image.

filter bank is via multiplication in the *DFT* domain, which is dual operation of circular convolution in the time/space domain. Thus there are wrap around errors which need to be removed to preserve perfect reconstruction.

After the error compensation stage the images are appropriately upsampled. The real part of the sum of the outputs of the synthesis filters gives the reconstructed image $J[n, m]$. Fig. 8.7 show the image analysis and synthesis algorithm used.

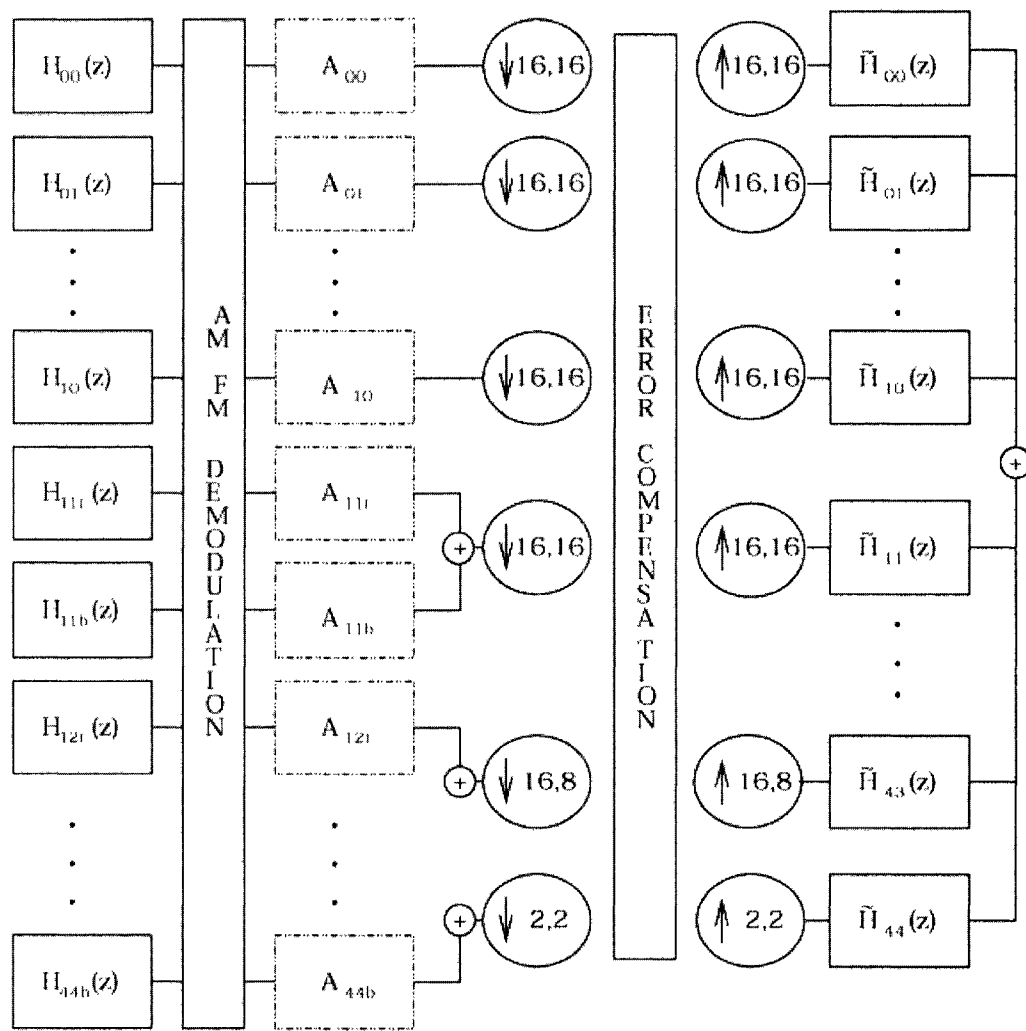


Figure 8.7: The image analysis algorithm.

8.2 Evaluation Using Some Well-Known QMF's

Several well known QMFs, the length six orthogonal Coiflet (Coif), the length six Daubechies orthogonal (DB_6), the biorthogonal length six lowpass analysis and length-two high pass analysis (BO6/2), the biorthogonal length three lowpass analysis and length five high pass analysis (BO3/5), and the length four biorthogonal (BO4/4) QMFs were tested. The criteria to judge the performance of each filter bank is the reconstruction cumulative squared error (CSE) which is defined as

$$CSE = \sum_{n,m=0}^{N,M} |I[n, m] - J[n, m]|^2. \quad (8.2)$$

The test images used in this evaluation are the 256×256 *lena*, *girl*, *gauss*, *burlap*, *mandril*, *mandril*, *clown*, *salesman*, *lady*, *baby*, and *Building0010* images. The pixel values of all the images are scaled to be zero mean and range from -1 to 1.

The original *lena* image is shown in Fig. 8.8. Table 8.1 shows the reconstruction CSE associated with each QMF. It is shown that using the Coiflet QMF produces the smallest CSE , followed by using the DB_6 QMF, followed by BO6/2, followed by BO3/5, followed by BO4/4 which has the largest CSE of all the QMFs tested. Comparing the result of Table 8.1 with the results of Table 7.1, we see that the same relation hold for CSE and filter bank uncertainty $\Gamma_5(\cdot)$.

Fig. 8.9 shows the best reconstruction of *lena* produced using a Gabor filter bank. This image has extensively been post processed. The *lena* image in Fig. 8.10 shows the reconstructed image using the length six Coiflet QMF. This image has the smallest reconstruction CSE and no post processing was done

	Coif	DB ₆	BO6/2	BO3/5	BO4/4
<i>CSE</i>	216.76	237.94	365.29	370.6	11083

Table 8.1: Reconstruction *CSE* of *lena* using the length six Coiflet (Coif) QMF, the Daubechies length 6 (DB_6) QMF, the biorthogonal 3/5 QMF (BO3/5), the biorthogonal 6/2 QMF (BO6/2), the biorthogonal 4/4 QMF (BO4/4).

	Coif	DB ₆	BO6/2	BO3/5	BO4/4
<i>CSE</i>	358.26	378.32	386.66	407.54	10393

Table 8.2: Reconstruction *CSE* of *girl* using the length six Coiflet (Coif) QMF, the Daubechies length 6 (DB_6) QMF, the biorthogonal 3/5 QMF (BO3/5), the biorthogonal 6/2 QMF (BO6/2), the biorthogonal 4/4 QMF (BO4/4).

on this image. This image looks somewhat washed out, but this is due to large errors on a few pixels effecting the dynamic range when the image is contrast stretched. Nonetheless, the overall image has the least *CSE*. Fig. 8.11 shows the *lena* image reconstructed using the length six Daubechies orthogonal QMF, DB_6 . The reconstruction error *CSE* is not much worse than the reconstruction error using the Coiflet. The image quality of the two are roughly the same.

Table 8.2 lists the reconstruction *CSE* of the *girl* image shown in Fig. 8.12. This table shows the relationship of the reconstruction *CSE*'s is the same as the relationship of the filter bank uncertainties. The data in this table re-enforcing the notion that smaller filter bank uncertainty translates to smaller reconstruction errors.

Table 8.3 lists the *CSE* of the *gauss* image shown in Fig. 8.13.

Again, the results of Table 8.3 shows that smaller filter bank uncertainty implies smaller reconstruction *CSE*.

Table 8.4 lists the reconstruction *CSE* of the *burlap* image shown in



Figure 8.8: The original *lena* image.

	Coif	DB_6	BO6/2	BO3/5	BO4/4
<i>CSE</i>	14296	14463	15429	18867	87899

Table 8.3: Reconstruction *CSE* of *gauss* using the length six Coiflet (Coif) QMF, the Daubechies length 6 (DB_6) QMF, the biorthogonal 3/5 QMF (BO3/5), the biorthogonal 6/2 QMF (BO6/2), the biorthogonal 4/4 QMF (BO4/4).

	Coif	DB_6	BO6/2	BO3/5	BO4/4
<i>CSE</i>	928.09	1117.7	1785.3	2516	82271

Table 8.4: Reconstruction *CSE* of *burlap* using the length six Coiflet (Coif) QMF, the Daubechies length 6 (DB_6) QMF, the biorthogonal 3/5 QMF (BO3/5), the biorthogonal 6/2 QMF (BO6/2), the biorthogonal 4/4 QMF (BO4/4).



Figure 8.9: The best reconstructed *lena* image using Gabor filter bank.



Figure 8.10: Reconstructed *lena* image using Coiflet QMF filter bank.



Figure 8.11: Reconstructed *lena* image using DB_6 QMF filter bank.



Figure 8.12: The original *girl* image.

Fig. 8.14. Once again, my theory is supported by the data of Table 8.4. In addition, I can give a subjective comparison with the reconstruction using a Gabor filter bank ² Fig. 8.15 is the reconstructed *burlap* image when a Gabor filter bank was used to determine the AM-FM image modulations. This image has undergone extensive post processing to arrive at the reconstruction seen in Fig. 8.15. The image shown in Fig. 8.16 is the reconstructed *burlap* image using the orthogonal Coiflet QMF. Though this image may seem washed, *i.e.*, poor contrast, the reconstruction *CSE* is still less than using the other filter banks, which are not as well-localized. Poor contrast is due to a few pixels exhibiting

²Comparison on some images are only available, if my committee chair, Professor Joe Havlicek, has not lost the image in a past hard disk failure.

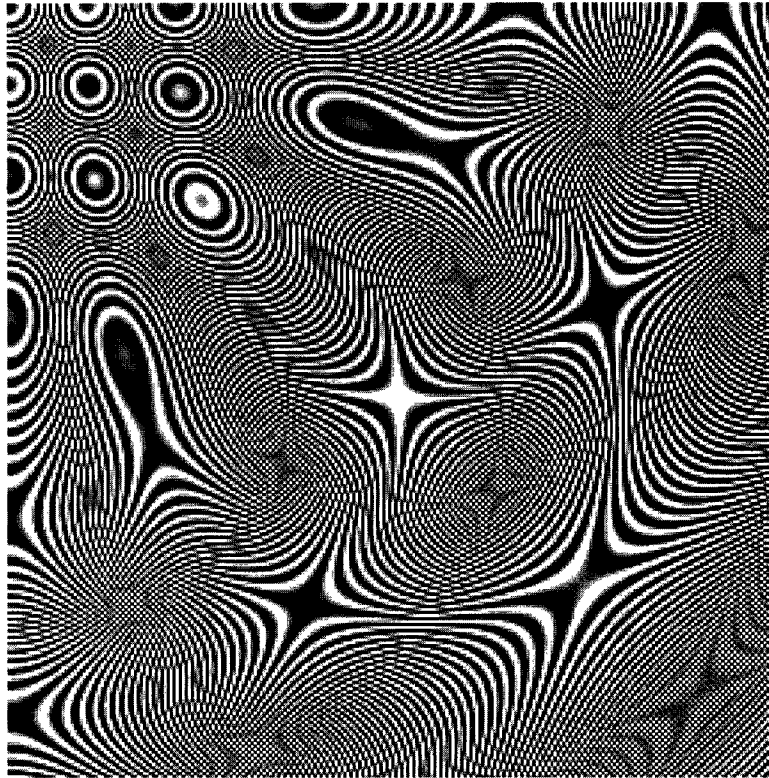


Figure 8.13: The original *gauss* image.

large errors that is not accounted for when contrasted stretched. Thus effecting the dynamic range of the reconstructed image. The image in Fig. 8.17 is the reconstructed *burlap* image using the orthogonal length-six QMF, DB_6 . The reconstruction error of this image is greater than the image in Fig. 8.16 which is consistent with the filter bank uncertainty of DB_6 being greater than the filter bank uncertainty of the Coiflet QMF.

Table 8.5 lists the reconstruction *CSEs* of the *mandril* image shown in Fig. 8.18. Since the extensively post processed reconstructed *mandril* image using Gabor filter bank is available, a comparison is given. Fig. 8.19 is subjectively the best reconstructed *mandril* image when a Gabor filter bank was used in determining the AM-FM modulations. When comparing this image with the

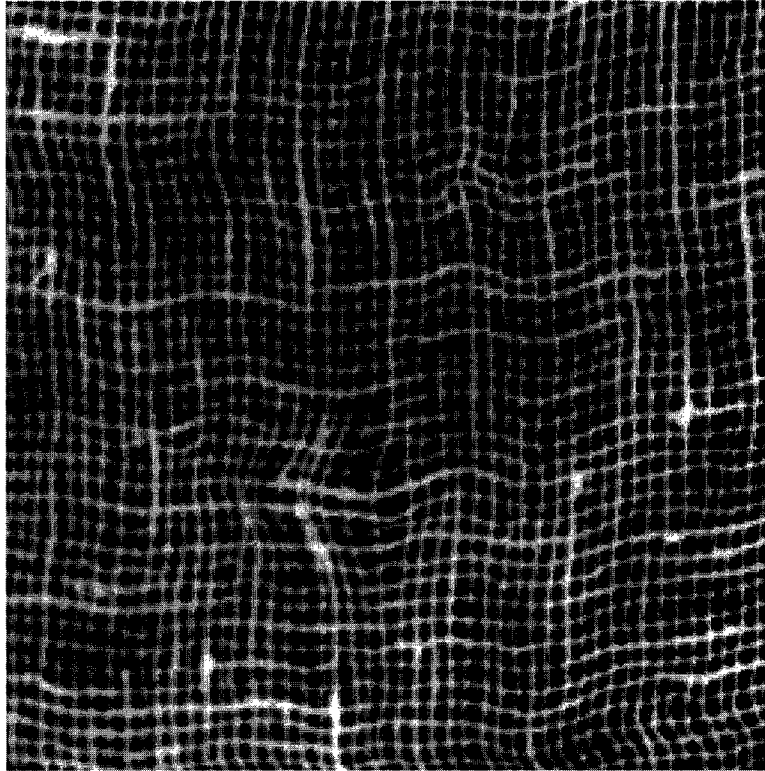


Figure 8.14: The original *burlap* image.

	Coif	DB_6	BO6/2	BO3/5	BO4/4
<i>CSE</i>	351.31	339.44	568.48	576.46	11503

Table 8.5: Reconstruction *CSE* of *mandril* using the length six Coiflet (Coif) QMF, the Daubechies length 6 (DB_6) QMF, the biorthogonal 3/5 QMF (BO3/5), the biorthogonal 6/2 QMF (BO6/2), the biorthogonal 4/4 QMF (BO4/4).

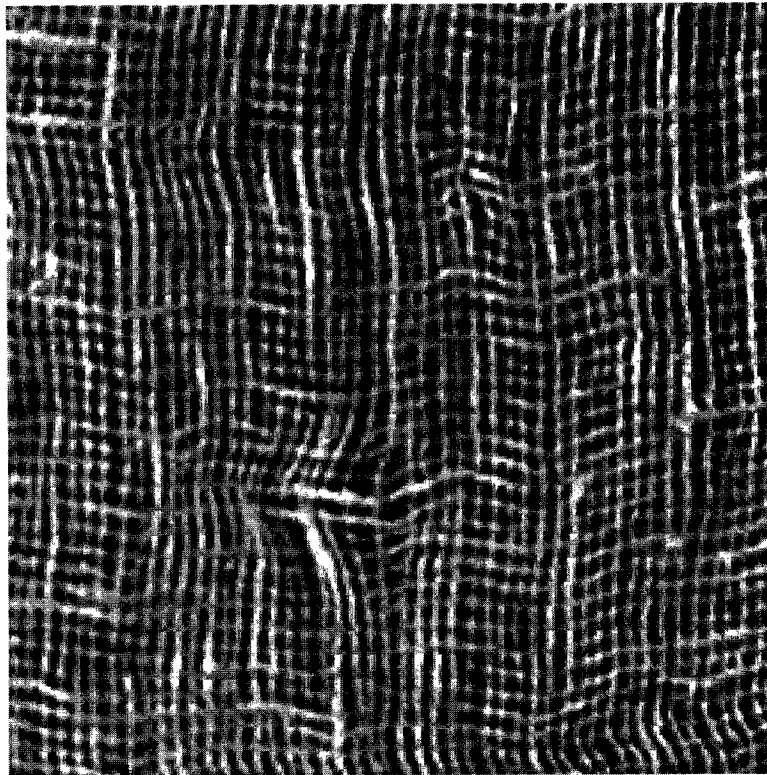


Figure 8.15: The best reconstructed *burlap* image using Gabor filter bank.

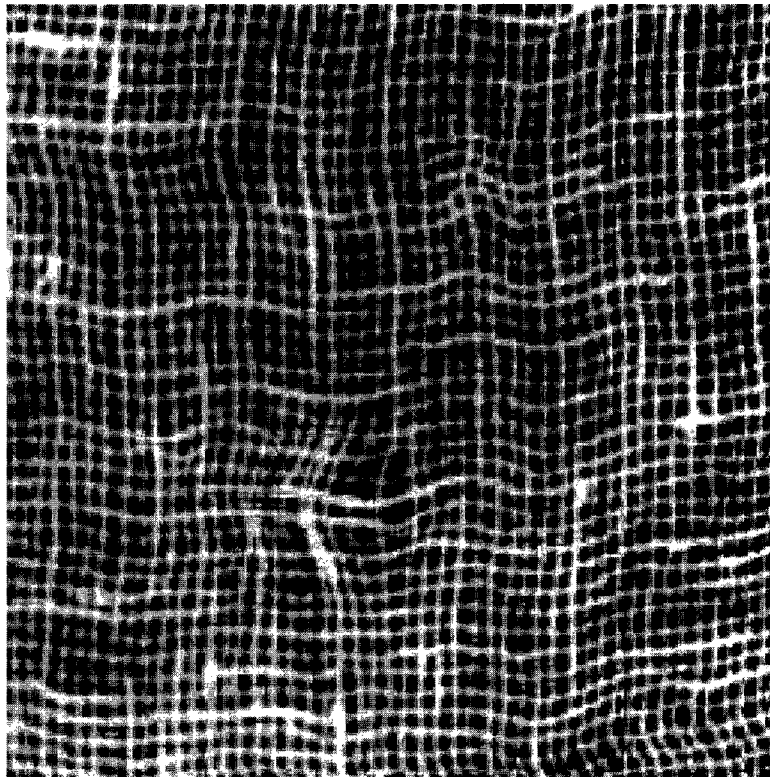


Figure 8.16: Reconstructed *burlap* image using Coiflet QMF filter bank.

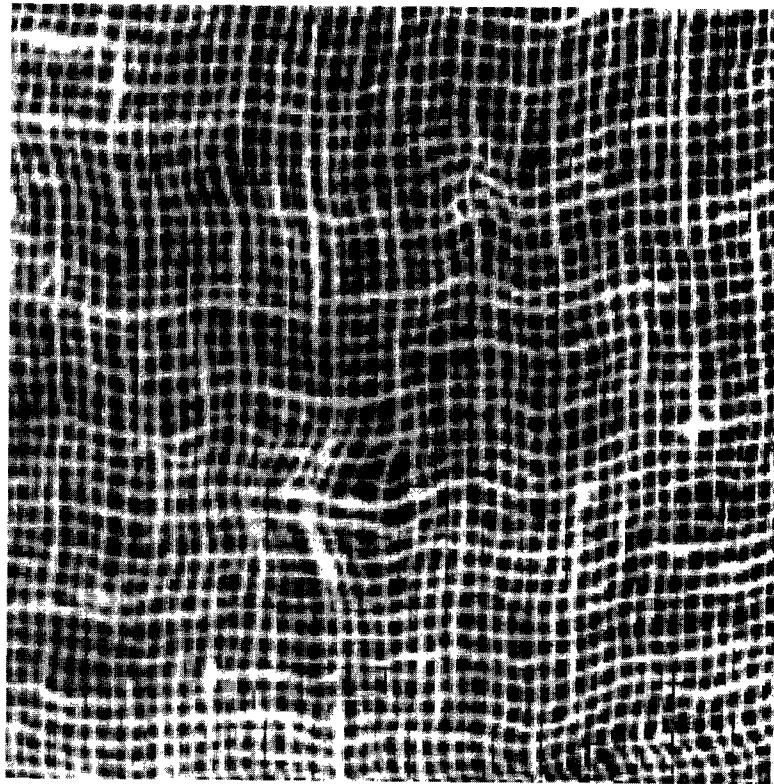


Figure 8.17: Reconstructed *burlap* image using DB_6 QMF filter bank.

	Coif	DB ₆	BO6/2	BO3/5	BO4/4
<i>CSE</i>	149.11	161.96	311.93	268.71	9949.3

Table 8.6: Reconstruction *CSE* of *clown* using the length six Coiflet (Coif) QMF, the Daubechies length 6 (DB_6) QMF, the biorthogonal 3/5 QMF (BO3/5), the biorthogonal 6/2 QMF (BO6/2), the biorthogonal 4/4 QMF (BO4/4).

original *mandril* image, noticeable intercomponent interference can be detected on the cheeks just below the eyes. In addition, there is blurring of the uncorrelated noise like texture of the hair. The contrasted stretched reconstructed *mandril* image using the Coiflet QMF can be seen in Fig. 8.20. The contrast stretched reconstructed *mandril* using the orthogonal DB_6 QMF is shown in Fig. 8.21. The reconstruction *CSE* using the Coiflet QMF is slightly and uncharacteristically larger than the reconstruction *CSE* using the DB_6 QMF. The subjective differences between the two images is impossible to detect.

Table 8.6 lists the reconstruction *CSE* of the *clown* image shown in Fig. 8.22. In this example, the reconstruction *CSE* using the biorthogonal BO3/5 QMF is less than the reconstruction *CSE* of biorthogonal BO6/2 QMF. This relationship is the reverse of their filter bank uncertainty, $\Gamma_5(\cdot)$. Nevertheless the reconstruction *CSE*s using the Coiflet and DB_6 QMF out performs the other three QMFs with the Coiflet reconstruction *CSE* being less than the DB_6 reconstruction *CSE*.

Table 8.7 lists the reconstruction *CSE* of the *salesman* image shown in Fig. 8.23. Fig.s 8.24, 8.25, and 8.26 shows the reconstructed *salesman* using a Gabor filter bank, using the Coiflet QMF, and using DB_6 QMF, *resp.* The reconstructed image using the Gabor filter bank has been extensively post

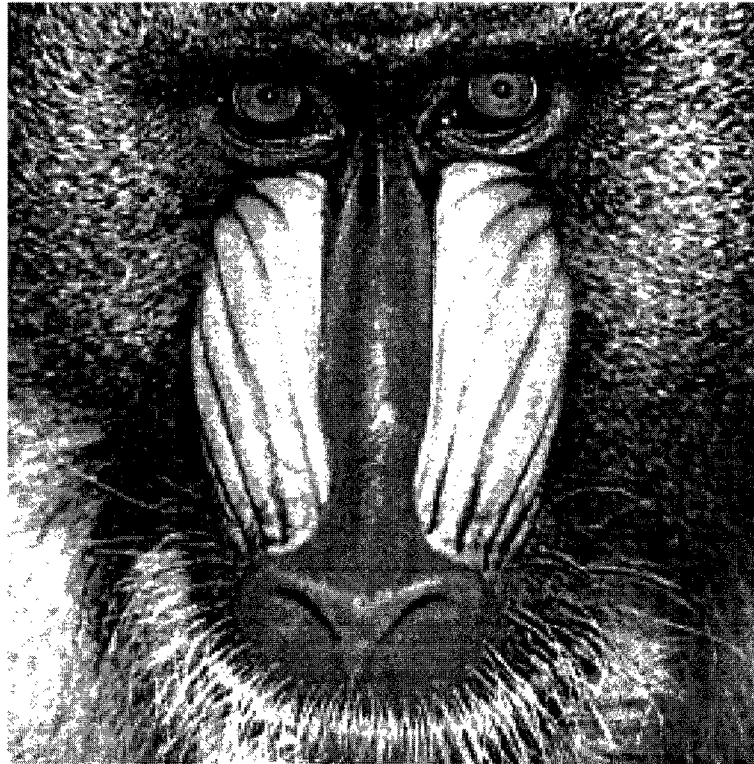


Figure 8.18: The original *mandril* image.

	Coif	DB_6	BO6/2	BO3/5	BO4/4
<i>CSE</i>	85.56	133.83	129.77	129.93	4246.8

Table 8.7: Reconstruction *CSE* of *salesman* using the length six Coiflet (Coif) QMF, the Daubechies length 6 (DB_6) QMF, the biorthogonal 3/5 QMF (BO3/5), the biorthogonal 6/2 QMF (BO6/2), the biorthogonal 4/4 QMF (BO4/4).

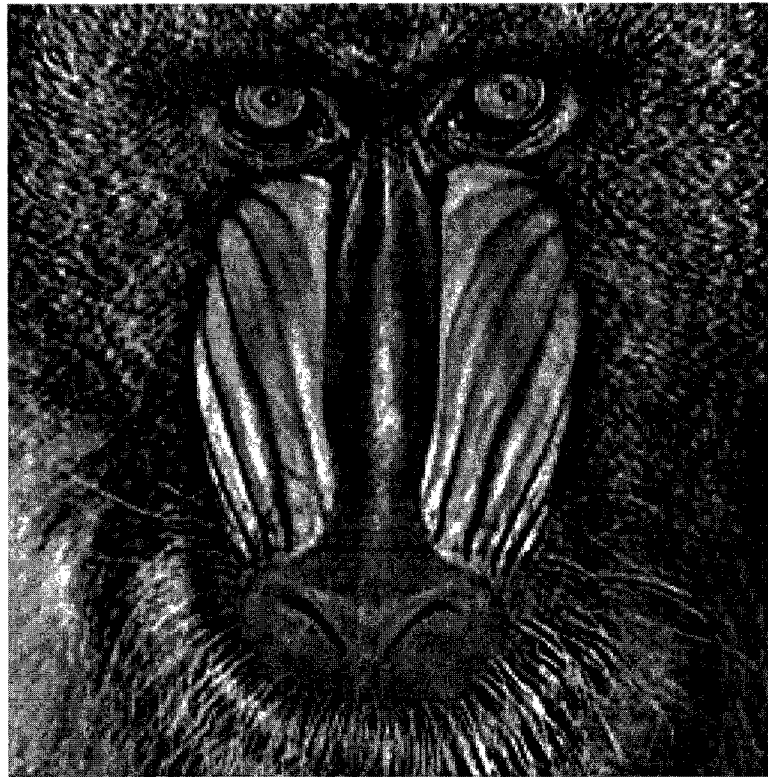


Figure 8.19: The best reconstructed *mandril* image using Gabor filter bank.

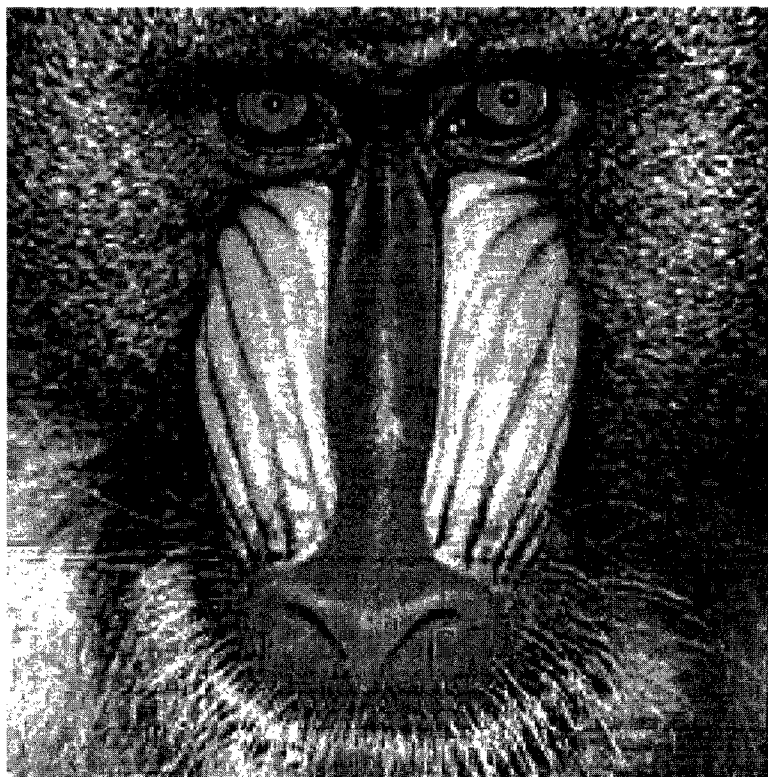


Figure 8.20: Reconstructed *mandril* image using Coiflet QMF filter bank.

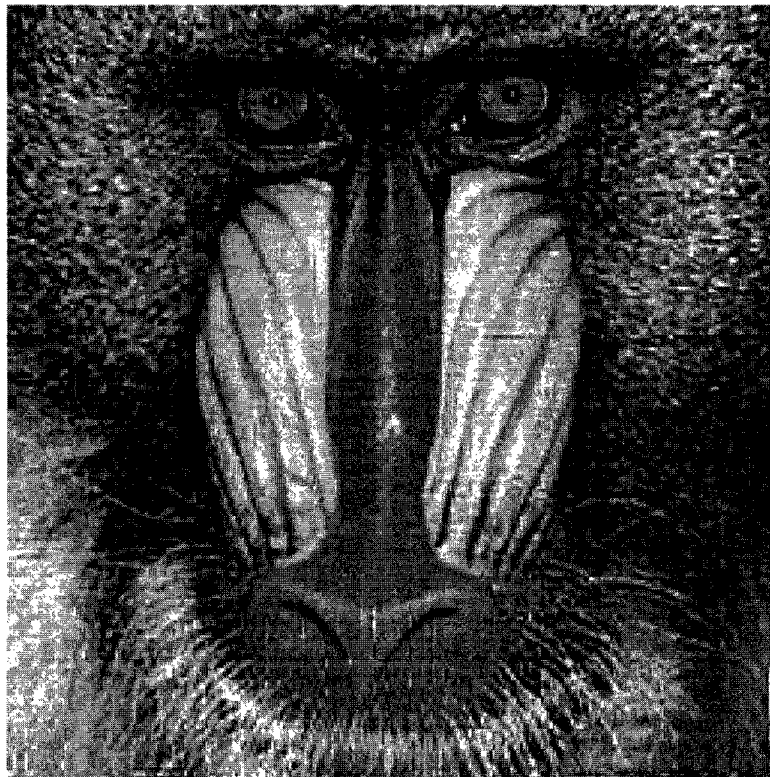


Figure 8.21: Reconstructed *mandril* image using DB_6 QMF filter bank.



Figure 8.22: The original *clown* image.

	Coif	DB ₆	BO6/2	BO3/5	BO4/4
<i>CSE</i>	16.7	10.32	31.6	23.94	1477

Table 8.8: Reconstruction *CSE* of *lady* using the length six Coiflet (Coif) QMF, the Daubechies length 6 (DB_6) QMF, the biorthogonal 3/5 QMF (BO3/5), the biorthogonal 6/2 QMF (BO6/2), the biorthogonal 4/4 QMF (BO4/4).

	Coif	DB ₆	BO6/2	BO3/5	BO4/4
<i>cse</i>	164.8	153.65	154.31	213.02	2392

Table 8.9: Reconstruction *CSE* of *baby* using the length six Coiflet (Coif) QMF, the Daubechies length 6 (DB_6) QMF, the biorthogonal 3/5 QMF (BO3/5), the biorthogonal 6/2 QMF (BO6/2), the biorthogonal 4/4 QMF (BO4/4).

processed. Ringing effects are noticeable and intercomponent interference are detectable in the reconstructed image using a Gabor filter bank. The reconstruction *CSE* of the DB_6 is slightly larger than the *CSE* of BO6/2 and BO3/5. The reconstruction *CSE* of the optimally localized orthogonal Coiflet is distinctly lower than the others.

Table 8.8 lists the reconstruction *CSE* of the *lady* image shown in Fig. 8.27. The reconstruction *CSE* for the *lady* image using the any of the QMF except BO4/4 is such a small quantity, I consider the reconstruction to be perfect in all four cases.

Table 8.9 lists the reconstruction *CSE* of the *baby* image shown in Fig. 8.28. Though the reconstruction *CSEs* are unusually permuted, I do not consider the differences in the reconstruction error great enough to exclude this case as an example.

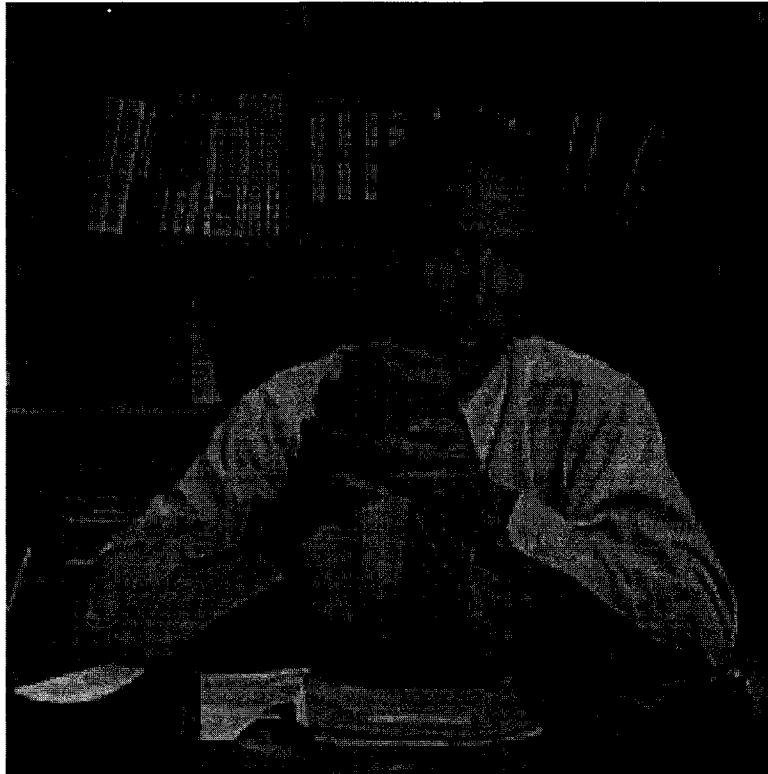


Figure 8.23: The original *salesman* image.

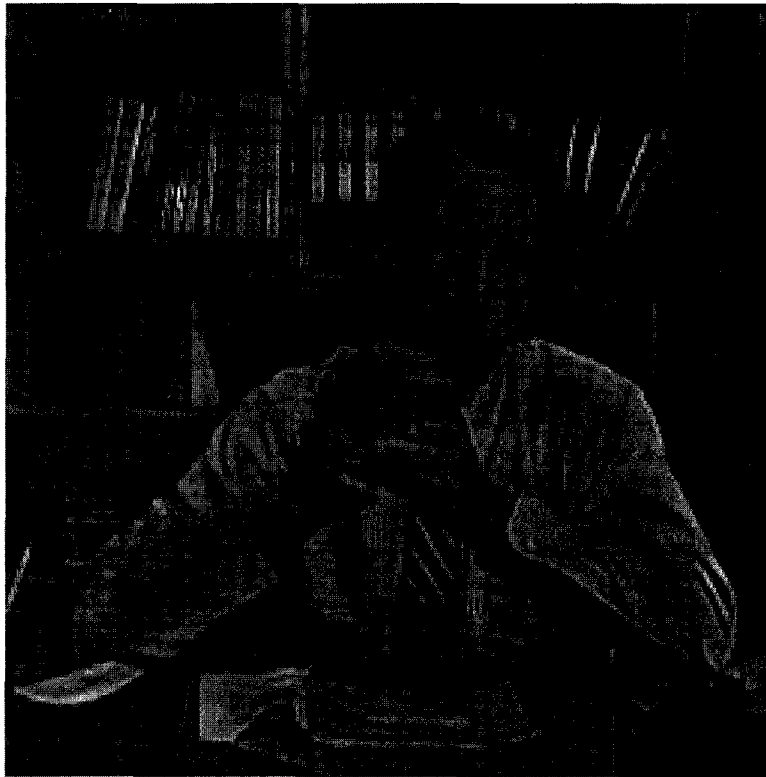


Figure 8.24: The best reconstructed *salesman* image using Gabor filter bank.

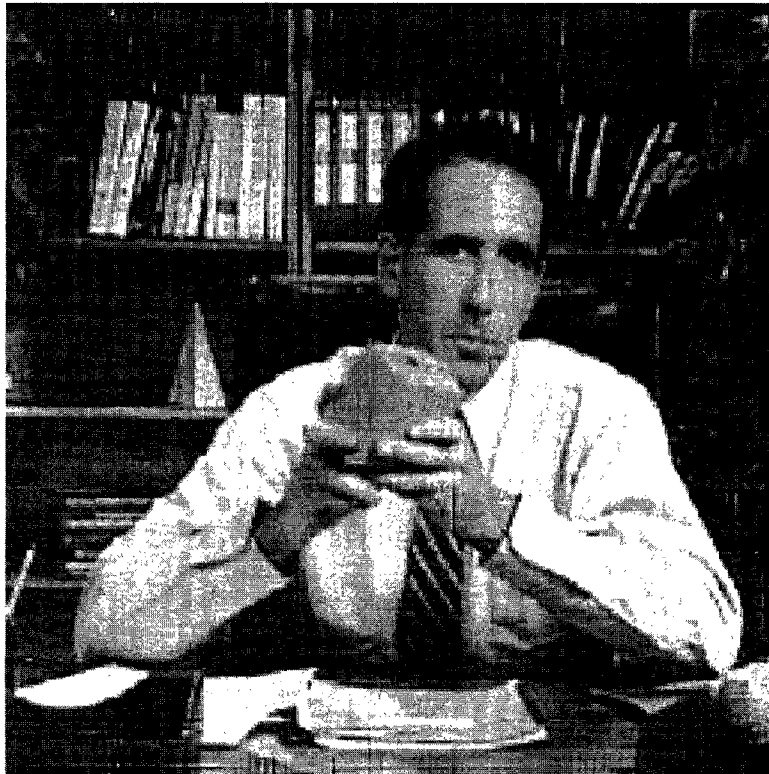


Figure 8.25: Reconstructed *salesman* image using Coiflet QMF filter bank.

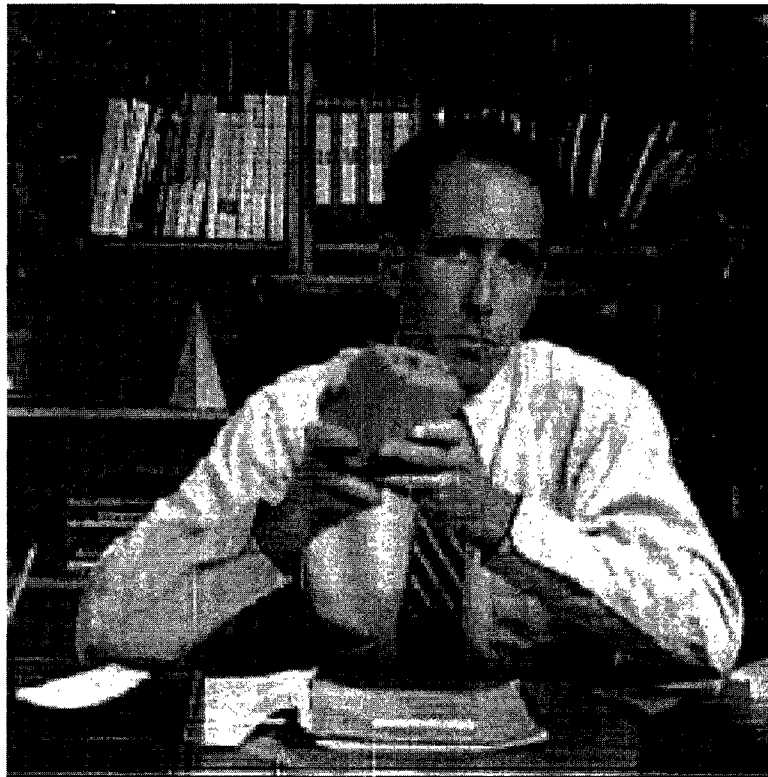


Figure 8.26: Reconstructed *salesman* image using DB_6 QMF filter bank.



Figure 8.27: The original *lady* image.



Figure 8.28: The original *baby* image.

Chapter 9

Conclusion and Future Work

9.1 Conclusion

The principle of indeterminacy originally described by W. Heisenberg and agreed upon by H. Weyl has been influential in fields other than quantum mechanics. D. Gabor's uncertainty relation of continuous finite energy signals is an example of this notion. Currently, many digital signal/image processing models discrete signals as a sampling of continuous signals and Gabor's elementary functions are shown to minimize HWUP, finitely discrete sampled versions or approximations of Gabor functions are thought to be conjointly well-localized. Many applications in signal and image processing require filters and/or filter banks, which are conjointly well-localize such as the AM-FM Image Model described in Chapter 2.2. Thus, quantification and conceptualization of uncertainty in the finite discrete time and finite discrete frequency domain is not only of great academic interest but practical in application.

Chapter 2.4 briefly describes the major current uncertainty principles used in signal/image processing. Some of these measures of uncertainty attempt to resemble the uncertainty measure used in HWUP, *i.e.* based on a probability distribution, characterized as a product of second moments, translation and modulation invariant, etc. An original contribution of this dissertation is a

novel measure of uncertainty applicable to finite length discrete sequences. This measure is taken directly from the context of discrete probability distributions and discrete random variables. It is analogous to HWUP in that it admits an attractive, intuitive interpretation as a product of variance in time and variance in frequency. The new uncertainty measure is made invariant to shifts in time and in frequency by defining it on equivalence classes of sequences. The fact that modulations and translations of finite sequence determine an equivalence class which is respected by the discrete Fourier transform has made time and frequency invariance possible for other uncertainty measures. The uncertainty measure proposed in this dissertation is classically defined as the minimum product of time variance and frequency variance taken from the class of all possible translations and modulations. Thus, the new measure is both shift invariant and modulation invariant.

When restricted to scaling function of a orthogonal or biorthogonal QMF¹, an unattainable non-zero² lower bound for the uncertainty maybe formulated as the product of smallest time variance given by the Haar scaling function and the smallest fequency variance given the ideal finite discrete filter. In both the orthogonal and biorthogonal case, a search algorithm was used to determine a conjointly well-localized scaling FIR function. Since the only linear phase orthogonal scaling function is given by the zero padded Haar function, the search algorithm determined a non-orthogonal linear phase FIR filter. Though still not an attainable lower bound for orthogonal scaling functions, the uncertainty measure of these symmetric filters provided a better lower bound

¹This restriction is made to emulate the restriction of Gabor's HWUP only applies to continous functionsl.

²For lengths greater than two.

than the product of the time variance of the Haar filter and the frequency variance of the ideal filter.

When the search was applied to symmetric scaling functions of biorthogonal QMFs, better conjoint localization (compared to the orthogonal case) was possible. A conjointly, well localized biorthogonal length six and eight scaling functions $f^{\text{opt}}[n]$ (as compared to the zero padded Haar scaling function, Daubechies wavelets, and symlet wavelets), were constructed using the search algorithm in Section 6.4.2. In addition, these quantities were attainable by biorthogonal scaling functions. The other three filters of the length six and eight biorthogonal QMF were found using a technique develop by Vetterli and Le Gall described in Section 6.4.2. This rendered a perfect reconstruction QMF in which the low pass analysis filter is conjointly well-localized.

The principle of indeterminacy was extended to L -channel PRPFB, which correspond to an $L - 1$ level DWT. Since the filters in the L -channel PRPFB exhibit strong interdependencies, it was necessary to define uncertainty of a filter bank with these dependencies in mind. Though it may be necessary for future work to include the localization of the synthesis filters in the filter bank uncertainty, in this dissertation only the localization of the analysis filters are used. The weighted arithmetic mean of the time variances and frequency variances, in which the frequency variances of the band pass channels were modified, of the analysis filters were used to quantify the localization of the L -channel PRPFB. The weighting function was determined by the manner in which the $L - 1$ level wavelet transform dyadically partitions the spectral domain.

From a set of well know QMFs the Coiflet QMF provided the best L -

channel PRPFB localization for $L = 2, 3, 4,$ and 5 as determined by smallest uncertainty $\Gamma_L(\cdot)$. The five channel PRPFB was used to separate spectral components of an image. The two dimensional perfect reconstruction filter bank was constructed by implementing the one dimensional five channel PRPFB on the rows of the image then the filter bank was applied to the columns, *i.e.* separably. In the two dimensional band pass channels the spectrum of the corresponding analysis filter was decomposed to provide orientation selectivity. This decomposition affected neither the localization nor the reconstruction ability of the filter bank. This construction provided a two dimensional filter bank in which optimal localization³, orientation selectivity, and perfect reconstruction are all attained.

Using *lena*, *girl2*, *gauss*, *burlap*, *mandril*, *clown*, *salesman*, *lady*, and *baby* as test images, it was shown that the *CSE* of the reconstructed image is lower when using a filter bank with smaller filter bank uncertainty measure $\Gamma_L(\cdot)$. This experiment supports our expectation: the multicomponent AM-FM image model found in [10] is better at representing the original image and lowering reconstruction errors when a conjointly well localized analysis filter bank is used.

9.2 Future Work

The science of digital signal processing is relatively new when compared to fields like mathematics and physics. It is neither amazing nor undesirable that ideas and concepts from mathematics and physics apply to signal processing. There

³Optimal localization is in the one dimensional case. Optimizing in multi- dimension will be left for future work.

are tremendous advancements to be made in signal/image/video processing by rigorously applying the knowledge and practices of these fields. There are many questions which were raised during the course of this research. These questions will require extensive research and creativity to answer. Some of the questions were pursued in a literary search, which ended in a unsatisfactory result. Hence are included in this dissertation as a declaration for future work.

It is always a worthwhile pursuit to generalize one dimensional signal processing concepts to multi-dimensions. It is not so large a step to generalize the uncertainty measure $\gamma_{N,f}^2$ in equation (4.15) to multi-dimensions. Rather, restricting the the multi-dimension uncertainty measure to finite discrete multi-dimensional signals which correspond to multi-dimensional continuous functions with compact support will be a work of great proportion. Mathematically precise working defintions and properties in which to construct multi-dimensional QMF will be a monumental task. Completion of this task will allow the use of a two dimensional non-separable filter bank to be implemented in the image analysis technique described in Chapter 8.

It is not necessary to wander into higher dimension to find interesting research. QMFs are a specific class of filter banks commonly know as L -channel maximally decimated perfect reconstruction filter bank (MDPRFB). An L -channel MDPRFB requires L analysis filters and L synthesis filters. In addition, the output of the analysis filter bank in each channel is down sampled by a factor of L and subsequently up sampled by L prior to applying the synthesis filters. When L is equal to two, this filter bank is the well studied QMF. When L is equals two raised to some positive integer power, like four, eight, sixteen, *etc.*, then a L -channel MDPRFB can be constructed simply by cas-

cading the two channel QMF to the all the branches. This is generally known as a wavelet packet. When our attention turns to L 's, which are not two to some positive power, Some interesting questions arise. For example, does a six channel MDPRFB exist? If they do exist are they equivalent to a filter bank composed of cascading all the P_i channel MDPRFB where P_i is a prime factor of L ? For example, given a six channel MDPRFB, is there a filter bank composed of cascading a QMF with a three channel MDPRFB or by cascading a three channel MDPRFB with a QMF which is equivalent to the given six channel MDPRFB? If odd channel MDPRFB's are possible then the problems encountered using multi-sampling rates would be alleviated.

In the Chapter 8, a conventional DWT at four level was used to determine AM-FM components of an image. The DWT at successive levels splits the low frequency channel. This is not necessary for perfect reconstruction. It is possible to devise a transform where the split into two channel does not always occur at the low frequency channel. It maybe more advantageous to construct a transform in which the filter bank resolves a band pass channel as opposed to the low pass channel. The channel to be resolved may be dependent on the frequency content of the signal or image. It maybe advantageous to devise the filter bank based on some image statistics. Which statistics and how they related to filter bank construction are of practical interest.

There are other interesting topics related to the work in this dissertation to explore. The few listed in this declaration seem the most prominent in extending the research presented in this dissertation. The rigorous and concise study of the topics outline in this chapter will provide immediate and insightful contributions to the field of signal and image processing.

Bibliography

- [1] D. Cassidy, *Dictionary of Scientific Biography*, vol. 3, p. 369. Charles Scribner's Sons, 1971.
- [2] D. Cassidy, *Dictionary of Scientific Biography*, vol. 17, pp. 394–403. Charles Scribner's Sons, 1991.
- [3] W. Heisenberg, "The physical content of quantum kinematics and mechanics," in *Quantum Theory and Measurement* (J. A. Wheeler and W. H. Zurek, eds.), pp. 63–86, Princeton, NJ: Princeton University Press, 1983.
- [4] H. Weyl, *The Theory of Groups and Quantum Mechanics*. New York, NY: Dover Publications, Inc., 1950.
- [5] D. Gabor, "Theory of communication," *J. Inst. Elect. Eng. London*, vol. 93, no. III, pp. 429–457, 1946.
- [6] J. P. Havlicek and A. C. Bovik, "Image modulation models," in *Handbook of Image and Video Processing* (A. Bovik, ed.), pp. 313–324, San Diego: Academic Press, 2000.
- [7] J. G. Daugman, "Uncertainty relation for resolution in space, spatial frequency, and orientation optimized by two dimensional visual cortical filters," *J. Opt. Soc. Am. A*, vol. 2, pp. 1160–1169, July 1985.

- [8] J. P. Havlicek, A. C. Bovik, and D. Chen, "AM-FM image modeling and Gabor analysis," in *Visual Information Representation, Communication, and Image Processing* (C. W. Chen and Y. Zhang, eds.), pp. 343–385, New York: Marcel Dekker, 1999.
- [9] J. P. Havlicek, D. S. Harding, and A. C. Bovik, "Multidimensional quasi-eigenfunction approximations and multicomponent AM-FM models," *IEEE Trans. Image Proc.*, vol. 9, pp. 227–242, February 2000.
- [10] J. P. Havlicek, D. S. Harding, and A. C. Bovik, "The multi-component AM-FM image representation," *IEEE Trans. Image Proc.*, vol. 5, pp. 1094–1100, June 1996.
- [11] J. P. Havlicek, J. W. Havlicek, N. D. Mamuya, and A. C. Bovik, "Skewed 2D Hilbert transforms and computed AM-FM models," in *Proc. IEEE Int'l. Conf. Image Proc.*, (Chicago, IL), pp. 602–606, October 4-7 1998.
- [12] S. G. Mallat, "A theory for multiresolution signal decomposition: the wavelet representation," *IEEE Trans. Pattern Anal. Machine Intell.*, vol. 11, pp. 674–693, July 1989.
- [13] T. P. Barnwell III and M. Smith, "Filter banks for analysis-reconstruction systems: a tutorial," in *Proc. IEEE Int'l. Symp. Circuits, Syst.*, (New Orleans, LA), pp. 1999–2003, May 1-3 1990.
- [14] O. Rioul and P. Duhamel, "A Remez exchange algorithm for orthonormal wavelets," *IEEE Trans. Circuits, Syst.-II: Analog, Digital Sig. Proc.*, vol. 41, pp. 550–560, Aug. 1994.

- [15] K. Nayebi, T. P. Barnwell III, and M. Smith, "The time domain analysis and design of exactly reconstructing FIR analysis/synthesis filter banks," in *Proc. IEEE Int'l. Conf. Acoust., Speech, Signal Proc.*, (Albuquerque, NM), pp. 1735–1738, Apr. 3-6 1990.
- [16] M. Vetterli and D. L. Gall, "Perfect reconstruction FIR filter banks: some properties and factorizations," *IEEE Trans. Acoustics, Speech, and Signal Proc.*, vol. 37, pp. 1057–1071, July 1989.
- [17] M. Smith and T. P. Barnwell III, "Exact reconstruction techniques for tree-structured subband coders," *IEEE Trans. Acoust., Speech, Signal Proc.*, vol. ASSP-34, pp. 434–441, June 1986.
- [18] M. Smith and S. L. Eddins, "Analysis/synthesis techniques for sub-band image coding," *IEEE Trans. Acoust., Speech, Signal Proc.*, vol. 38, pp. 1446–1456, Aug. 1990.
- [19] K. Nayebi, T. P. Barnwell III, and M. Smith, "The time domain analysis and design of exactly reconstructing FIR analysis/synthesis filter banks," in *Proc. IEEE Int'l. Conf. Acoust., Speech, Signal Proc.*, (Albuquerque, NM), pp. 1735–1738, Apr. 3-6 1990.
- [20] M. Antonini, M. Barlaud, and I. Daubechies, "Image coding using wavelet transform," *IEEE Trans. Image Proc.*, vol. 1, pp. 205–220, April 1992.
- [21] I. Daubechies, "Orthonormal bases of compactly supported wavelets," *Commun. Pure Appl. Math.*, vol. 51, pp. 909–996, 1988.
- [22] M. Vetterli and C. Herley, "Wavelets and filter banks: theory and design," *IEEE Trans. Signal Proc.*, vol. 40, pp. 2207–2232, Sept. 1992.

- [23] K. Nayebi, T. P. Barnwell III, and M. Smith, "A time domain view of filter banks and wavelets," in *Proc. 25th Asilomar Conf. Signals, Syst., Comput.*, (Pacific Grove, CA), pp. 736–740, Nov. 4-6 1991.
- [24] A. Cohen, I. Daubechies, and J. Feauveau, "Biorthogonal bases of compactly supported wavelets," *Comm. Pure Appl. Math*, vol. 45, no. 5, pp. 485–560, 1992.
- [25] P. Stoica and R. Moses, *Introduction to Spectral Analysis*. New Jersey: Prentice Hall, 1997.
- [26] R. Ishii and K. Furukawa, "The uncertainty principle in discrete signals," *IEEE Trans. Circ. Syst.*, vol. CAS-33, pp. 1032–1034, Oct. 1986.
- [27] M. Doroslovački, "Discrete-time signals and uncertainty relations involving ordinary second moments in time and frequency," in *Proc. IEEE Int'l. Symp. Signal Proc.*, (Philadelphia, PA), pp. 186–189, Oct. 1994.
- [28] L. Calvez and P. Vilbé, "On the uncertainty principle in discrete signals," *IEEE Trans. Circuits, Syst.-II: Analog, Digital Sig. Proc.*, vol. 39, pp. 394–395, June 1992.
- [29] D. L. Donoho and P. B. Stark, "Uncertainty principles and signal recovery," *SIAM J. Appl. Math.*, vol. 49, pp. 906–931, June 1989.
- [30] D. M. Monro, B. E. Bassil, and G. J. Dickson, "Orthonormal wavelets with balanced uncertainty," in *Proc. IEEE Int'l. Conf. Image Proc.*, (Lausanne, Switzerland), pp. 581–584, Sept. 16-19, 1996.

- [31] D. M. Monro and B. G. Sherlock, "Space-frequency balance in biorthogonal wavelets," in *Proc. IEEE Int'l. Conf. Image Proc.*, (Santa Barbara, CA), pp. 624–627, October 26-29 1997.
- [32] V. DeBrunner, M. Özaydin, and T. Przebinda, "Resolution in time-frequency," *IEEE Trans. Signal Proc.*, vol. 47, pp. 783–788, March 1999.
- [33] J. J. Kulikowski, S. Marčelja, and P. O. Bishop, "Theory of spatial position and spatial frequency relations in the receptive fields of simple cells in the visual cortex," *Biol. Cybern.*, vol. 43, no. 3, pp. 187–198, 1982.
- [34] J. P. Jones and L. A. Palmer, "The two-dimensional structure of simple receptive fields in cat striate cortex," *J. Neurophysiol.*, vol. 58, no. 6, pp. 1187–1211, 1987.
- [35] J. P. Jones, A. Stepnoski, and L. A. Palmer, "The two-dimensional spectral structure of simple receptive fields in cat striate cortex," *J. Neurophysiol.*, vol. 58, no. 6, pp. 1212–1232, 1987.
- [36] J. P. Jones and L. A. Palmer, "An evaluation of the two-dimensional Gabor model of simple receptive fields in cat striate cortex," *J. Neurophysiol.*, vol. 58, no. 6, pp. 1233–1258, 1987.
- [37] W. Mendenhall and T. Sincich, *Statistics for Engineering and the Sciences*. San Francisco: Dellen Publishing Company, third ed., 1992.
- [38] Y. Meyer, *Wavelets and Operators*. New York, NY: Cambridge University Press, 1992.

- [39] A. Papoulis, *The Fourier Integral and Its Applications*. New York: McGraw-Hill Publishing Company, 1962.
- [40] L. J. Corwin and R. H. Szczarba, *Calculus in Vector Spaces*. New York, NY: Marcel Dekker, Inc., second ed., 1995.
- [41] D. Wei and A. C. Bovik, "The generalized coiflets with nonzero-centered vanishing moments," *IEEE Trans. Circ. and Syst.-II*, vol. 45, pp. 988–1001, August 1998.

Appendices

Appendix A

Plots of Functions Γ_{\max} and Γ_{\min}

The following figures in this appendix are plots of $\Gamma_{\max}(\lambda)$ and $\Gamma_{\min}(\lambda)$ where $0 \leq \lambda \leq 1$ for lengths $N = 6, 8, 10, 12, 14, 16, 18, 20$. The functions $\Gamma_{\max}(\lambda)$ and $\Gamma_{\min}(\lambda)$ are defined in chapter 6.3 equations (6.43) and (6.45), *resp.* Though these figures do not conclusively prove the claim that the phase terms of equations (6.23) and (6.24) are a global maximum and a global minimum when the magnitude terms satisfy the conditions specified in chapters 6.4.1 and 6.4.2, these figures do support this claim. Thus the use of the function in equation (6.22) as the phase term in the search algorithm of chapters 6.4.1 and 6.4.2 is justified by this claim.

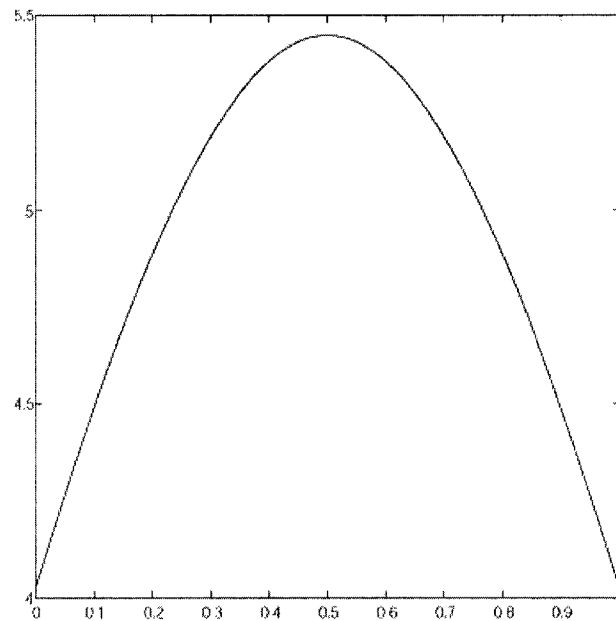


Figure A.1: Plot of $\Gamma_{\max}(\lambda)$ of the length 6 filter \mathbf{f} defined in equation (6.44) for $0 \leq \lambda \leq 1$.

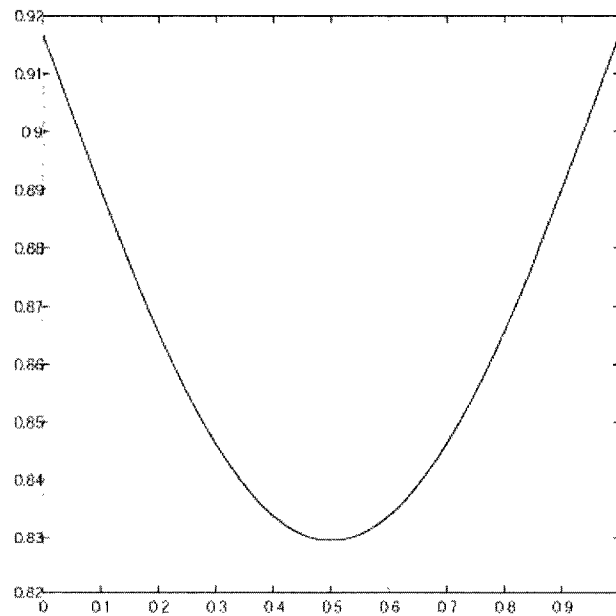


Figure A.2: Plot of $\Gamma_{\min}(\lambda)$ of the length 6 filter \mathbf{f} defined in equation (6.44) for $0 \leq \lambda \leq 1$.

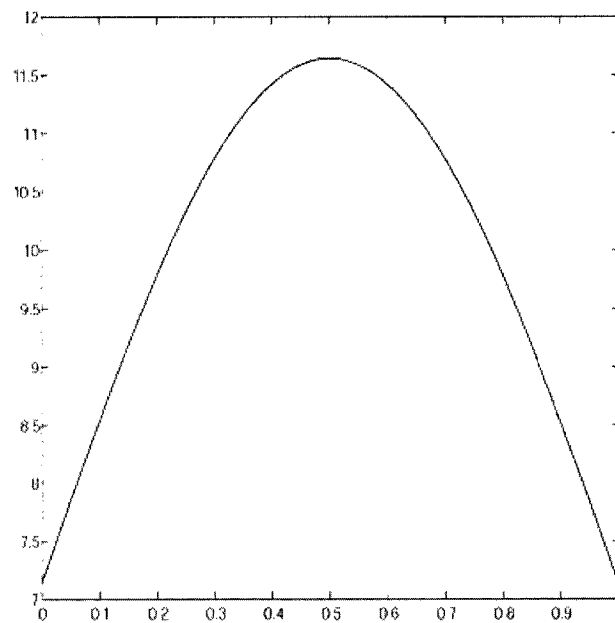


Figure A.3: Plot of $\Gamma_{\max}(\lambda)$ of the length 8 filter \mathbf{f} defined in equation (6.44) for $0 \leq \lambda \leq 1$.

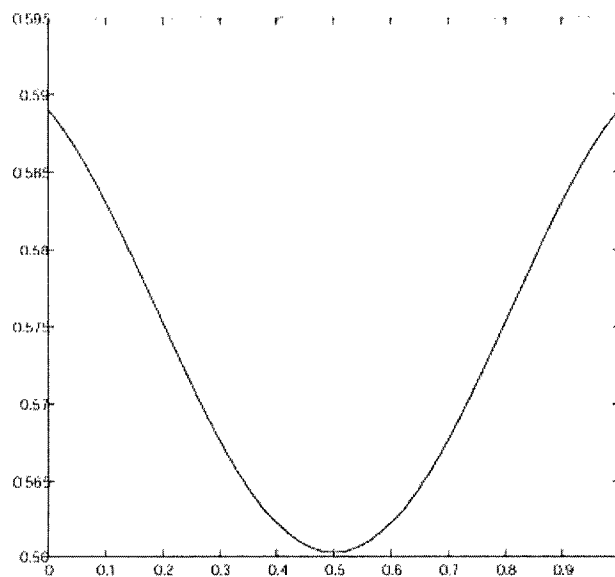


Figure A.4: Plot of $\Gamma_{\min}(\lambda)$ of the length 8 filter \mathbf{f} defined in equation (6.44) for $0 \leq \lambda \leq 1$.

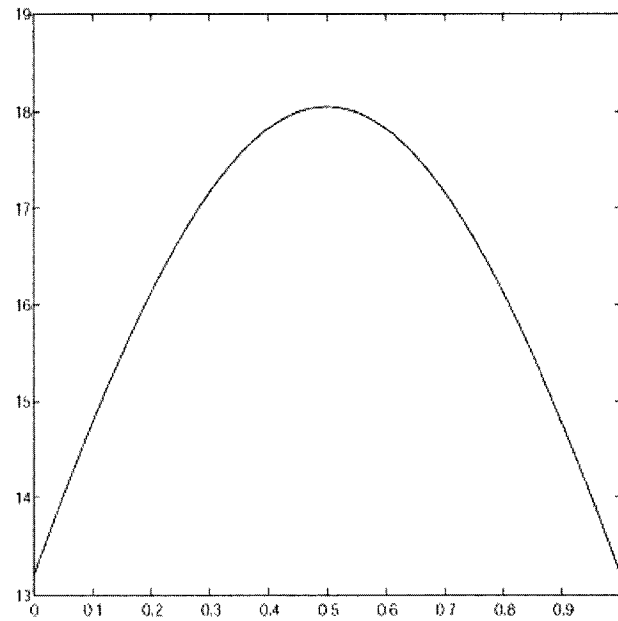


Figure A.5: Plot of $\Gamma_{\max}(\lambda)$ of the length 10 filter \mathbf{f} defined in equation (6.44) for $0 \leq \lambda \leq 1$.

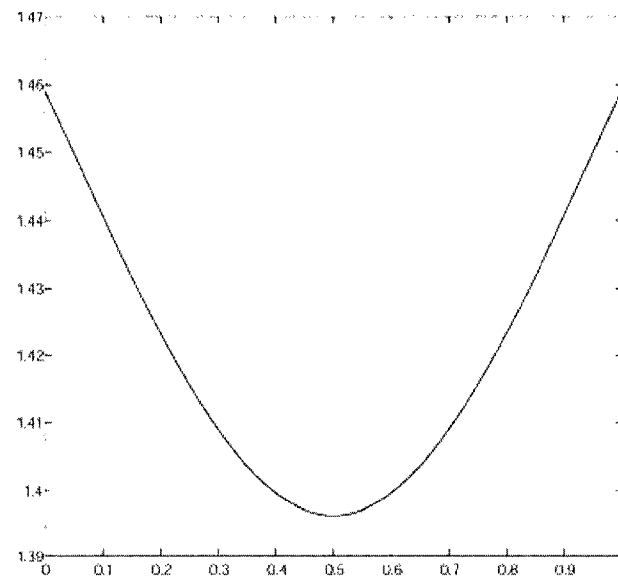


Figure A.6: Plot of $\Gamma_{\min}(\lambda)$ of the length 10 filter \mathbf{f} defined in equation (6.44) for $0 \leq \lambda \leq 1$.

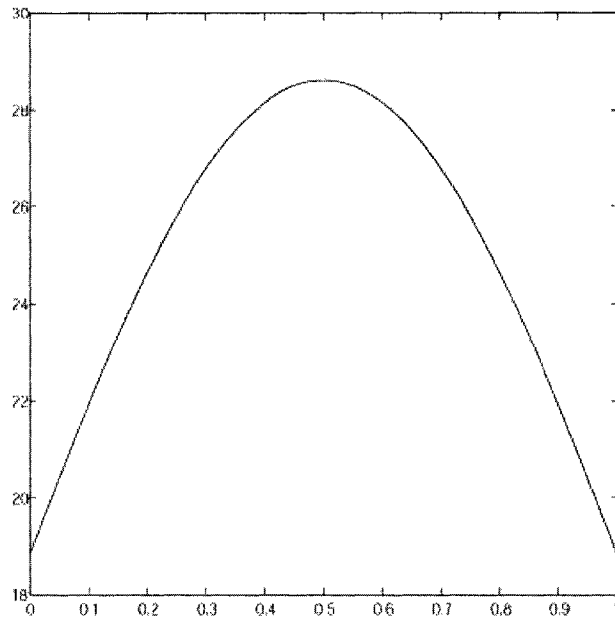


Figure A.7: Plot of $\Gamma_{\max}(\lambda)$ of the length 12 filter \mathbf{f} defined in equation (6.44) for $0 \leq \lambda \leq 1$.

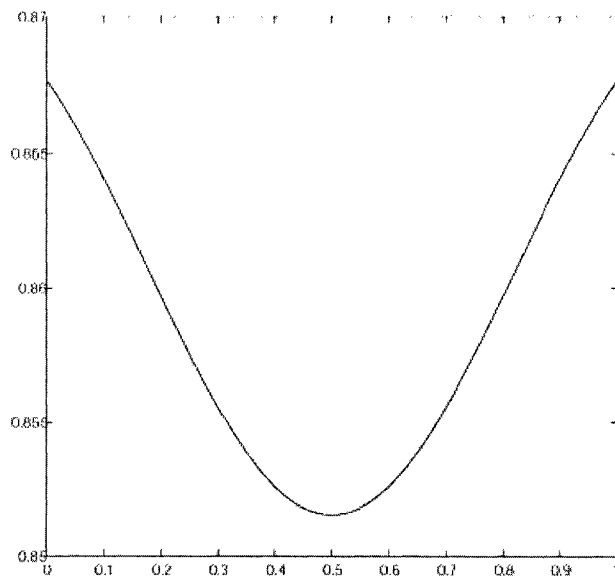


Figure A.8: Plot of $\Gamma_{\min}(\lambda)$ of the length 12 filter \mathbf{f} defined in equation (6.44) for $0 \leq \lambda \leq 1$.

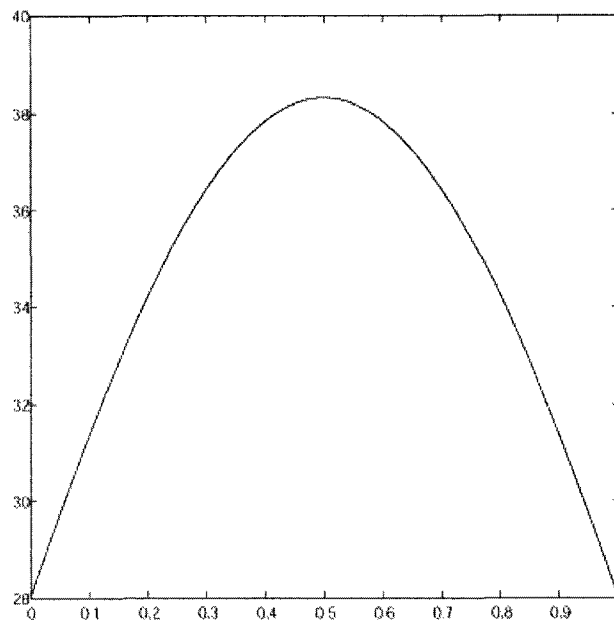


Figure A.9: Plot of $\Gamma_{\max}(\lambda)$ of the length 14 filter \mathbf{f} defined in equation (6.44) for $0 \leq \lambda \leq 1$.

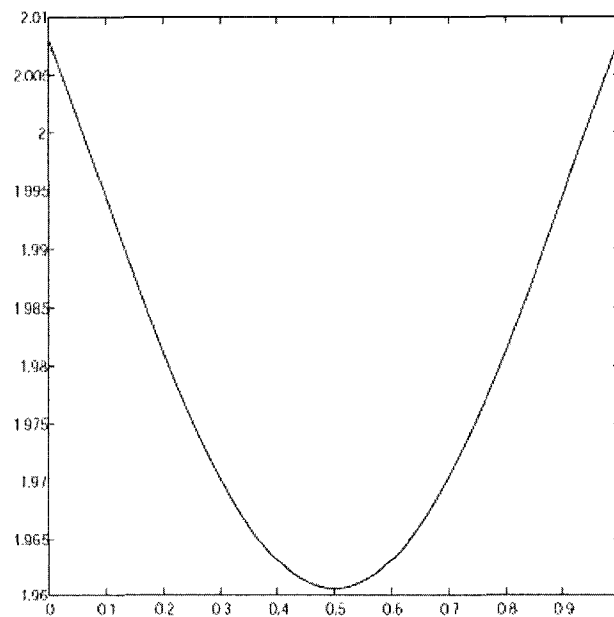


Figure A.10: Plot of $\Gamma_{\min}(\lambda)$ of the length 14 filter \mathbf{f} defined in equation (6.44) for $0 \leq \lambda \leq 1$.

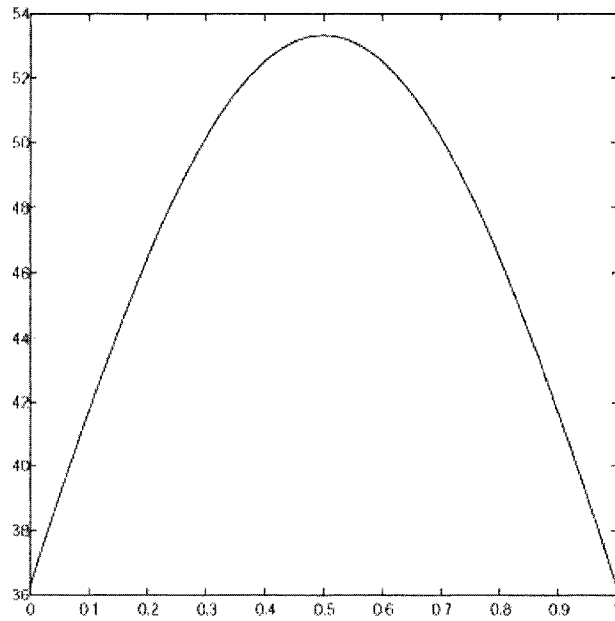


Figure A.11: Plot of $\Gamma_{\max}(\lambda)$ of the length 16 filter \mathbf{f} defined in equation (6.44) for $0 \leq \lambda \leq 1$.

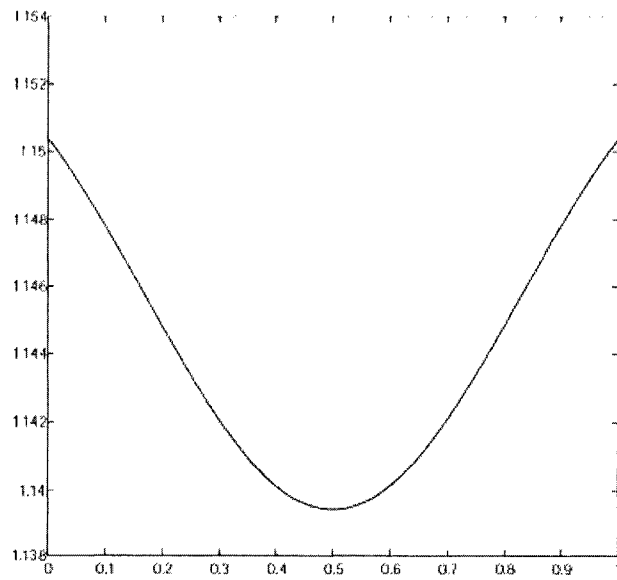


Figure A.12: Plot of $\Gamma_{\min}(\lambda)$ of the length 16 filter \mathbf{f} defined in equation (6.44) for $0 \leq \lambda \leq 1$.

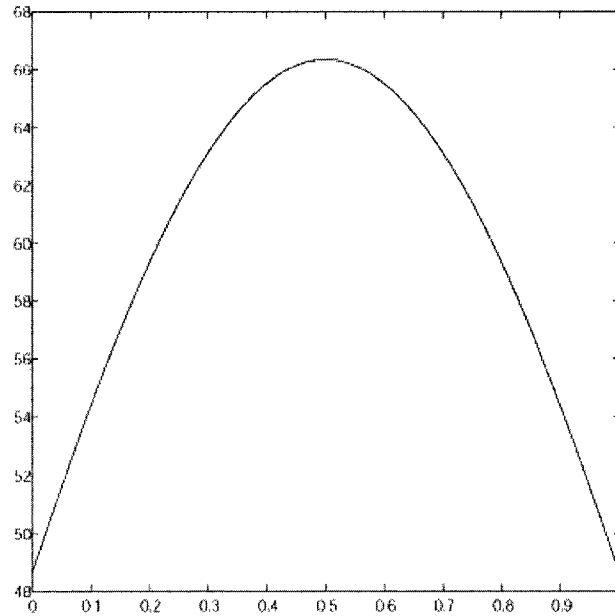


Figure A.13: Plot of $\Gamma_{\max}(\lambda)$ of the length 18 filter \mathbf{f} defined in equation (6.44) for $0 \leq \lambda \leq 1$.

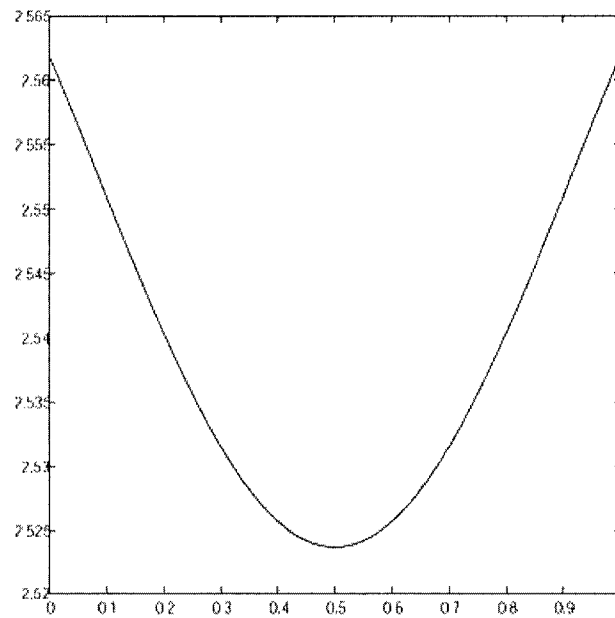


Figure A.14: Plot of $\Gamma_{\min}(\lambda)$ of the length 18 filter \mathbf{f} defined in equation (6.44) for $0 \leq \lambda \leq 1$.

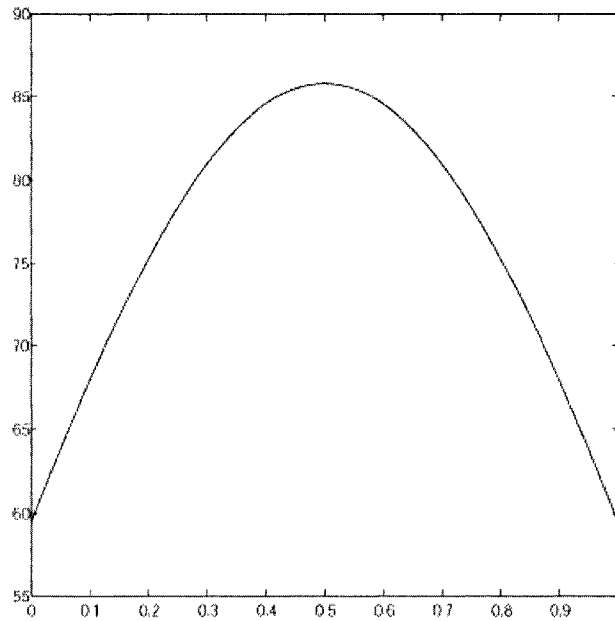


Figure A.15: Plot of $\Gamma_{\max}(\lambda)$ of the length 20 filter \mathbf{f} defined in equation (6.44) for $0 \leq \lambda \leq 1$.

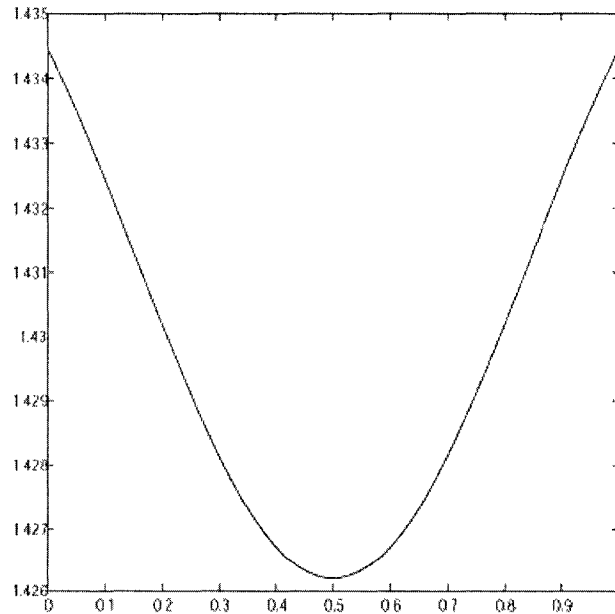


Figure A.16: Plot of $\Gamma_{\min}(\lambda)$ of the length 20 filter \mathbf{f} defined in equation (6.44) for $0 \leq \lambda \leq 1$.

Appendix B

Search Results of Section 6.4.1

The best localized filter $\mathbf{f}^{opt} \in \mathcal{B}'_{10}$ is

$$\begin{aligned} f^{opt}[0] &= 0.00097755285610 &= f^{opt}[9] \\ f^{opt}[1] &= 0.00020212581019 &= f^{opt}[8] \\ f^{opt}[2] &= -0.0292317911516 &= f^{opt}[7] \\ f^{opt}[3] &= 0.02926361329492 &= f^{opt}[6] \\ f^{opt}[4] &= 0.70589528037703 &= f^{opt}[5]. \end{aligned}$$

The time variance for this filter is

$$\sigma_{n, [\mathbf{f}^{opt}]}^2 = 0.2637$$

and the frequency variance is

$$\sigma_{\omega, [\mathbf{f}^{opt}]}^2 = 2.9263.$$

The joint uncertainty is

$$\gamma_{10, \mathbf{f}^{opt}}^2 = 0.7717.$$

The best localized filter $\mathbf{f}^{opt} \in \mathcal{B}'_{12}$ is

$$\begin{aligned} f^{opt}[0] &= -0.00000289471504 &= f^{opt}[11] \\ f^{opt}[1] &= 0.00065979348988 &= f^{opt}[10] \\ f^{opt}[2] &= 0.00059110696006 &= f^{opt}[9] \\ f^{opt}[3] &= -0.02971968049867 &= f^{opt}[8] \\ f^{opt}[4] &= 0.02972257521371 &= f^{opt}[7] \\ f^{opt}[5] &= 0.70585588073661 &= f^{opt}[6]. \end{aligned}$$

The time variance for this filter is

$$\sigma_{n, [\mathbf{f}^{opt}]}^2 = 0.2642$$

and the frequency variance is

$$\sigma_{\omega, [\mathbf{f}^{opt}]}^2 = 4.2079.$$

The joint uncertainty is

$$\gamma_{12, \mathbf{f}^{opt}}^2 = 1.1116.$$

The best localized filter $\mathbf{f}^{opt} \in \mathcal{B}'_{14}$ is

$$\begin{aligned}
 f^{opt}[0] &= -0.00158529669169 &= f^{opt}[13] \\
 f^{opt}[1] &= 0.00192275459981 &= f^{opt}[12] \\
 f^{opt}[2] &= -0.00141183651197 &= f^{opt}[11] \\
 f^{opt}[3] &= 0.00263148266877 &= f^{opt}[10] \\
 f^{opt}[4] &= -0.03111890876758 &= f^{opt}[9] \\
 f^{opt}[5] &= 0.03093528385826 &= f^{opt}[8] \\
 f^{opt}[6] &= 0.70573330203094 &= f^{opt}[7].
 \end{aligned}$$

The time variance for this filter is

$$\sigma_{n, [\mathbf{f}^{opt}]}^2 = 0.2661$$

and the frequency variance is

$$\sigma_{\omega, [\mathbf{f}^{opt}]}^2 = 5.7033.$$

The joint uncertainty is

$$\gamma_{14, \mathbf{f}^{opt}}^2 = 1.5178.$$

The best localized filter $\mathbf{f}^{opt} \in \mathcal{B}'_{16}$ is

$$\begin{aligned}
 f^{opt}[0] &= -0.00003487499231 &= f^{opt}[15] \\
 f^{opt}[1] &= 0.00058416625621 &= f^{opt}[14] \\
 f^{opt}[2] &= -0.00059007570920 &= f^{opt}[13] \\
 f^{opt}[3] &= 0.00042956131426 &= f^{opt}[12] \\
 f^{opt}[4] &= 0.00022402630573 &= f^{opt}[11] \\
 f^{opt}[5] &= -0.02089780602489 &= f^{opt}[10] \\
 f^{opt}[6] &= 0.02090371547788 &= f^{opt}[9] \\
 f^{opt}[7] &= 0.70648806855886 &= f^{opt}[8].
 \end{aligned}$$

The time variance for this filter is

$$\sigma_{n, [\mathbf{f}^{opt}]}^2 = 0.2570$$

and the frequency variance is

$$\sigma_{\omega, [\mathbf{f}^{opt}]}^2 = 7.7251.$$

The joint uncertainty is

$$\gamma_{16, \mathbf{f}^{opt}}^2 = 1.9857.$$

The best localized filter $\mathbf{f}^{opt} \in \mathcal{B}'_{18}$ is

$$\begin{aligned}
 f^{opt}[0] &= 0.00061899820684 &= f^{opt}[17] \\
 f^{opt}[1] &= -0.00064969560982 &= f^{opt}[16] \\
 f^{opt}[2] &= -0.00026258320251 &= f^{opt}[15] \\
 f^{opt}[3] &= 0.00017939412897 &= f^{opt}[14] \\
 f^{opt}[4] &= 0.00226696548146 &= f^{opt}[13] \\
 f^{opt}[5] &= -0.00113839278178 &= f^{opt}[12] \\
 f^{opt}[6] &= -0.02842125053982 &= f^{opt}[11] \\
 f^{opt}[7] &= 0.02856067064159 &= f^{opt}[10] \\
 f^{opt}[8] &= 0.70595267486162 &= f^{opt}[9].
 \end{aligned}$$

The time variance for this filter is

$$\sigma_{n, [\mathbf{f}^{opt}]}^2 = 0.2633$$

and the frequency variance is

$$\sigma_{\omega, [\mathbf{f}^{opt}]}^2 = 9.5103.$$

The joint uncertainty is

$$\gamma_{18, \mathbf{f}^{opt}}^2 = 2.5041.$$

The best localized filter $\mathbf{f}^{opt} \in \mathcal{B}'_{20}$ is

$$\begin{aligned}
 f^{opt}[0] &= -0.00004324906913 = f^{opt}[19] \\
 f^{opt}[1] &= 0.00055735837877 = f^{opt}[18] \\
 f^{opt}[2] &= -0.00046835044924 = f^{opt}[17] \\
 f^{opt}[3] &= -0.00096769015396 = f^{opt}[16] \\
 f^{opt}[4] &= 0.00106040023790 = f^{opt}[15] \\
 f^{opt}[5] &= 0.00006499402194 = f^{opt}[14] \\
 f^{opt}[6] &= 0.00119337996413 = f^{opt}[13] \\
 f^{opt}[7] &= -0.03084394524167 = f^{opt}[12] \\
 f^{opt}[8] &= 0.03079448422686 = f^{opt}[11] \\
 f^{opt}[9] &= 0.70575939927094 = f^{opt}[10].
 \end{aligned}$$

The time variance for this filter is

$$\sigma_{n, [\mathbf{f}^{opt}]}^2 = 0.2655$$

and the frequency variance is

$$\sigma_{\omega, [\mathbf{f}^{opt}]}^2 = 11.6458.$$

The joint uncertainty is

$$\gamma_{20, \mathbf{f}^{opt}}^2 = 3.0915.$$

Appendix C

Well Known Quadrature Mirror Filter Banks

This Appendix gives the filters which compose the QMF's used in Chapters 7 and 8.

n	$f_a[n]$	$g_a[n]$	$f_s[n]$	$g_s[n]$
0	0.03522629188210	-0.33267055295096	0.33267055295096	0.03522629188210
1	-0.08544127388224	0.80689150931334	0.80689150931334	0.08544127388224
2	-0.13501102001039	-0.45987750211933	0.45987750211933	-0.13501102001039
3	0.45987750211933	-0.13501102001039	-0.13501102001039	-0.45987750211933
4	0.80689150931334	0.08544127388224	-0.08544127388224	0.80689150931334
5	0.33267055295096	0.03522629188210	0.03522629188210	-0.33267055295096

Table C.1: The Daubechies length six (DB_6) QMF.

n	$f_a[n]$	$g_a[n]$	$f_s[n]$	$g_s[n]$
0	0	0	0	0
1	0.35355339059327	0.17677669529664	-0.17677669529664	0.35355339059327
2	0.70710678118655	0.35355339059327	0.35355339059327	-0.70710678118655
3	0.35355339059327	-1.06066017177982	1.06066017177982	0.35355339059327
4	0	0.35355339059327	0.35355339059327	0
5	0	0.17677669529664	-0.17677669529664	0

Table C.2: The biorthogonal 3/5 ($BO3/5$) QMF.

n	$f_a[n]$	$g_a[n]$	$f_s[n]$	$g_s[n]$
0	-0.08838834764832	0	0	-0.08838834764832
1	0.08838834764832	0	0	-0.08838834764832
2	0.70710678118655	-0.70710678118655	0.70710678118655	0.70710678118655
3	0.70710678118655	0.70710678118655	0.70710678118655	-0.70710678118655
4	0.08838834764832	0	0	0.08838834764832
5	-0.08838834764832	0	0	0.08838834764832

Table C.3: The biorthogonal 6/2 (*BO6/2*) QMF.

n	$f_a[n]$	$g_a[n]$	$f_s[n]$	$g_s[n]$
0	0	0	0	0
1	0.17677669529664	-0.35355339059327	-0.35355339059327	-0.17677669529664
2	0.53033008588991	-1.06066017177982	1.06066017177982	0.53033008588991
3	0.53033008588991	1.06066017177982	1.06066017177982	-0.53033008588991
4	0.17677669529664	0.35355339059327	-0.35355339059327	0.17677669529664
5	0	0	0	0

Table C.4: The biorthogonal 4/4 (*BO4/4*) QMF.

n	$f_a[n]$	$g_a[n]$	$f_s[n]$	$g_s[n]$
0	-0.01565572813546	0.07273261951285	-0.07273261951285	-0.01565572813546
1	-0.07273261951285	0.33789766245781	0.33789766245781	0.07273261951285
2	0.38486484686420	-0.85257202021226	0.85257202021226	0.38486484686420
3	0.85257202021226	0.38486484686420	0.38486484686420	-0.85257202021226
4	0.33789766245781	0.07273261951285	-0.07273261951285	0.33789766245781
5	-0.07273261951285	-0.01565572813546	-0.01565572813546	0.07273261951285

Table C.5: The length six Coiflet (*Coif*) QMF.